

https://dspace.org/

Characterisation of a Titanium precursor salt and study of some of the treatment steps used for the extraction process

Mutava, Tapiwa David

2010-07-19T07:59:58Z
http://hdl.handle.net/10539/8294

Downloaded from a DSpace repository. https://dspace.org/

Characterisation of a Titanium precursor salt and study of some of the treatment steps used for the extraction process

Tapiwa David Mutava

A dissertation submitted to the Faculty of Engineering and the Built Environment, University of the Witwatersrand, Johannesburg, in partial fulfillment of the requirements for the degree of Master of Science in Engineering.

Johannesburg, 2009

DECLARATION

I declare that this dissertation is my own unaided work. It is being submitted for the Degree of Master of Science in Engineering in the University of Witwatersrand, Johannesburg. It has not been submitted before for any degree or examination in any other University.

(Signature of candidate)

---------- Day of----------2009

ABSTRACT

The advancement of a material and its usage, particularly for civilian applications, are dependent primarily on cost considerations regardless of the superior properties that the material might possess. Titanium is a material with superior properties which could make a significant impact on civilian life if used on a much larger scale. However, the use of this metal is up to this day limited to highly specialized applications, those being predominantly military owing to its very high cost. The high cost is a direct result of the very expensive commercial method of extraction which has been in existence for more than sixty years now since its inception. Efforts are now made to formulate new methods of extracting titanium from its ores which will be simpler, more economic and therefore more affordable for ordinary applications. This work involved the development and elaboration of a novel titanium extraction method from its ores, particularly ilmenite. A novel titanium complex salt, herein called the precursor, was used for all the work that is presented. It was fully characterised using a wide range of techniques to ascertain its chemical and physical properties. Further to that, the precursor was taken through various pyrometallurgical steps which saw its thermal decomposition and final reduction to titanium metal. The emphasis was on making the process simple and much cheaper.

DEDICATIONS

This work is dedicated to my twin daughters, Eunice and Nokutenda Mutava. Although Eunice failed to make it at birth, she still lives with us today and in a big way you passed on my dear flawless. We love you, and when we see your kid sister everyday we think of you. For the five hours that you were with us, we thank you. Without the support of my wife, Eunice, and my parents, Clemence and Enica Mutava, as well as my family, Petronilla, Desmond, Emmanuel and Tafadzwa Clemence Mutava, this work would not have been possible. This great piece of work is also dedicated to the unbelievably strong people of Zimbabwe.

ACKNOWLEDGEMENTS

This work could not have been without Prof. Sigalas (Jack) and Dr. Herrmann, thanks Jack. The funding from The Centre of Excellence in Strong Materials made all this work possible and for that I will always be indebted to them, thank you. There are also a number of people and organizations that made this work a success. I need to thank Retha Rossouw of CSIR for all the microscopy work, Anita Naick of Mintek for X-ray fluorescence, Dr. Shackleton for ToF-SIMS, Vuyisi of the Witwatersrand Chemistry department for ICP-MS and Mr. Adri Watkins of AJ Electrical for all the training on TGA-DTA.

TABLE OF CONTENTS

ABSTRACT ..... **iii**
DEDICATIONS ..... **iv**
ACKNOWLEDGEMENTS ..... **v**
LIST OF FIGURES ..... **viii**
LIST OF TABLES ..... **xi**
ABBREVIATIONS ..... **xiii**
Chapter 1: Introduction **1**
1.1 Project Overview 3
Chapter 2: Literature Review **4**
2.1 The discovery of titanium 4
2.2 Chemistry of titanium 5
2.2.1 Titanium as a biomaterial 6
2.3 Metallurgy of titanium 8
2.3.1 Common ores of titanium 8
2.3.2 Metallurgical extraction of titanium from its concentrates 10
2.3.3 Phase equilibria of titanium alloys 14
2.3.4 Classification of titanium alloys 17
2.3.5 Titanium forming processes 19
2.4 Alternative extraction routes 23
2.4.1. The ITP/ Armstrong Process 25
2.4.2 Electrolytic processes 26
2.4.2.1 The Fray-Farthing-Chen (FFC) Cambridge process 27
2.4.2.2 The Preform Reduction process (PRP) 28
2.4.2.3 The Process 30
Chapter 3: Experimental Procedure **34**
3.1 Characterisation of the titanium precursor 35
3.1.1 Precursor particle size distribution 36
3.1.2 Determination of the chemical composition of the precursor 36
3.1.2.1 Scanning Electron Microscopy and Energy Dispersive X-ray spectrometry (SEM/EDX) 37
3.1.4.2 X-ray Fluorescence (XRF) Spectrometer 37
3.1.4.3 Inductively Coupled Plasma Mass Spectrometer (ICP-MS) 37
3.1.4.3 X-ray diffraction (XRD) analysis 38
3.2 Thermal analysis: Thermogravimetric and thermal differential analyser (TGA-DTA) and Differential Scanning Calorimeter (TGA-DSC) 38
3.2.1 Pyrolysis of the precursor powder in a tube furnace 39
3.3 .Optimisation of inert gas flow rate 41
3.3.1 Optimisation of soaking time 42
3.3.2 Stepwise decomposition of the titanium precursor powder 43
3.3.3 Reaction kinetics studies 44
3.3.4 Mass balances and Optimization of the amount of reductant 45
3.4 Precursor reduction experiments 46

3.5 Chemical Vapour Deposition (CVD) experiments 47
Chapter 4: Results..... 49
4.1 Characterisation of the starting precursor 49
4.1.1 Particle size distribution of the precursor and final titanium product..... 49
4.1.2 SEM Analysis of the precursor 51
4.2 Thermal Analysis 54
4.2.1 SEM analysis of product at various gas linear flow rates 56
4.3 Stepwise thermal decomposition of the precursor 58
4.4.3 Characterisation of product after soaking the reduced powder at..... 71
1300^{o}C
4.5 Chemical Vapour Deposition (CVD) of AlF_3 on Titanium 73
4.6 Kinetics of the decomposition of the precursor and sublimation of AlF_3..... 74
4.6.1 Thermal analysis 74
Chapter 5: Discussion of Results 78
5.1 Particle size distribution of the precursor and the titanium product 78
The shrinking core model 80
SEM Analysis of product before and after sublimation of AlF_3..... 80
5.2 Characterisation of the starting precursor 81
5.2.3 Thermogravimetric and thermal analysis of the precursor 83
5.2.3 XRD Analysis of products of pyrolysis 86
5.2.4 SEM Analysis of products 87
5.3 Optimization of gas linear flow rate 89
5.4 Reduction of the precursor with aluminum 93
5.4.1 Characterisation of the titanium product..... 95
5.5 Kinetics Studies 99
5.6 Recovery of titanium..... 104
5.8 Summary and proposed process flow sheet 107
Chapter 6: Conclusions and Recommendations 110
6.0 Conclusions..... 110
6.1 Recommendations..... 112
References:..... 114

LIST OF FIGURES

Figure 2. 1: Distribution of the most abundant titanium ore reserves in the world [5]**Figure 2. 2: Flowchart for titanium production by the Kroll or Hunter process** [44].

Figure 2. 3: The Ti-O phase diagram [41]

Figure 2. 4: Phase diagram of the Ti-Al system [41].

Figure 2. 5: The Ti-C phase diagram [41]

Figure 2. 6: Effect of alloying elements on the phase fields of the constitutional diagram [42]

Figure 2. 7: Schematic of a vacuum arc melter (after H.Sibum [5].)

Figure 2. 8: Process flow chart for titanium sponge [40]

Figure 2. 9: Schematic of the FFC electrolytic cell

Figure 2. 10: Flowchart of the Process [1].

Figure 3. 1: Schematic of the tube furnace

Figure 3. 2: Heat treatment cycle during precursor reduction trials

Figure 3. 3: Heat treatment cycle during CVD trials

Figure 4. 1: Particle size distribution of raw precursor

Figure 4. 2: Particle size distribution of the final titanium product

Figure 4. 3: SEM analysis of the precursor (a) SEM micrograph (b) Overall EDS spectrum (c) EDS

Figure 4. 4: XRD pattern of the raw precursor

Figure 4. 5: TGA/DTA trace of precursor in UHP argon

Figure 4. 6: SEM micrographs of pyrolysis products after heating the precursor for 2 hours at

Figure 4. 7: XRD patterns for product after soaking at 1300oC with linear gas flow rate at

Figure 4. 8: SEM analysis of product after decomposing precursor at 400oC and soaking for

Figure 4. 9: XRD Analysis of product after decomposing precursor at 400oC in UHP Argon

Figure 4. 10: SEM analysis of product after decomposing precursor at 600oC (a) SEM (b)

Figure 4. 11: XRD Analysis of product after decomposing precursor at 600oC in UHP Argon

Figure 4. 12: SEM analysis of product after decomposing precursor at 800oC and soaking for

Figure 4. 13: XRD of product after decomposing precursor at 800oC and soaking for 2 hours

Figure 4. 14: SEM analysis of product after decomposing precursor at 1000oC for 2 hours (a)

Figure 4. 15: XRD Analysis of product after decomposing precursor at 1000oC for 2 hours

Figure 4. 17: XRD Analysis of product after decomposing precursor at 1200oC in UHP Ar

Figure 4. 18: SEM analysis of product after decomposing precursor at 1300oC (a) SEM (b)

Figure 4. 19: XRD Analysis of product after decomposing precursor at 1300oC in UHP Ar

Figure 4. 20: SEM analysis of the titanium product after reduction aluminium

Figure 4. 21: XRD pattern after reduction of precursor with aluminium at 800oC

Figure 4. 23: XRD pattern of product after reduction and soaking at 1300oC for 2 hours

Figure 4. 24: ToF-SIMS images of passivated product (a) Al ion image before sputtering (b) Ti ion

Figure 4. 25: TGA-DSC trace of precursor in UHP Argon

Figure 4. 26: TGA/DTA trace of AlF3

Figure 4. 16: SEM analysis of product after decomposing precursor at 1200oC for 2 hours

Figure 4. 22: SEM analysis of product after reduction of precursor with aluminium at 1300oC for 2 hours (a)

Figure 5. 1: Superimposed particle size distributions of the precursor and Ti product

Figure 5. 2: Schematic showing (a) a pre-existent volatile phase and (b) Volatile phase forming due to thermal decomposition

Figure 5. 3: Schematic of the shrinking core model

Figure 5. 4: SEM Analysis (a) 800oC (b) 1200oC after sublimation of AlF3

Figure 5. 5: Elemental composition of precursor determined from XRF and ICP-MS in weight %.**Figure 5. 6 (a) Variation of EDS peak intensities (b) Variation of XRD peak intensities with temperature**

Figure 5. 7: Variation of mass loss with gas flow rate at 1300oC after soaking for 2 hrs

Figure 5. 8: Variation of AlF3 XRD intensities normalised to its value at 0.5m/min with gas flow rate

Figure 5. 9: SEM micrographs of product (a) 1.3m/min 10 minutes (b) 1.3 m/min 60 minutes

Figure 5. 10 (a): Variation of AlF3 relative peak intensities with soaking time at 1300oC

Figure 5. 11: Superimposed TG/DTA traces of precursor and premixed with Al

Figure 5. 12: Schematic of (a) Unsintered product and (b) sintered product

Figure 5. 13: Variation of vapour pressure of Ti fluorides and Aluminium fluorides with temperature

Figure 5. 14: TGA-DTA trace of pure AlF3

Figure 5. 15: $t_{1/2}$ **vs. mass loss for varying temperatures**

Figure 5. 16: A plot of natural log of rate constants versus the inverse absolute T/K

Figure 5. 17: Vapour pressure over AlF3 as a function of temperature

Figure 5. 188: Flow sheet for the pyrolysis of the titanium precursor

Figure 5. 19: Flow sheet of the process with the precursor premixed with Aluminium

LIST OF TABLES

Table 2. 1: Physical and chemical properties of pure titanium *[42]*

Table 2. 2: ***Ore production levels of world producers in 1999*** *[40]*

Table 2. 3: ***Composition of several titanium slags***

Table 3. 1: ***Process conditions during determination of optimum soaking temperature***

Table 3. 2: ***Experimental conditions during optimization of inert gas flow rate***

Table 3. 3: ***Reaction conditions during the thermogravimetric analysis of the precursor***

Table 4. 1: ***Comparison of particle size parameters of the precursor and titanium product***

Table 4. 2: ***XRF and ICP-MS scan results for the precursor***

Table 4. 3: ***Mass losses observed under varying gas linear flow rate at 1300oC***

Table 4. 4: ***Linear gas flow rate and the corresponding relative XRD peak intensities (Ii/Io)*** *of AlF3 after reduction of the precursor to Ti with Al and soaking for 2 hours at 1300oC*

Table 4. 5: ***Nitrogen analysis of product after decomposing precursor at 400oC*** *for 2 hours*

Table 4. 6: ***Nitrogen analysis of product after decomposing precursor at 600oC*** *for 2 hours*

Table 4. 7: ***Nitrogen analysis of product after decomposing precursor at 800oC*** *for 2 hours*

Table 4. 8: ***Mass variation of precursor with temperature and soaking time***

Table 4. 9: ***Mass variation with soaking temperature, time and linear flow rate***

Table 4. 9: ***Mass variation with soaking temperature, time and linear flow rate***

Error! Reference source not found.

Table 5. 1: ***lattice parameters of the three complex salts***

Table 5. 2: ***Mass losses and residue composition at various soaking temperatures***

Table 5. 3: ***XRD Peak positions of the product and cp titanium***

Table 5. 4: ***Rate constants in mg/s for various soaking temperatures***

Table 5. 5: ***Composition of precursor and of the titanium product from ICP-MS***

ABBREVIATIONS

XRD: X-ray diffraction

SEM: Scanning Electron Microscope

EDS: Energy Dispersive X-ray spectrum

TGA: Thermogravimetric analyser

DTA: Differential Thermal Analysis

ICP-MS: Inductively Coupled Plasma Mass Spectrometer

ToF-SIMS: Time of Flight Secondary Ion Mass Spectrometer

XRF: X-Ray Fluorescence

Chapter 1: Introduction

The cost of producing titanium has until this day hindered the progress of the usage of the metal compared to other commodity metals present in the market. Although titanium is the fourth most abundant structural metal, at 0.6%, in the earth's crust after iron, magnesium and aluminium, it still remains exotic due to its prohibitive cost [2 and 5]. Furthermore, all the common commodity metals are inferior to titanium in terms of both specific mechanical as well as chemical properties yet this metal has not been fully exploited [1, 2 and 5]. As will be further discussed in Chapter 2, titanium offers unique properties, some of which are exclusive to it, that could help it replace the common metals and alloys like steel and aluminium in many applications [3]. The current commercial method of producing titanium is the Kroll process commercialized by DuPont Germany in 1948[7]. It is an energy and labour intensive batch process with stringent conditions that make it expensive. Therefore researchers all over the world are investigating novel methods of extracting titanium from its ores.

It is arguable that to a large extent the future of engineering lies in engineering materials and our ability to continually develop them to suit our ever changing needs [2and 3]. As will be described in detail in chapter 2, titanium as a metal and in alloy form has a special place in terms of properties required of a metal. The most used metal at present is iron. In fact steel is the second most used engineering material on earth after concrete. However, steels have their inherent weaknesses particularly low specific strength and poor corrosion resistance [4]. Although steels can be processed to achieve extreme levels of

strength and hardness, this is usually done with some addition of weight and cost to the final product due to the alloying elements. These limitations of steel and many other common metals are countered convincingly by titanium and its alloys. The major advantages of titanium are its extremely high specific strength, particularly when alloyed, and exceptional corrosion resistance even at elevated temperature [2 and 3].

Unfortunately to date titanium is not a commodity metal because of its exorbitant cost. Based on the wide geographical distribution and abundance of the metal in the earth's crust, there should be at first sight no justification for such a cost. However, the processing route employed to this day is highly energy and labour intensive making it extremely expensive. Therefore, there is great motivation to find alternative extraction routes. Without new extraction processes for titanium, and hence reduction in production cost, titanium will never have its place as a commodity metal and its exceptional properties will not be taken advantage of especially for civilian applications.

It is interesting and encouraging noting that before the development of the Hall-Heroult process, aluminium was more expensive than gold [7] but now it is one of the cheapest and most readily available metals.

1.1 Project Overview

The project involved full characterisation of a titanium precursor powder followed by the evaluation of a pyrometallurgical process to extract pure titanium from the precursor. The patent on the titanium precursor used in this study describes in detail how the precursor is manufactured and how it should be processed to extract titanium [1]. However, the patent lacks technical data of the relevant metallurgical, thermodynamics and kinetics principles of the process.

The scope of the work included handling and characterisation of a wide range of materiel, evaluating an extractive process and the kinetics as well as application of a wide range of methods in analyzing products of the various stages of processing. The precursor was produced and characterised in order to understand its composition elementally as well as the phase composition. Since the preferred route of extraction was pyrometallurgical, another necessary task was to conduct full thermal analysis of the precursor as well as that of the precursor combined with aluminium in order to observe the thermal behaviour. It is important to note that the precursor is indeed novel as described in the patent [1]. In particular, the salt NH_4TiF_4, which was found out to be one of the phases in the precursor, had never been produced anywhere else before and this made characterisation quite challenging [1].

The main task of the work was to establish if it was possible to process this precursor thermally and then reduce it with aluminium to produce grade 1 titanium. Finally, the titanium powder that was expected to be produced had to be characterised fully and compared to the present grades of commercial titanium, particularly grade 1.

Chapter 2: Literature Review

This chapter covers the basics known about titanium. It encompasses in brief everything from the history of the metal to the most recent advancements made in its applications, processing and alternative routes of extraction.

2.1 The discovery of titanium

Titanium, chemical symbol Ti, was discovered by the British reverend William Gregor in 1791[2]. He isolated black sand from a river in England by removing iron using a magnet, and upon treating this sand with hydrochloric acid he produced an impure oxide of a new element, which he named machanite after its location [2]. The metal was only formed in its pure state more than one and a half centuries later by William Justin Kroll in Luxembourg in 1932 and the process was commercialized almost twenty years later in DuPont Germany [1, 2, 7and8]. He used $TiCl_4$ which he had obtained by carbochlorination of a titanium ore and reduced this to titanium using magnesium as a reductant [1-8]. This is the commercial process used to date and is known as the Kroll process. Titanium is not a rare element but actually the ninth most abundant element and fourth most abundant structural metal in the earth's crust [2, 3and 5]. Unfortunately, it is never found in high concentrations and, due to its high reactivity at high temperature, it is not possible to crystallize in its pure form during its geological formation. The main ore of titanium is ilmenite ($FeTiO_3$) and is named after the Ilmen Mountains of Russia where it was originally found [2]. Another common ore is rutile (TiO_2) from the beach sands of Mexico,

India and Australia. There are other less common ores like Leucoxene and perovskite ($CaTiO_3$) [2-5].

2.2 Chemistry of titanium

Titanium is a group 4 transitional metal with the electronic configuration [Ar] $3d^2$ $4s^2$. Its common chemical and physical properties are listed in table 2.1 below

Table 2. 1: Physical and chemical properties of pure titanium [42]

Molecular weight/ $kgkmol^{-1}$	47.88
Melting point/^oC	1670
Boiling point/^oC	3287
Electronic configuration	$[Ar]3d^24s^2$
Common oxidation states	+2, +3 and **+4**
Crystallographic forms	hcp (c/a=1.587) below 882^oC and bcc above 882^oC
Transition temperature/^oC	882+/-2
Colour	Lustrous white
Specific gravity	4.51
Latent heat of fusion/ KJ/mol	18.8
Atomic radius/ (pm)	147

Titanium has 13 known isotopic forms although of these only five are naturally occurring and these have atomic weights ranging from 46 to 50 [10 and 43]. It is a light metal whose density is about 45% that of mild steel but double that of aluminium. Pure titanium is an allotropic metal which exits in two forms depending on the temperature and pressure to which it is subjected [2, 3, 42 and 43]. Under atmospheric pressure, pure titanium exists with a close packed hexagonal (hcp) crystal structure and this structure undergoes an allotropic transformation to body centered cubic (bcc) around 882^{o}C. Titanium has a high affinity for oxygen even at ambient temperature but quickly passivates in oxidising environments. This property gives titanium its ability to resist corrosion even at elevated temperature. The passivation renders the metal unreactive to a point that the only known acid that can attack titanium is boiling hydrofluoric acid [2 and 4]. Partly this is the reason why titanium and a great number of its alloys are non reactive and non toxic to living tissue and for its use as a biomaterial.

2.2.1 Titanium as a biomaterial

There has been increased use of metals as biomaterials in the past few decades [2 and 6]. The use of metals in biomedicine encompasses a whole range of their properties from the strength they offer in structural prosthesis and even their ability to be in contact with blood in their application as coronary stents for example [2 and 6]. The main requirements for structural prostheses are strength, non toxicity, durability and, increasingly, bioactivity. The requirements when used as stents are high flexibility, high cold deformability and sufficient static and dynamic strength [6]. Titanium and a number of its alloys offer all these property requirements rather very well. In particular, as clinically

required, titanium and a multitude of its alloys offer high axial flexibility, good expansion behaviour, radio opacity and haemocompatibility. Although titanium has found use in these sophisticated bioapplications, the main use of titanium in biomedicine is as a structural prosthesis [2, 5 and 6]. Titanium and a selection of its alloys have excellent compatibility with human tissue and are extremely resistant to corrosion from body fluids. Coupled with their elastic deformability as thin foil, they have become key materials in medical engineering [2, 5 and 6]. Further to this, titanium and its alloys offer an outstanding strength to weight ratio and excellent fatigue behaviour making them the natural choice for orthopedic devices [5 and 6]. The relatively low modulus of elasticity of titanium reduces the difference in stiffness between the human bone and the implant making the implant and the natural bone compatible [5]. The other major advantage of using titanium as a biomaterial is its paramagnetism [2]. Titanium is nonmagnetic and this allows surgery in the presence of the magnetic field of nuclear spin tomography apparatus. Secondly, paramagnetism of the metal eliminates the risk of damage to small and sensitive implanted electronic devices [2, 5 and 26]. Another important application of titanium in biomedicine is as a dental implant. Its major advantage is that, unlike gold-based alloys, titanium comes as a pure element thus avoiding chemiophysical reactions in the mouth and excludes the danger of metal allergy while providing the strength and hardness necessary for the high forces encountered during mastication [2, 5, and 6]. The biocompatibility of titanium is due to its high affinity for oxygen. Titanium forms a tenacious layer of oxide film which creates this neutrality. Added to this, the dielectric constant of titanium oxides is similar to that of water hence titanium dental implants are

neutral in taste. Finally, titanium is the only dental metal that can easily be x-rayed making a proper diagnosis possible without removing crowns or bridges [5 and 6].

2.3 Metallurgy of titanium

This section discusses those aspects of titanium with a bearing on how it is extracted from its ores and processed to the final usable product.

2.3.1 Common ores of titanium

Titanium deposits are enormous with today's estimates assuming a worldwide reserve of 650 billion metric tones of titanium oxide. Deposits suitable for mining are found in South Africa at Namaka and Richards Bay, Australia, Canada, Norway and Ukraine [5]. The two main ores considered for use are ilmenite and rutile and although these are the minerals available for economic mining, TiO_2 is part of almost all minerals, sands and rock [5]. The ores are usually precleaned and enriched on site. Ilmenite, which is relatively inexpensive, is usually smelted resulting in a titan ferrous slag which is usually enriched to a point where its composition is comparable to that of rutile [2 and 23]. In South Africa this ilmenite enrichment process is done by Richards Bay Minerals [5]. The global distribution of titanium ores is shown in the pie chart in figure 2.1

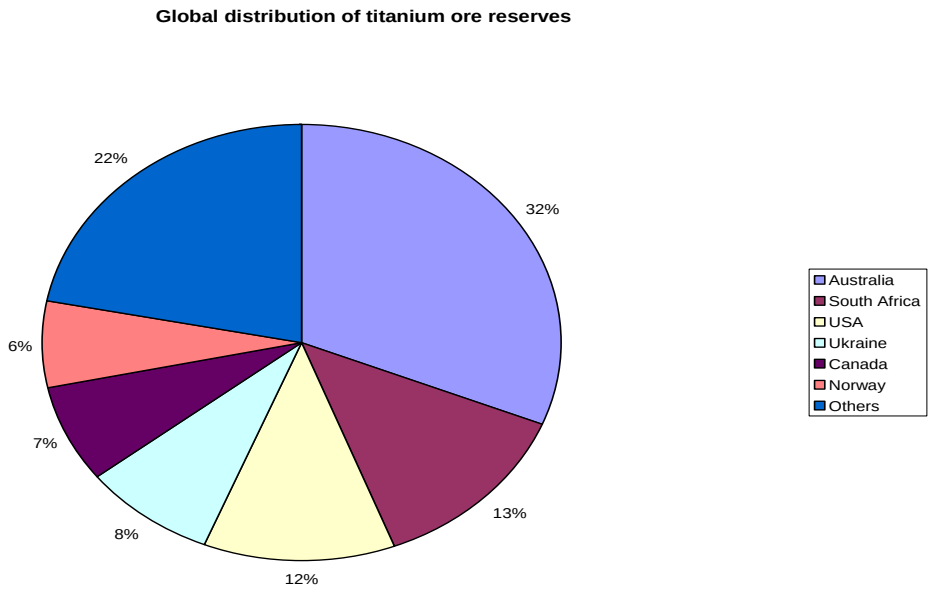


Figure 2. 1: **Distribution of the most abundant titanium ore reserves in the world** [5]

The production levels of titanium ores by various world producers are also shown in table 2.2.

Table 2. 2*: Ore production levels of world producers in 1999* [40]

Producer	Thousands of tons	% of total
Australia	1291	30.6
South Africa	850	20.1
Canada	767	18.2
Norway	382.9	9.1
Ukraine	357	8.5
Other countries	573.1	13.6
Total world	4221	100.1

Table 2. 3: ***Composition of several titanium slags***

Country	Producer	TiO_2	Fe_2O_3	SiO_2	MnO	MgO	CaO
Australia	BHP	96.5	0.8	0.9		0.14	0.06
South Africa	Richards Bay	95.0	-	1.4	0.03	0.05	0.05
USA	Cable Sands	95.5	0.8	0.6	0.50	0.03	0.04

It is clear from table 2.3 that after enrichment the concentrates can be quite high in the desired mineral, TiO_2. The gangue materiel, SiO_2, MgO, MnO and CaO, is similar to the gangue encountered in other ores, e.g. iron ores. There has been extensive research on the separation processes applicable to this type of gangue and a number of these are successful commercial processes today [5 and 23]. It is important to note that a number of these processes are applicable to titanium ores as well, and, as a result, separation processes ranging from simple magnetic separation for magnetic gangue to suppression of gangue during froth flotation are used in the enrichment of titanium ores [23].

2.3.2 Metallurgical extraction of titanium from its concentrates

A number of extraction techniques have been tried with the most cited being pyrometallurgical and hydrometallurgical [5]. To date the commercial method for producing titanium is the Kroll process. It is a complex batch pyrometallurgical process involving chlorination of titanium ores to form $TiCl_4$, also known as "tickle" [7], as an intermediate. The intermediate $TiCl_4$ is then reduced with magnesium, or sodium in the

Hunter process, to form titanium sponge and magnesium chloride ($MgCl_2$) or NaCl [1-12]. The sponge forms on the walls of the reactor and thus the process is not continuous as the accretions have to be physically removed from the reactor walls before further processing [2, 3, 8 and 9]. Figure 2.2 shows the flow diagram of the production of titanium from ilmenite or rutile by the Kroll or the Hunter process.

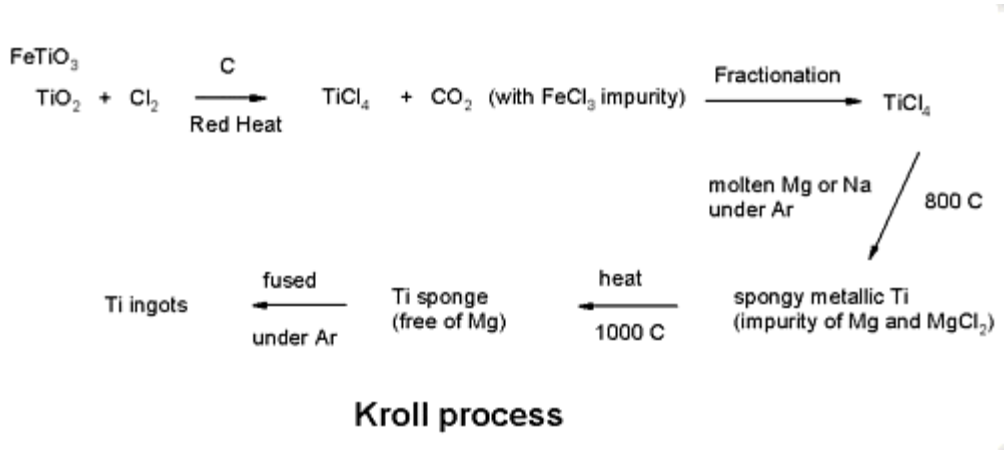


Figure 2. 2: Flowchart for titanium production by the Kroll or Hunter process [44].

The only difference between the Kroll and the Hunter process is that in the Hunter process sodium is used as the reductant instead of magnesium. The Hunter process is less favoured because of the difficulties associated with handling of sodium and excessive enthalpy associated with the reduction [8 and 44].

The processes shown in Figure 2.2 are individually described below including the chemistry involved. The Kroll process first involves the carbochlorination of titanium oxides to produce an oxygen-free tetrachloride (tickle) [1, 3, 5-8 and 44]. This is done in a fluidized bed at about 1300K as described by eqn (2.1) below

$TiO_2 + 2Cl_2 + C \rightarrow TiCl_4 + CO_2$ eqn (2.1)

The titanium tetrachloride is then distilled at 400K to rid it of any remaining impurities before further processing can be done. The purified tetrachloride is subsequently slowly fed into a large steel retort containing pure liquid magnesium at a temperature of between 1073 and 1173K. The feeding is slow as the reaction is highly exothermic [2 and 8]. There is thus need to continuously cool the steel retort as the reduction of the tetrachloride progresses. The rate determining process during the reduction is the extraction of heat from the retort and, as this is slow, the reduction period is generally long, as long as five days in some cases [40]. The reduction of $TiCl_4$ is represented by equation 2.2 below

$TiCl_4 + 2Mg \rightarrow Ti + 2MgCl_2$ eqn (2.2)

The titanium is formed as a sponge and usually sticks to the walls of the steel retort making continuity of the process virtually impossible. The sponge is then pressed or jack hammered out of the retort and is crushed. Thereafter, the crushed titanium is alloyed and can either be consolidated into a welded electrode for vacuum arc remelting (VAR) or fed directly in to an electron beam cold hearth melting furnace (EBCHM) [5, 40 and 44]. The cast product from either of these processes then undergoes extensive thermomechanical processes to acquire the final product shape, size and microstructure [2 and 5].

Whatever the process currently in use or being tried, the final starting material during the production of titanium is rutile (TiO_2). The rutile is then combined with petroleum coke and subsequently chlorinated in a fluidized bed reactor at about 1300K to produce $TiCl_4$ as earlier mentioned. Less expensive materials can be ilmenite or titanferrous slag but this is always at the expense of purity as this materiel contains substantial amounts of

iron and other impurities [1-8]. Titanium producers either purchase pure $TiCl_4$ from pigment manufactures or they produce their own [7]. In the Kroll process about 90% of $TiCl_4$ is oxidised back to TiO_2 for the pigment industry. Gerdemann [7] claims that $TiCl_4$ is the starting point for all commercial titanium processes and most proposed new routes because of its high purity and also that titanium is separated from oxygen. Gerdemann [7] further claims that any new process that proposes to eliminate the chlorination step will have to find a way to replace these functions mentioned above [7]. To this day very minimal changes have taken place from the Kroll process that DuPont developed to produce titanium in 1948 [7]. Since then and until now the Kroll process involves pumping down and filling a stainless steel retort with argon and then pushing in enough magnesium plus 15-30% excess to reduce the $TiCl_4$. The retort is heated to between 800 and 900^oC and $TiCl_4$ is slowly pumped in (due to the highly exothermic nature of the reaction) to the retort for reduction. As mentioned before and according to eqn (2.2), the reduction produces titanium sponge and $MgCl_2$ as a byproduct. $MgCl_2$ is periodically tapped off as the reduction proceeds and after several days, depending on the size of the retort, the reaction stops and the retort pressure rises. At this point approximately 30% of the initial magnesium charge is still unreacted while the titanium formed is a porous mass that resembles a sponge [7]. At this stage the retort contains a mixture of titanium sponge, magnesium and magnesium chloride and these impurities may be removed by either vacuum distillation or leaching. Vacuum distillation removes unreacted magnesium and magnesium chloride, which are both volatile, leaving behind the titanium sponge. The retort is then opened and the sponge is pressed or jack hammered out [2, 5, and 7]. This is followed by shearing the titanium into rough 6mm chunks and the simultaneous addition

of alloying elements and scrap titanium for charge make up. These blended chunks are then melted to produce an ingot and, to ensure uniformity and to remove inclusions, the ingot is remelted once or twice more. The original melting step adds approximately $1/lb (which is more than double the price of steel) and each subsequent remelt adds another $0.50[5]. The major developments on the Kroll process are quite subtle and only include the enlargement of retorts and that the magnesium reduction and vacuum distillation steps are now carried out in the same reactor [7].

2.3.3 Phase equilibria of titanium alloys

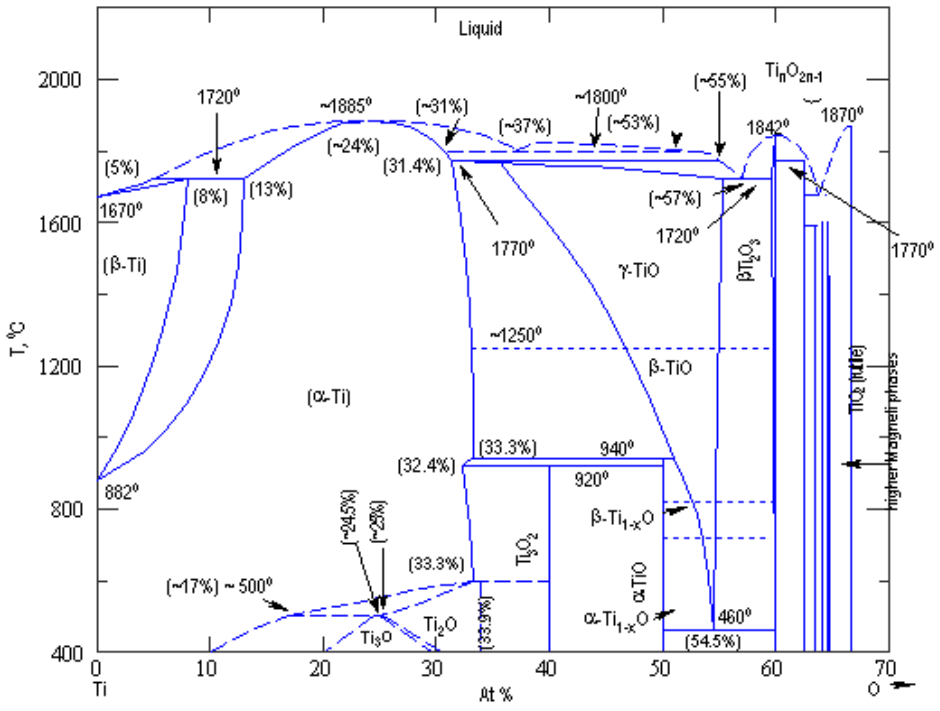


Figure 2. 3: The Ti-O phase diagram [41]

It is evident that oxygen shifts the β transition temperature upwards and hence it is an α stabiliser. The phase diagram shows that α-Ti can solve large amounts of oxygen.

Therefore, for high quality titanium, it is necessary to work in oxygen-free environments and, ideally, under reducing conditions [11].

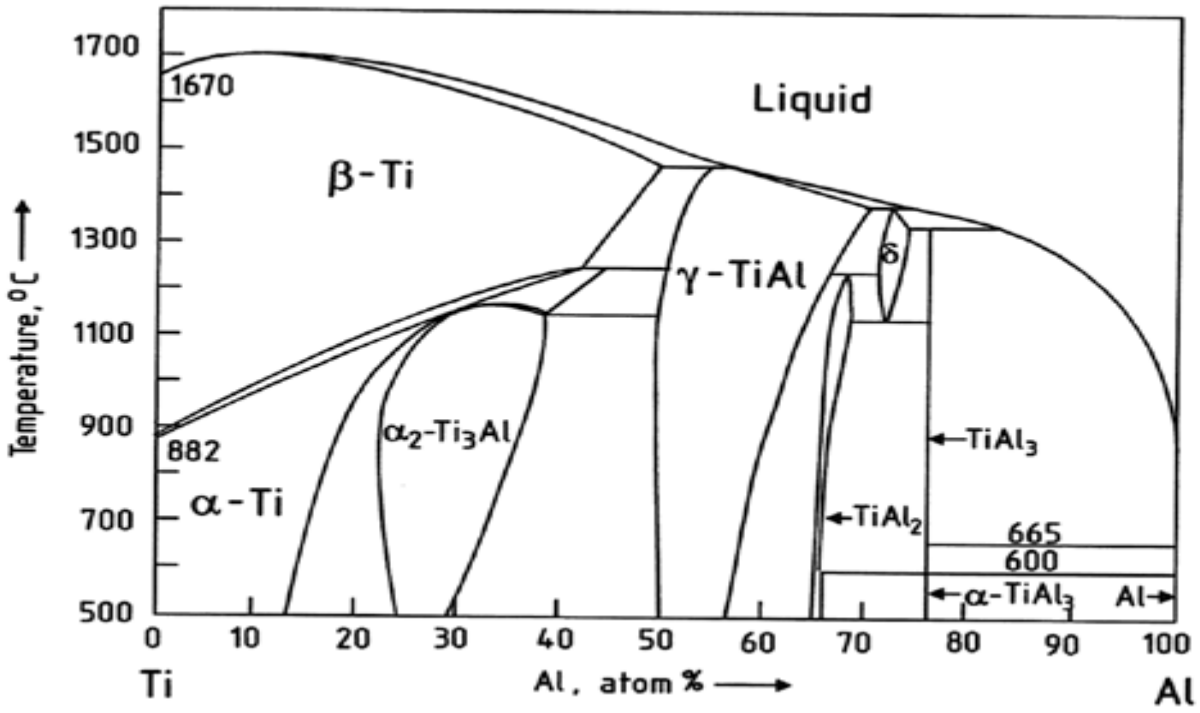


Figure 2. 4: **Phase diagram of the Ti-Al system [41].**

The presence of aluminium shifts the α-β transition temperature to higher temperature regions significantly making aluminium a strong α stabiliser [2 and 42]. Aluminum by virtue of its big atomic size relative to the titanium atom can not interstitially dissolve in titanium but rather forms substitutional alloys [2, 11 and 42]. It, however, forms large areas of solid solutions and most of the intermetallics formed have a large homogeneity area.

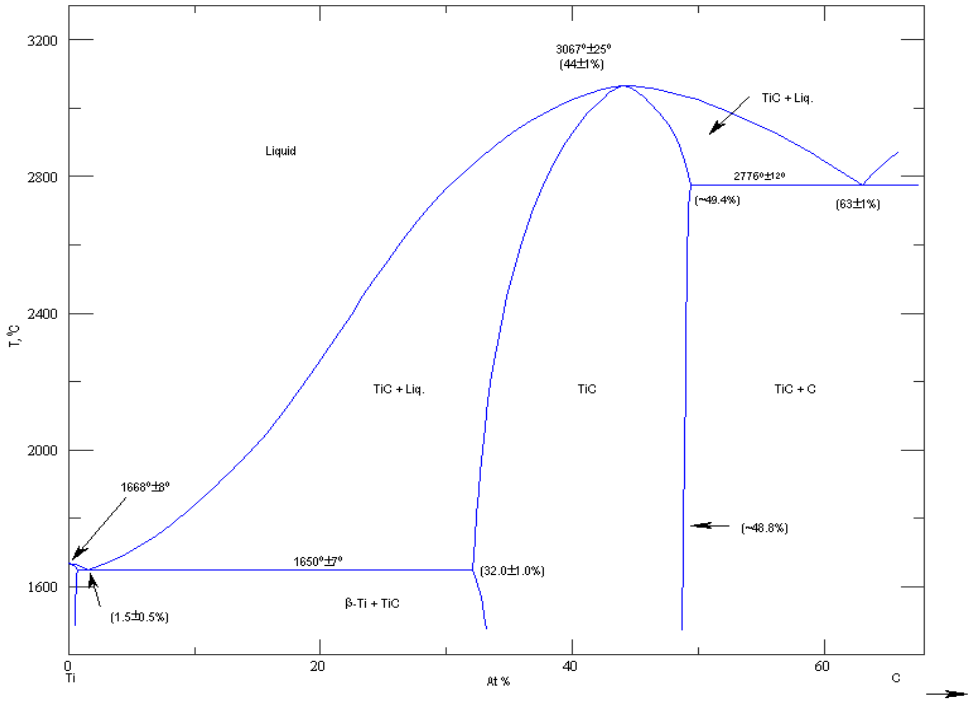


Figure 2. 5: The Ti-C phase diagram [41]

The phase diagram in figure 2.6 above gives an insight as to why it is not feasible to obtain pure titanium by carbothermic reduction of titanium oxides. The reduction of titanium oxides with carbon forms titanium carbide which will not react further with any titanium oxides.

2.3.4 Classification of titanium alloys

As mentioned earlier, pure titanium exists as a hexagonal close packed (hcp) structure at room temperature. This structure is known as the α phase for titanium and such titanium can thus be referred to as α titanium. At 882+/2 ^{o}C the α hcp structure transforms to a body centered cubic structure (bcc) known as the β phase or β titanium. The classification of titanium alloys is based on the effect of the alloying element on the α and β fields on the phase diagrams. It has been observed that any elements with atomic radii in the range of 0.85 to 1.15 to that of titanium alloy substitutionally while elements with radii less 0.59 that of titanium alloy interstitially and generally have a good solubility in titanium [42]. H, N, O, C and B interstitially dissolve in titanium and all exhibit substantial solubility while Al, Cu, Ni and Fe substitutionally alloy with titanium. The alloys are classified according to whether the element stabilizes the α phase to a higher temperature, such elements are called α-stabilizers and the alloys are termed α alloys, or the element stabilizes the β phase to a lower temperature, β-stabilizers and correspondingly β alloys. Al, O, N and Ga are known common α-stabilizers while V, W, Ta and Mo are common β-stabilizers. Cu, Mn, Fe, Ni, Co and H are also β-stabilisers but form the eutectoid [2 and 42]. Some elements like Sn, Zn and Si do not show any effect on the titanium phase diagram and hence are said to be neutral alloying elements. The effect of the elements on the phase regions is shown in figure 2.7 below and it is that consideration which is the basis of titanium alloys' classification.

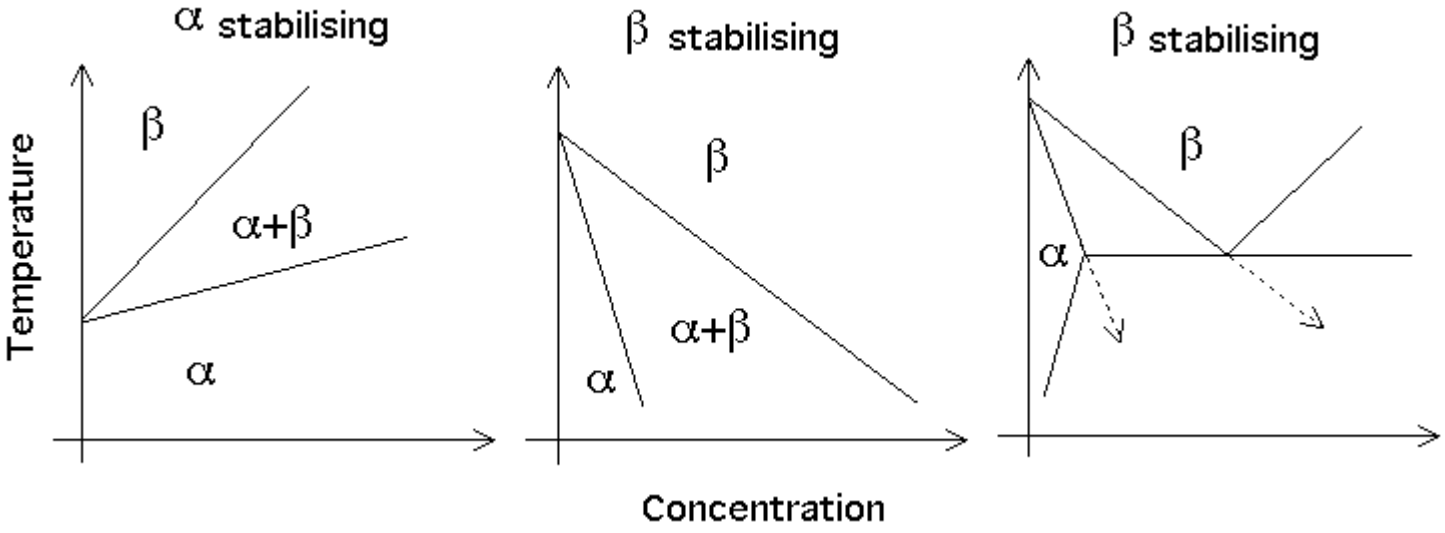


Figure 2. 6: Effect of alloying elements on the phase fields of the constitutional diagram [42]

The fact that all the elements exhibiting interstitial solubility in titanium have substantial solubility makes precipitation-hardening of titanium challenging. Boron is the only common element used in this regard by inducing titanium-boride precipitation [42]. Alpha alloys are easily weldable and are usually based on aluminium and are tough even at cryogenic temperature. The β alloys are ductile and therefore easier to work. Most titanium alloys are made to be between these two extremes by judiciously having both forms of alloying elements so that on solidification some β phase is retained in the final structure [2 and 42]. Such alloys which are formed in the two-phase region are termed $\alpha + \beta$ alloys and depending on whether the composition is closest to α or the β phase region the alloys termed near-α or near-β alloys respectively [2 and11].

2.3.5 Titanium forming processes

This section describes in brief the various processes that titanium sponge undergoes in order to obtain a semi-finished titanium product. The section also includes a discussion of specialized techniques used in the transformation of the wrought metal to specialized engineering materials or components.

When the titanium sponge has been pressed or jack hammered out of the steel retort, it is necessary to process it further in a bid firstly to remove impurities, in the form of magnesium and magnesium chloride predominantly, and then compact the sponge so that it acquires the theoretical density of titanium [5]. In sponge form, even if 100% pure titanium, the metal is unusable for any meaningful purpose particularly as a structural component owing to very low strength, hardness, toughness and basically all other mechanical properties that a structural material should possess[42]. From the sponge, therefore, the first step is to purify the sponge and thereafter once the necessary specifications have been achieved the material can then be subjected to the conventional metal forming techniques such as investment casting, sintering, rolling, drawing et cetera. In fact, the very same methods used in forming steel are applicable to titanium and for reduction of capital costs some companies have adopted exactly the same step ups found in steel forming shops when they developed their own titanium forming shops [2].

Titanium sponge is currently the base material for the production of all titanium based semi finished products as well as for alloying additions to titanium-stabilized specialized steels [2 and 5]. The major contaminants in the sponge are magnesium and magnesium chloride, and multiple remelting in vacuum is necessary to remove them and to obtain the required morphology as well as the final alloy composition [2, 5, 7 and 8]. Volatile

contaminants like chlorides are removed in this way through their sublimation and, depending on the specific melting process, castings, slabs and ingots can be produced with a homogeneity required for further processing [2,4 and 5]. Before melting, the titanium sponge has a density of between 1.2 and 3g/cc. It is predensified in a cold hydraulic press and the compacts are assembled into an electrode for the melting process [5]. Before densifying the sponge would have been mixed with prealloys and/or elements in order to obtain a specific alloy composition. The densified compacts are then welded to an electrode in a plasma-welding chamber up to a maximum weight of 13 tones per electrode [2, 5, 7, 11, 12 and 42]. The schematic of a vacuum arc melter (VAM) is shown in figure 2.7

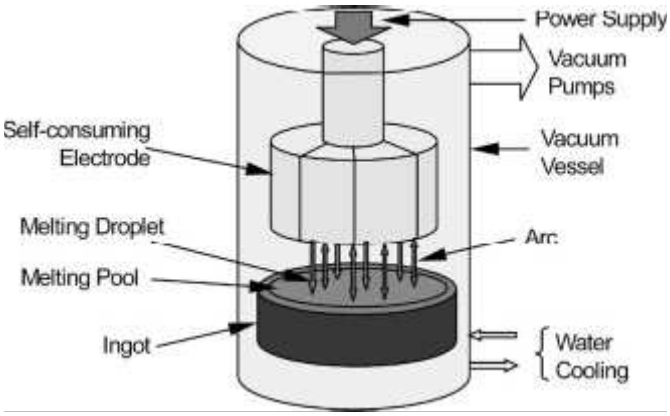


Figure 2. 7: Schematic of a vacuum arc melter (after H.Sibum [5].)

The electrode is then at least double remelted to get rid of almost all volatile contaminants. The need for vacuum is due to the high oxygen affinity of titanium as earlier discussed in this chapter. A full illustration of the processing of titanium sponge to various forms is shown in figure 2.8

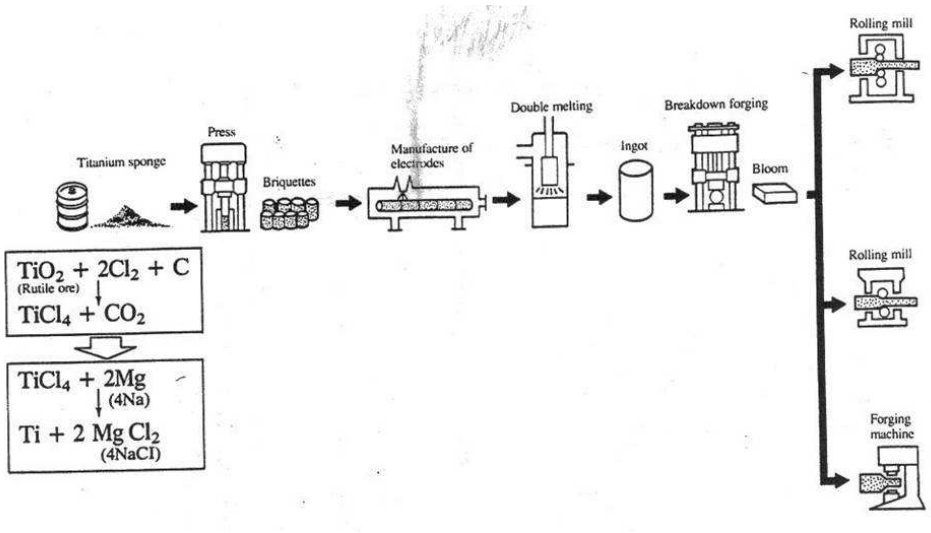


Figure 2. 8: Process flow chart for titanium sponge [40]

Machining of titanium and its alloys is usually avoided due to the wasteful nature and hence high cost of the technique. Near-net techniques like casting and HIPing become obvious options to consider. It is mentioned extensively in literature that all known titanium alloys are castable [1, 2, 5 and 7]. Investment casting is the common casting method employed by most titanium foundries world wide and the principles of the technique are available in detail in literature [2 and 5]. Casting of titanium and its alloys not only offers cost saving advantages but allows the production of highly complex component profiles which otherwise would be impossible with machining. The biggest challenge encountered during the casting of titanium and its alloys is the extreme reactivity of the metal particularly in the molten state. For instance, conventional Al_2O_3-SiO_2 moulds can not be used for titanium casting because molten titanium reacts with these materials. With conventional Al_2O_3-SiO_2 moulds, titanium attacks them dissolving aluminium, silicon as well as the oxygen resulting inevitably in the detriment of the final titanium cast [2 and 5]. Apart from reacting with the mould walls, molten titanium also reacts with oxygen,

nitrogen and carbon monoxide in the ambient air leading to embrittlement or outright formation of titanium compounds like refractory compounds such as carbides and nitrides. So, as a rule, any melting of titanium or its alloys is always carried out either in vacuum or under an inert gas, usually UHP argon [1, 2, 5 and 13]. In the extreme, the use of conventional Al_2O_3-SiO_2 moulds risks breakouts and spilling of titanium in to the furnace. To counter this problem of the inadequacy of conventional Al_2O_3-SiO_2 moulds there are basically three alternatives, which are

(a) refractory metals whose melting points are much higher than the temperature of liquid titanium and with low solubilities in titanium

(b) chill materials with high thermal conductivities such that there is formation of a solid titanium skin on the mould wall thus creating a barrier between the mould and the molten titanium. There is thus a solid-solid reaction between titanium and the mould wall only [2]. This is the same mechanism used in a blast furnace hearth, wherein carbon brick is used for thermal solution, and

(c) Ceramics which have higher melting points than titanium and whose enthalpies of oxide formation are much higher than that of Ti_xO_y like Y_2O_3 [2].

Again, as a rule of thumb, the more complex the shapes are the more economical it will be to design them as cast parts. It is important, however, to note that in almost all cases mould wall-titanium reactions do take place forming an α case on the surface of the titanium cast usually with a thickness of a few tenths of a millimeter [3]. This α case is subsequently removed by pickling, also known as chemical milling, using a solution of nitric and hydrofluoric acids as will be discussed later in section 2.3.6.2 of this chapter [2 and 4]. As with any other investment casting operation, the normal practices of gating et

cetera are necessary for titanium castings. However, unlike most cast metals, defects like cavities during solidification of titanium casts can not be prevented by improved gating [2]. One common way of countering this problem is to sinter any cast titanium parts under pressure. This is a necessary condition for all aerospace titanium parts wherein the smallest imperfections could act as stress initiation points. For titanium and its alloys, hot isostatic pressing (HIPing) is used to densify casts, and even powder, to remove casting defects and produce components with similar properties as the wrought counterparts. Hot isostatic pressing of titanium typically uses 1000 bar pressure of an inert atmosphere at about 900^{o}C [2]. In the case of sintering precast parts, these conditions of temperature and pressure are sufficient to close any macro or micro cavities. The walls of the former cavities in the cast join and completely diffusion weld together. Under these conditions the material can creep without adversely affecting macroscopic dimensional stability [2 and 40]. A strict requirement to achieve successful sintering of titanium is the purity of the metal.

2.4 Alternative extraction routes

The inadequacies of the Kroll process have brought about great impetus on researchers all over the world to find new ways to extract titanium from its ores. The two major weaknesses of the current commercial process, as described in chapter 2, are the high production cost and the handling of the extremely hazardous intermediate salt, $TiCl_4$. It has become difficult, if not impossible, particularly in developed countries to obtain a practicing license for a Kroll process plant because of the hazards associated with $TiCl_4$[19]. Greener processes have been, and are still being, sought. The need to move

away from the labour and energy intensive process to a continuous low cost one has become even more pressing because of rising energy and labour costs.

This section reviews efforts made and still underway to find alternative extraction routes of titanium from its ores. The Kroll process is already highly advanced and optimized and any further improvements are likely to be heat extraction from the steel retort by improved design and maybe improving the efficiency of $MgCl_2$ electrolysis [1, 2 and 5]. However, these changes will only be evolutionary and will not result in significant cuts in the production cost of titanium [2]. To achieve the production costs and, as a result, volumes associated with commodity metals, a step change in the extractive metallurgy process is required [1, 2 and 5]. To add to this, the elimination of or minimizing of downstream multiple melting and remelting operations and possibly ingot homogenization stages could result in significant cuts in the production cost of pure titanium, titanium alloys and components. Equally importantly and both for economy and the environment, any new developments should strive to bypass the production of the $TiCl_4$ intermediate salt. Firstly, $TiCl_4$ is classified as in the top ten most hazardous materials and is listed as a “highly toxic” chemical in various pieces of international legislation on major hazards [19]. Secondly, there is need for ultra purity resulting in the distillation stage which adds to the final production cost. Therefore foregoing the carbochlorination step would not only contribute to reducing cost but would eliminate the environmental hazards associated with tickle [2, 7 and 19]. The next subsections describe in detail the known methods being tried or that have been tried or developed to date as alternative processes for the production of titanium.

2.4.1. The ITP/ Armstrong Process

The process is a continuous version of the Hunter process [3, 5, and 7]. The process still involves the reduction of $TiCl_4$ with sodium except that it is continuous. The continuity of the process obviously suggests an improvement over the Hunter or even the Kroll process but the process is still not environmentally friendly. It was developed by International Titanium Powder (ITP) Company in Chicago.

$TiCl_4$ vapour is reacted with molten sodium, which sodium will be in excess of the stoichiometric requirement. The purpose of the excess sodium is to cool the reaction products and carry them to a separation unit where excess sodium and salt are removed [2]. The reaction product is a continuous stream and, with little modification, it is possible make vanadium and aluminium titanium alloys. The process has managed to produce titanium with lower than 0.2wt% oxygen which makes it comparable to grade 2 titanium. The major disadvantages of the process are that it still uses $TiCl_4$ and involves the use of sodium which is a reactive metal that is difficult to handle. The use of $TiCl_4$ makes the prospects of a drastic cost reduction very slim. There are, however, advantages associated with the process. For a start it is a continuous and low temperature process and this has a significant bearing on both capital and labour costs. Secondly, no further rigorous purification of the formed titanium powder is necessary compared to titanium sponge. Another interesting aspect of the process is that the titanium powder product is directly amenable to all powder metallurgy (PM) forming methods and PM methods by their nature are usually cheaper than other traditional metal forming techniques [15].

2.4.2 Electrolytic processes

In 1953 Kroll is said to have predicted that an electrolytic route would produce titanium in 15 years yet up to now, almost 60 years later, there is no commercial electrolytic process that has been developed [5, 7 and 9]. Electrolytic processes by their nature are usually cheaper than their pyrometallurgical counterparts. Before the introduction of Hall-Heroult process, aluminium was produced by reduction of its oxides with sodium. Aluminum was more expensive than gold yet it now costs less that $1/lb [7]. An electrolytic reduction process for titanium would have to deal with a molten bath just like alumina and cryolite but the biggest problem is that titanium's melting point is 1000^{o}C higher than that of aluminium[3,7and 40]. This high melting point results in the production of solid titanium that results in dendritic structures and loss of catholyte due to drag out. Compared to aluminium which has only one valance state in its molten form, titanium can exhibit a multiplicity of these. The multiplicity in valence states results in serious losses in current efficiency due to redox recycling as shown below

$$Ti^{4+} + 2\bar{e} \rightarrow Ti^{2+} \qquad \text{eqn (2.10)} \quad \text{Cathode}$$

$$Ti^{2+} \rightarrow Ti^{4+} + 2\bar{e} \qquad \text{eqn (2.11)} \quad \text{Anode}$$

The two reactions shown above become a reversible reaction which consumes energy without the actual deposition of titanium. The biggest problem with electrolytic processes is that all of them begin with the hazardous $TiCl_4$ salt, which is quite expensive at about $1.45/ lb Ti just like in the Kroll process. The company Dow-Howmet, RMI, has built a pilot plant and has not reported any significant savings compared to the Kroll process [7].

There has been a lot of research on electrolytic reduction of titanium but so far there has not been any commercial plant commissioned. Where commercial plants have been built they have all been abandoned at one point or the other usually after spending a significant amount of money [7]. The remainder of this section is devoted to two processes that have been developed to electrolytically produce titanium from its ores.

2.4.2.1 The Fray-Farthing-Chen (FFC) Cambridge process

This process was developed by Derek Fray of Cambridge [7 and 9]. In this process TiO_2 is pressed into pellets to make a cathode in a calcium chloride bath at 950^oC while a graphite electrode is used as the anode. Upon application of a current, oxygen is ionized and dissolves in $CaCl_2$ bath [7, 9]. Effectively, the TiO_2 is deoxidized since oxygen is removed into solution. The FFC process and many other such processes are referred to as electrochemical reduction processes. A schematic of the electrolytic cell is shown in Figure 2.9

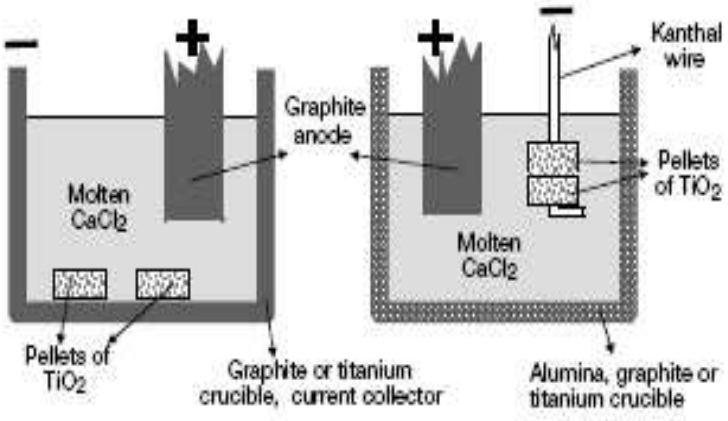


Figure 2. 9: Schematic of the FFC electrolytic cell

2.4.2.2 The Preform Reduction process (PRP)

Another recent development in alternative methods of producing titanium is the preform reduction process (PRP). Okabe *et al* [13] report that they managed to produce ultrapure titanium powder through the calciothermic reduction of a preform containing TiO_2 [13]. The feed preform was fabricated from slurry which was made by mixing TiO_2 powder, flux e.g. $CaCl_2$ and a binder. Conventional techniques were used to prepare various forms of the preforms such as spheres, and tubes. Before reduction, the preforms are sintered at 1073K in order to remove the binder and water. The sintered solid TiO_2 is then placed into a stainless steel container wherein it is reacted with calcium at a constant temperature ranging from 1073 to 1273K for 6 hours. Titanium powder is then recovered by leaching the reduction product with acid. Okabe *et al* [13] claim that the method produces pure titanium powder with a purity of above 99wt%. The overall reaction is for the process is

$TiO_2 + 2Ca \rightarrow Ti + 2CaO$ eqn (2.12)

The calciothermic reduction of titanium is a huge exothermic reaction and in general it is difficult to achieve a homogeneous reaction unless calcium vapour is used [13]. There are two reduction reactions that take place in the electrolytic cell. Firstly, there is oxygen ionization leading to the reduction of Ti^{2x+} to $Ti^{2(x-n)+}$ as the primary reduction reaction. The O^{2-} ions then combine with free Ca^{2+} ions in the molten bath to form CaO. The second reduction on the other cathode is that of Ca^{2+} to Ca atoms. The reductions reactions are shown below

$TiO_x + 2n\bar{e} \rightarrow TiO_{x-n} + nO^{2-}$ eqn (2.13). Cathode

$nO^{2-} + nCa^{2+} \rightarrow nCaO$ eqn (2.14), then

$nCa^{2+} + 2n\bar{e} \rightarrow nCa$ eqn (2.15) Cathode

$TiO_x + nCa \rightarrow TiO_{x-n} + nCaO$ eqn (2.16)

Reactions 2.13 and 2.15 occur on the cathode and are real electrochemical reactions. Reactions 2.14 and 2.16 occur in the melt using products of reactions 2.13 and 2.15. The secondary reduction is referred to as calciothermic reduction just because calcium is used as the reductant. The anodic reduction produces CO and CO_2 which escape as gases. The operational voltage for this process is between 2.8 and 2.5V while the TiO_2 feedstock can either be in the form of a pellet or is bagged as a powder [13]. The choice of using $CaCl_2$ is based on the low melting point of the salt (1055K), high solubility of oxygen in the salt as well as its low cost. Although the method still uses a chloride, it has the advantage of eliminating the expensive and hazardous $TiCl_4$ and since the route starts with rutile ($0.48/lb Ti) it appears the route could lower the production cost of titanium [7]. However, rutile is not pure TiO_2 and therefore something should be done to achieve the purification done by carbochlorination if titanium of ultrahigh purity is to be produced by the PRP method. The other disadvantage is that the process produces CaO (eqn 2.14 and 2.16) that later precipitates in the pellet pores at the cathode and CaO also reacts with TiO_2 to form $CaTiO_3$. The precipitation of CaO in the cathode pores and the formation of $CaTiO_3$ lead to a significant decrease in current efficiency as the reduction progresses. The diffusion of oxygen from the cathode into the molten bath becomes more difficult as TiO_2 is transformed into solid titanium due to a longer and restricted diffusion path [13]. The slow diffusion of oxygen in metallic titanium at these reaction temperatures leads to a long reduction time for the reduction to go to completion. Elemental calcium also reacts

with the graphite anodes leading to contamination of the electrolyte and the titanium cathodes with carbon [13].

2.4.2.3 The Process by Pretorius et al.

Pretorius [1] managed to produce a novel titanium powder processing route and the work was patented in 2005. The patent claims that the novel precursor can be processed to produce titanium in an inexpensive and efficient manner. According to the invention, the process commences with producing a solution of M"TiF_6 from a titanium ore or any other titanium-containing material for that matter. Where M" is a cation from the type that forms a hexafluotitanate e.g.Fe^{2+}, Mn^{2+}, Cu^{2+}, Ni^{2+} and so on. This is followed by precipitating M'$_2TiF_6$ from that solution by the addition of M_aX_b where M' is selected from the ammonium and alkali metal cations while X is an anion from the halide, nitrite, nitrate or acetate group [1].

The powder that was finally produced was through the digestion of ilmenite with aqueous hydrofluoric acid meaning then that $X=F^-$ $M'=H^+$, $M"=Fe^{2+}$ and a=b=1. Excess ilmenite was used and the concentration of HF (aq) was maintained between 20 and 24wt%. The method also included a step of adding a reducing agent to the digested

solution to reduce any Fe^{3+} in the solution to Fe^{2+}.

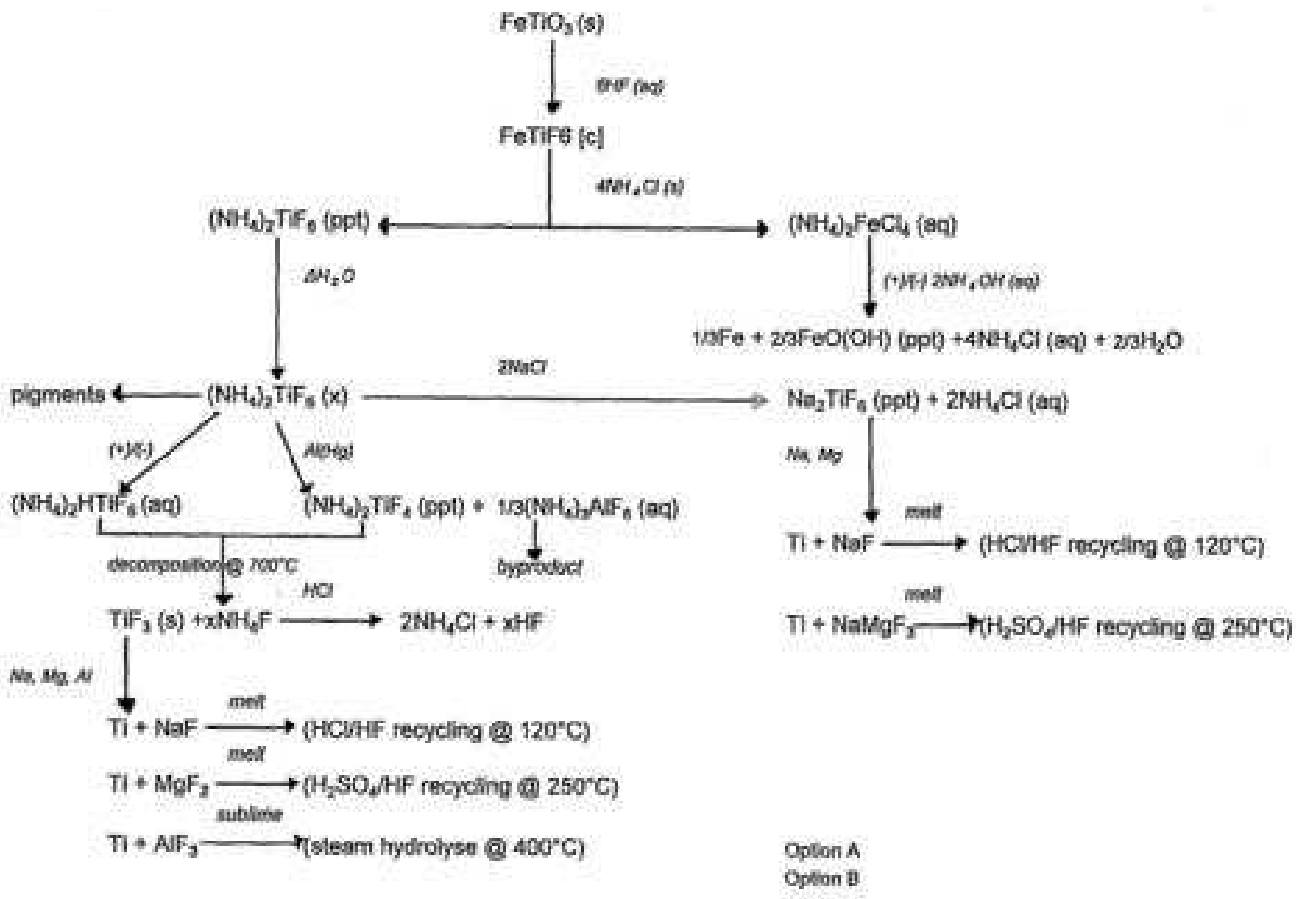


Figure 2. 10: Flowchart of the Process [1].

Considering the flow chart stage by stage, the following key points should be clear. In step 1 the digestion of ilmenite with HF (aq) does not just form the complex double salt ($FeTiF_6$). It also has the advantage of removing oxygen from the ilmenite forming water in the process. The digestion reaction is shown in eqn (2.17)

$$FeTiO_3 + 6HF \rightarrow FeTiF_6 + 3H_2O \qquad \text{eqn (2.17)}$$

The second stage involves the addition of NH_4Cl powder to the digested solution. The necessity of this stage is the ability of NH_4Cl to precipitate a complex salt containing all

the titanium while simultaneously leaving all the iron as an aqueous complex salt. So, apart from being a simple complexation reaction, this stage is also a separation and beneficiation stage too as shown in eqn (2.18)

$FeTiF_{6(s)} + 4NH_4Cl_{(s)} \rightarrow (NH_4)_2TiF_{6\ (ppt)} + (NH_4)_2FeCl_{4\ (aq)}$ eqn (2.18)

The products can thus be separated in to two distinct streams by filtration. The NH_4Cl can be regenerated by adding a quantitative equivalent of aqueous NH_4OH as shown in eqn (2.19)

$(NH_4)_2FeCl_4 + 2NH_4OH \rightarrow 1/3Fe + 2/3\ FeO\ (OH) + 4\ NH_4Cl + 3/2\ H_2O$ eqn (2.19)

The Fe produced in this regeneration step can be added to the digested solution to reduce Fe^{3+} to Fe^{2+} as shown in eqn (2.20)

$2Fe^{3+} + Fe \rightarrow 3Fe^{2+}$ eqn (2.20)

The NH_4Cl can be recycled to the process while the other products can be discarded or put to other uses elsewhere. The product of interest is ammonium hexafluorotitanate and is further processed by reducing it with mercury-activated aluminium to result with a complex salt wherein the oxidation state of titanium is +3 [1]. The reaction is shown in eqn (2.21) below

$(NH_4)_2TiF_6 + Al\ (Hg) \rightarrow NH_4TiF_4 + 1/3\ (NH_4)\ AlF_6$ eqn (2.21)

Pretorius [1] further argue that any of the ammonium flouro complexes of titanium formed in the process can be decomposed to TiF_3 between 400 and 700^oC in an inert atmosphere. Finally, the patent postulates that many common reductants can then be used to reduce this TiF_3 to titanium and the fluoride salt of the reductant as shown in eqn (2.22) below

$TiF_3 + M \rightarrow Ti + MF_3$ eqn (2.22),

Wherein M is the reductant and can be an alkali metal or aluminium. The titanium product can then be separated from the fluoride by melting while in the case of aluminium as a reductant, the AlF_3 sublimes off at around 1200^oC leaving behind pure titanium [1]. The patent further posits that a variety of titanium alloys can be made *in situ* by simply introducing an appropriate salt containing the desired alloying element(s) prior to the final reduction step so that the final product is a titanium alloy contain at least one other metal. For example, Pretorius [1] argues that the addition of a predetermined combination of Na_3AlF_6 and Na_2VF_7 can result in the formation of grade 5 titanium (i.e. Ti-6Al-4V). Of the possible reductants of TiF_3, this author shall limit the discussion to aluminium not only because it is the cheapest but also because aluminium fluoride sublimes at a relatively low temperature (1260^oC, 1 atm). The conclusion derived from this fact is that the need to melt and then separate the titanium from the byproduct fluoride salt is eliminated. Secondly, the patent claims that the final product mixture can be heated at a temperature and for a time that are sufficient to sublime off most of the AlF_3 but allow for its sufficient retention on the surface of the product to reduce the reactivity of the final titanium powder [1].

Chapter 3: Experimental Procedure

The work started with producing a titanium precursor powder according to the patented method. The precursor was characterised to determine its chemistry, physical and thermal properties. Chemical characterisation of the precursor was done using a scanning electron microscope (SEM) coupled with an energy dispersive x-ray spectrometer (EDX) to determine the elemental composition and the morphology of the precursor. Owing to the lower resolution of the SEM/EDX relative to X-ray Fluorescence (XRF), elements in quantities lower than 0.01% were determined using XRF and an inductively coupled plasma mass spectrometer (ICP-MS). X-ray diffraction (XRD) was used to identify the phases present in the precursor. The make up of the precursor being known, the thermal decomposition profile was determined using a thermogravimetric analyser (TGA) coupled to a differential thermal analyser (DTA). The aim was to establish the temperatures at which various reactions took place and then make logical deductions as to the nature of the reactions at those established temperatures. This information was important for the planning of the real experiments with reasonably sized samples in a tube furnace. The temperature profile from the TG/ DTA was used to mark the various temperatures and soaking periods that were used in the step by step processing of the precursor in a tube furnace. All samples from every stage of processing of the precursor in the tube furnace were fully characterised using all the techniques earlier mentioned. This was important as it allowed to substantiate or dismiss theoretical expectations as well as to have a full understanding of the reactions that take place in the previously established temperature regime.

In all the experiments, save for the later stages when all parameters had been established, there was only one degree of freedom. A single variable was investigated and optimized while holding all other variables constant. These variables were temperature (T), soaking time (t), gas linear flow rate (v) and the amount of the reductant (%Al). This stringent condition of one degree of freedom was relaxed later as a better understanding of the behaviour of the precursor became apparent. The final experimental work involved varying more than one variable at once to observe the synergistic effects of such and compare to theoretical expectations. The kinetics of precursor thermal decomposition were determined using thermogravimetric graphs, and this information was helpful in determining the heating rates and soaking times necessary to achieve the product composition required.

The remaining sections of this chapter describe in detail the various experiments that were carried out and the justifications of so doing. The description is in chronological order beginning with the first and ending with the last. Exceptions will be highlighted and justified.

3.1 Characterisation of the titanium precursor

The starting material for all the work that was done was a powder processed from ilmenite according to the patent. The powder had been prepared according to the patent of Pretorius [1] as briefly described in chapter 2 of this thesis. The first step was to determine the physical and chemical properties of the titanium precursor. This involved the particle size distribution and particle shape, elemental composition, phase

composition, impurity content and decomposition thermal profile as the important chemical and metallurgical properties.

3.1.1 Precursor particle size distribution

Particle size distribution was determined using a Malvern Master 2000 Particle size analyser. The equipment utilizes Fraunhofer diffraction of light formed by particles with a diameter larger than the incident laser beam wavelength [46]. The d_{10}, d_{50} and d_{90} values were determined while only the d_{50} values were used to describe the average size of the powder particles. The same analytical technique was used to characterise the particle size distribution of the final product.

3.1.2 Determination of the chemical composition of the precursor

The determination of the chemical make up of the precursor involved the use of three analytical techniques. First, 3 samples were extracted from the precursor after coning and quartering. The coning and quartering technique was important in making the samples representative portions of the precursor. A Mettler Toledo digital scale with a sensitivity of 0.01g was then used to weigh 50.00g for the sample that was used for X-ray Fluorescence (XRF) and ICP-MS and 5.00g for the sample that was analysed with a scanning electron microscope and energy dispersive X-ray spectrometer (SEM/EDX). The third sample was not necessary to weigh as it had to be analysed with an X –ray powder diffraction apparatus (XRD).

3.1.2.1 Scanning Electron Microscopy and Energy Dispersive X-ray spectrometry (SEM/EDX)

The precursor was anaysed using a LEO 1525 FE-SEM Scanning Electron Microscope (SEM) coupled with an Oxford link Pentafet Energy Dispersive X-ray (EDS) spectrometer in the SE2 secondary mode to determine elemental compositions as well as the morphologies of the precursor as received. The machine was set at a voltage of 10KV and magnifications 200x to 10kx. The resolution of the EDX was high and only elements with concentrations lower than 0.01% could not be detected by this technique. Light elements like hydrogen and lithium can not be detected using EDX.

3.1.4.2 X-ray Fluorescence (XRF) Spectrometer

This was necessitated by the need to quantitatively determine the elemental composition of the precursor since the EDS scan was only comparative. A Phillips PW1606 XRF spectrometer at Mintek laboratories in South Africa was used for this purpose.

3.1.4.3 Inductively Coupled Plasma Mass Spectrometer (ICP-MS)

An inductively coupled plasma mass spectrometer (ICP-MS) at the University of the Witwatersrand was used to quantitatively determine the elemental composition of the precursor. Its use was necessitated by the need to determine all other elements that the techniques mentioned above could not detect. In particular it was the only technique that could determine the amount of hydrogen in the samples. 1.00g of precursor was digested with 20% nitric acid and diluted with 20.00ml of water to lower elemental concentration to the specifications of the machine. The digested liquid was then passed through a

nebulizer wherein it was converted into small droplets of aerosol so that it could be ionized. The spectrometer could determine elements whose concentrations were in the order of 1 in 10^{12}. A dilution factor of 250 was used and the same figure was used in converting the spectrometer reading to the final composition figures.

3.1.4.3 X-ray diffraction (XRD) analysis

The precursor powder was then analysed with a Phillips X-ray diffraction machine PW1710 set at a voltage of 40KV, a current of 20mA, from 10 to 80^{o} 2theta with a step size of 0.02 2theta degrees. The JCPSD database (Xpert High Score) was used for phase identification.

3.2 Thermal analysis: Thermogravimetric and thermal differential analyser (TGA-DTA) and Differential Scanning Calorimeter (TGA-DSC)

The patent [1] on the precursor claims that the processing route to make titanium from the precursor involves thermal decomposition of the precursor but it does not specify exactly the temperature and conditions required. The thermal decomposition behaviour of the precursor was established by tracing mass and heat changes using a Setaram TG92 thermogravimetric analyser (TGA) coupled to a Setaram differential thermal analyser (DTA). The machine is of the bottom loading type with furnace gas flowing from the top end of the sample and its microbalance has a measuring range of 200.00mg with a sensitivity of 0.01mg.

20-40mg samples were loaded into a 100 μl , 4mm internal diameter and 8mm height, alumina crucible and heated from ambient temperature to 1400^{o}C at a scanning rate of 5K/minute in an argon atmosphere. The samples used in a TG/DTA are too small to be later subjected to any other characterisation technique. It was thus impossible to analyse products from this machine using XRD in particular where a sizeable sample is required. This is what necessitated the need to run these experiments separately in a tube furnace. This was important as sizeable samples could be used and hence analysed to establish the products from every stage of processing. A Perkin Elmer TGA/DSC was also used to check the reproducibility of results.

3.2.1 Pyrolysis of the precursor powder in a tube furnace

10.00g of the precursor were weighed and placed into a rectangular base, 75mm x 40mm x 40mm, alumina boat and placed into a tube furnace. An oxygen getter tube furnace preceded the tube furnace. The getter furnace was packed with copper turnings which were kept at 700^{o}C in order for the copper to be oxidised by, and hence capture, the oxygen in the UHP argon stream.

In the first experiment after having determined the necessary carrier gas flow rate, 10g of precursor were loaded into an alumina boat and this was surrounded by alumina boats containing commercially pure (cp) titanium on either side in order to avoid incidental oxidation from any reminiscent oxygen in the inert gas. The ends of the alumina tube were tightly sealed using brass enclosures with rubber o-ring as shown in the schematic in Figure 3.1. Vacuum grease was applied between the o-ring and brass covers to ensure an air-tight fit.

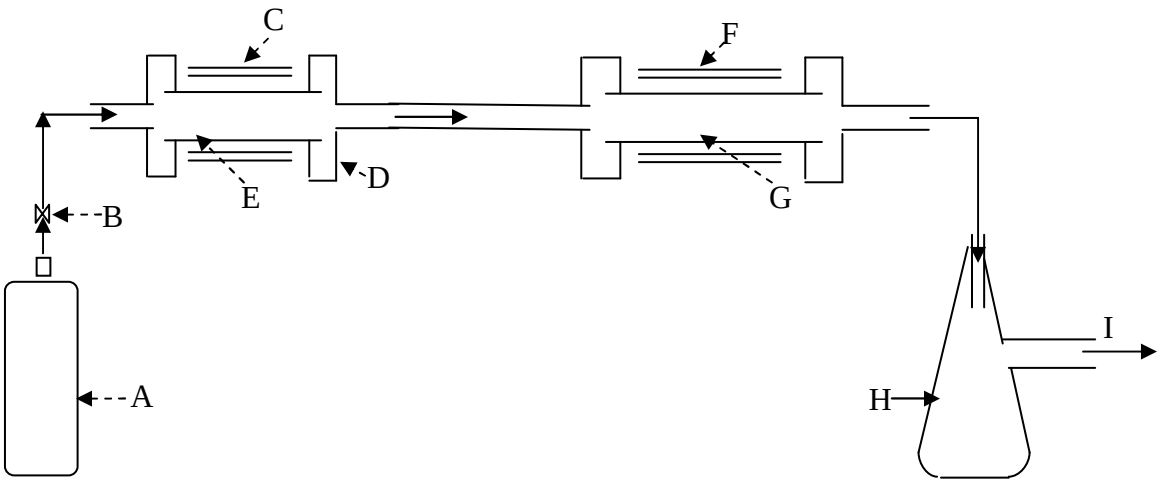


Figure 3. 1: Schematic of the tube furnace

Key:

A- UHP Argon cylinder

B- Flow control valve

C-Oxygen getter (Copper) Furnace

D-Brass seals with a rubber o-ring

E-Silica tube containing copper mesh

F- Tube furnace

G-Mullite or Alumina tube containing the sample

H-Water bubbler

I- Exhaust stream to the atmosphere.

The tightness of the seals was checked using a Gas Check leak detector to determine any gas leaks. The various soaking temperatures had been determined form thermogravimetric curve as shown in figure 4.4 in chapter 4. The table below shows these temperatures and the other variables that were controlled during the stepwise

decomposition tests. After cooling to room temperature the product was weighed and then analysed with the help of SEM and XRD.

Table 3. 1: ***Process conditions during determination of optimum soaking temperature***

Sample identity	Mass/g	Soaking temperature/^{o}C	Soaking time/mins	Linear gas flow rate/ m/min
Sample 1	10.00	400	120	2.60
Sample 2	10.00	600	120	2.60
Sample 3	10.01	800	120	2.60
Sample 4	10.01	1000	120	2.60
Sample 5	10.02	1100	120	2.60
Sample 6	10.00	1200	120	2.60
Sample 7	10.01	1300	120	2.60

3.3 .Optimisation of inert gas flow rate

The original intention of using an inert gas was to provide a non reactive atmosphere around the precursor and the final titanium product. Apart from protecting the precursor and product from reactions with the ambient air, the inert gas inert gas had the important functions of controlling the partial pressure of volatile products in the vicinity of the reactants as well as to carry away any gases or volatile particulate matter away from the reaction zone. Optimising of the gas flow rate was done on the basis of the mass of product collected in the bubbler and comparing this to the theoretical expected. This was

corroborated by examining the SEM micrographs and EDX spectra of decomposition products with gas flow rate being the independent variable. It was not possible to go further than 3.50m/min as the seals of the water bubbler would pop out leaving the whole set up open.

Table 3. 2: ***Experimental conditions during optimization of inert gas flow rate***

Sample identity	Mass/g	Soaking temperature/^{o}C	Soaking time/mins	Linear gas flow rate/ m/min
Sample 08	10.05	1300	120	0.00
Sample 09	10.10	1300	120	0.10
Sample 10	10.01	1300	120	0.50
Sample 11	10.00	1300	120	1.00
Sample 12	10.01	1300	120	2.00
Sample 13	10.03	1300	120	3.00
Sample 14	10.01	1300	120	3.50

3.3.1 Optimisation of soaking time

The dependence of decomposition progress on time was investigated by fixing temperature and gas linear flow rate at their optimal values and varying the time the precursor was kept at temperature. Of importance was the need to optimize the soaking time necessary to rid the final product of AlF_3. Five 10g samples of the precursor were prepared and loaded into five rectangular alumina boats. Each experimental run employed one of these identical precursors of the same mass. The precursors were soaked

at 1300oC for time periods ranging from 10 to 120 minutes and then cooled at 5K/min to room temperature. The mass of the product was measured and the product was studied using both SEM/EDX and X-ray diffraction with a special interest in noting the morphologies and the relative peak intensities of Al and F in SEM/EDX and AlF_3 in the XRD patterns.

3.3.2 Stepwise decomposition of the titanium precursor powder

The profile of the TGA/DTA experiments had to be explained and elaborated by conducting experiments with reasonably sized samples whose product masses would be large enough to allow for their full characterisation after every stage of processing. This was achieved by heat treating fresh precursor samples at the various temperatures that had been determined during thermogravimetric and differential thermal analysis. 10.00g of the fresh titanium precursor were loaded in to an alumina boat and placed into the tube furnace. Argon flow rate was maintained at 3.6m/min as had earlier been determined. Each run entailed heating up the precursor at a scanning rate of 5K/min and soaking at varying temperatures for 2 hours as shown in table 3.1. After soaking the samples were cooled to 20^oC at 5K/min and then removed for analysis. Product analysis involved measurements of product mass, SEM/EDX and X-ray diffractometry. These data allowed for the comparison of the products after soaking the precursor at various temperatures and also enabled the correlation of this with the DTA/TGA data.

3.3.3 Reaction kinetics studies

Rates of the various reactions that take place during the pyrolysis of the precursor had to be determined. This was necessitated by the need to limit the soaking time of products at temperature to the minimal necessary as one major objective of this work was to lower drastically the production cost of titanium. Determination of the kinetics of the decomposition and reduction of the precursor would allow for proper timing of the reactions and more importantly would reduce the risk of holding the pure titanium product at high temperature for too long as this would increase the probability of contamination.

30.00+/-5.00mg samples of the titanium precursor were loaded into a 100 μl alumina TGA/DTA crucible and analysed in an argon atmosphere. A Setaram thermogravimetric analyser coupled to a differential thermal analyser was used. The thermogravimetric curve was used to determine the kinetics of the reactions encountered. In this case the fresh precursor was heated to a predetermined temperature and soaked for two hours as tabulated in table 3.3.

Table 3. 3: ***Reaction conditions during the thermogravimetric analysis of the precursor***

Amount of powder/mg	**Temp/^{o}C**	**Ar Pressure/ bar**	**Soaking time/min**
30	400	1.50	30
32	400	1.50	45
28	400	1.50	60
30	600	1.50	30
35	600	1.50	45
30	600	1.50	60
31	1200	1.50	30
35	1200	1.50	45
33	1200	1.50	60
30	1300	1.50	30
30	1300	1.50	60

Argon at a pressure of 1.5bar was used to provide an inert atmosphere as well as to carry away volatile products for the reaction zone. All the rate equations that were obtained were normalized against the cross sectional area of the small crucible used so as to make them independent of size of reactor size.

3.3.4 Mass balances and Optimization of the amount of reductant

The determination of the required amount of aluminum to reduce the precursor was done based on the analysis results from XRF and/or ICP. The XRF and ICP results as shown in table 4.1 show that precursor contains an average of about 22% Ti by weight. Since pyrolysis of the precursor showed the ultimate residue as TiF_3 according to the XRD patterns, it was logical to conclude that it is TiF_3 that is finally reduced by aluminium. Using a 100g basis of the precursor with a titanium content of 22% means that the amount of titanium present is 22g. In pure TiF_3 , Ti is 45.7 wt%. 22g of titanium would then form 48.14g of TiF_3. Effectively, 100g of the precursor would produce 48.14g of TiF_3 when completely pyrolysed. The reduction of TiF_3 with aluminum, together with the associated molar masses, is as shown by eqn (3.1) below

$$TiF_3 + Al = Ti + AlF_3 \qquad \text{eqn (3.1).}$$

$$105g + 27g = 48g + 84g$$

1g of TiF_3 would thus require 27g/105g= 0.26g of aluminum and hence 100g of precursor would require 12.50 g of aluminum. Therefore on average the stoichiometric amount of aluminium required to reduce the precursor is 12.5% of the precursor by mass. The amount of aluminium needed to complete the TiF_3 reduction was determined this way.

3.4 Precursor reduction experiments

Based on the stoichiometric amount of aluminium determined above, batches of the stoichiometric composition of the precursor mixed with aluminium were prepared. Batches of 10.00g of the raw precursor mixed with 1.25g (12.5%) of aluminium were prepared by accurate weighing and then mixing the powders thoroughly in a mortar using a pestle. The mixing was done for 5 minutes to ensure no powder segregation. The mixture was then loaded into a rectangular alumina boat and placed in to the tube furnace. The furnace was sealed and the tube purged using UHP argon which had been passed through the oxygen getter furnace. Based on the information obtained from the TGA/DTA traces, the following heat treatment profile was selected: The mixture was heated at 5K/min to 400^{o}C and soaked for 30 minutes and then ramped up at the same rate to 800^{o}C, where reduction was expected, then soaked at that temperature for 30 minutes. The temperature was then raised to 1300^{o}C at the same scanning rate and soaked for 2 hours to allow for the sublimation of AlF_3 and then cooled at 5K/min to ambient temperature. The product was then retrieved from the furnace, weighed and analysed

using SEM/EDS and x-ray diffraction. The heat treatment cycle is shown in figure 3.2

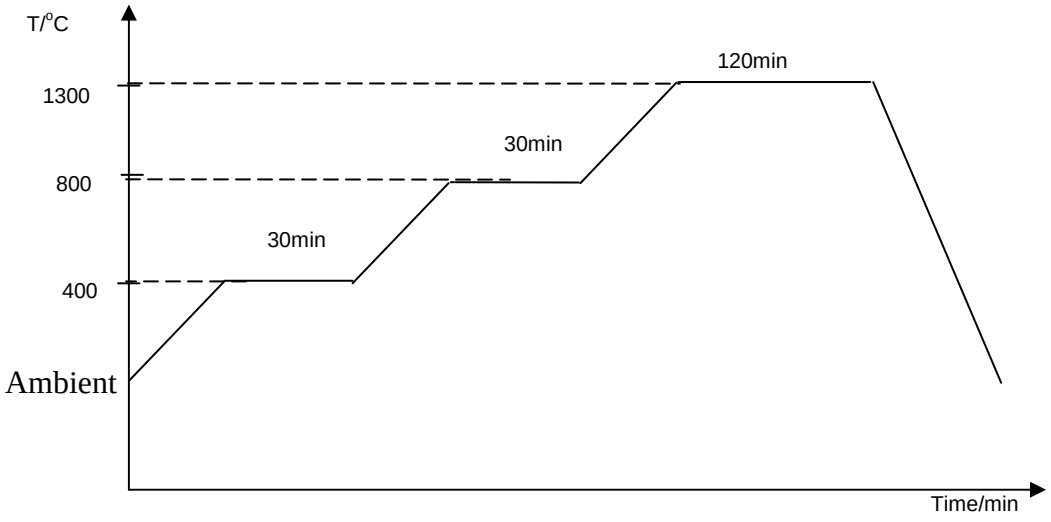


Figure 3. 2: Heat treatment cycle during precursor reduction trials

3.5 Powder coating experiments

12.50g of the raw mix (precursor + 12.5%Al) were loaded in to the tube furnace and treated according to the thermal profile in figure 3.2. However, the soaking time was reduced to 30 minutes in order to retain a significant amount of AlF_3 in the final product. After cooling to room temperature the product was removed from the furnace and the alumina boat was covered with an alumina sheet and placed back into the furnace. The enclosed powder was heated to 1300^{o}C at a scanning rate of 5K/min and soaked at that temperature for 1 hour before being cooled again to room temperature as shown in the thermal profile in figure 3.3

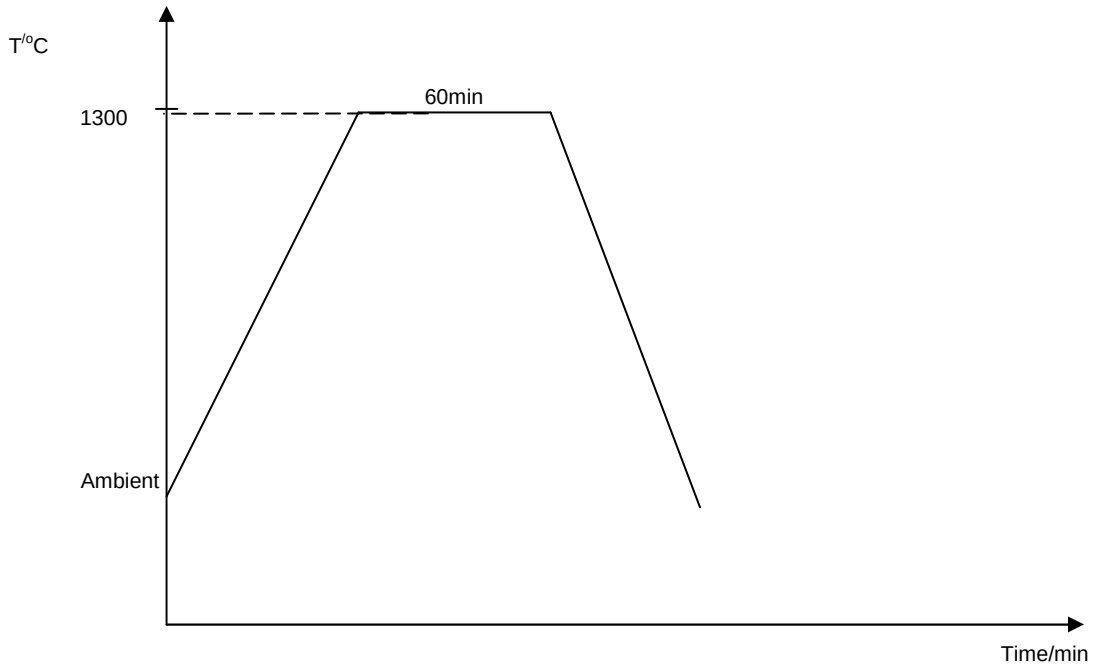


Figure 3. 3: Heat treatment cycle during CVD trials

The powder was then analysed using a *PHI nano* Time of Flight Secondary Ion Mass Spectrometer (ToF-SIMS) in order to check if the AlF_3 was a surface coating or part of the bulk powder. The principle was to bombard the powder surface with a pulsed ion beam and desorb the surface atoms as secondary ions and then pass these through a spectrometer for elemental determination. The analysis was also to determine if any coating that could exist would significantly passivate the titanium from oxidation. The powder was also taken through a thermal analysis process using the TG/DTA in an oxygen atmosphere and the trace was compared to that of cp titanium as a reference.

Chapter 4: Results

This chapter is a summary of the results that were obtained from the experimental work that was conducted. It is structured according to the order in which the experiments were described in chapter 3. A brief discussion is given after each result is presented. Chapter 5 focuses on discussing the results and particularly highlighting the synergies of the various parameters investigated and explaining the principles governing the processes observed. The results are presented in such a manner as to fully describe every stage of characterisation and processing. As a result, all the characterisation techniques, viz SEM/EDS, XRD, TGA/DTA, XRF, ICP and mass measurements are presented together for every stage considered beginning with the raw precursor and ending with the final product in that order.

4.1 Characterisation of the starting precursor

4.1.1 Particle size distribution of the precursor and final titanium product

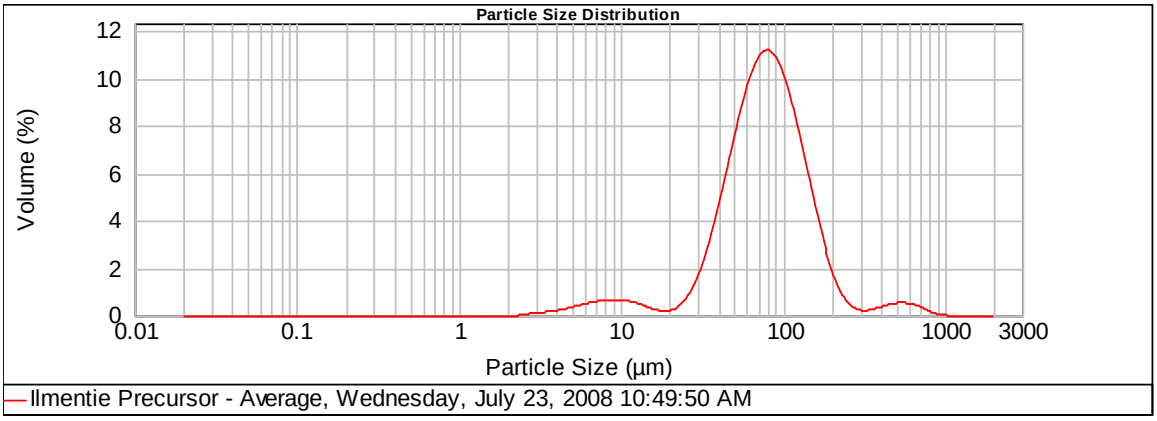


Figure 4. 1: Particle size distribution of raw precursor

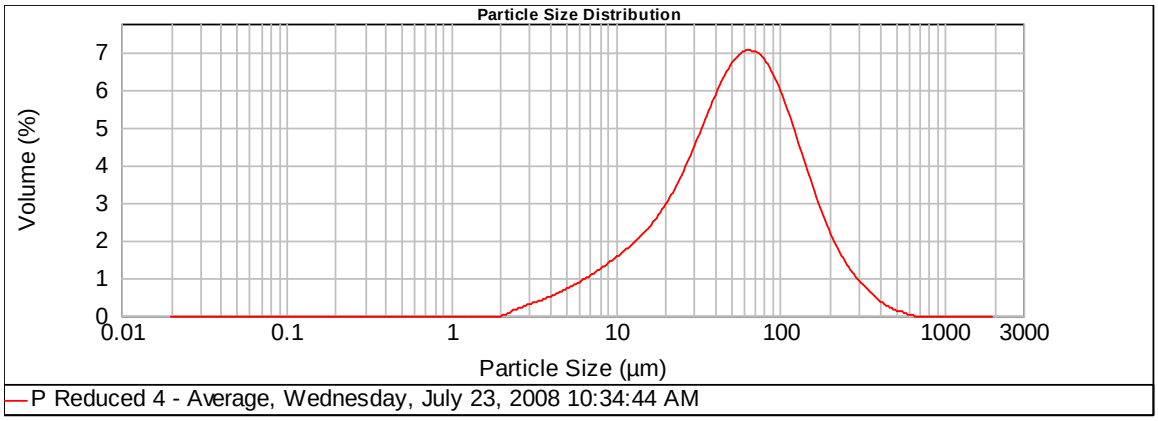


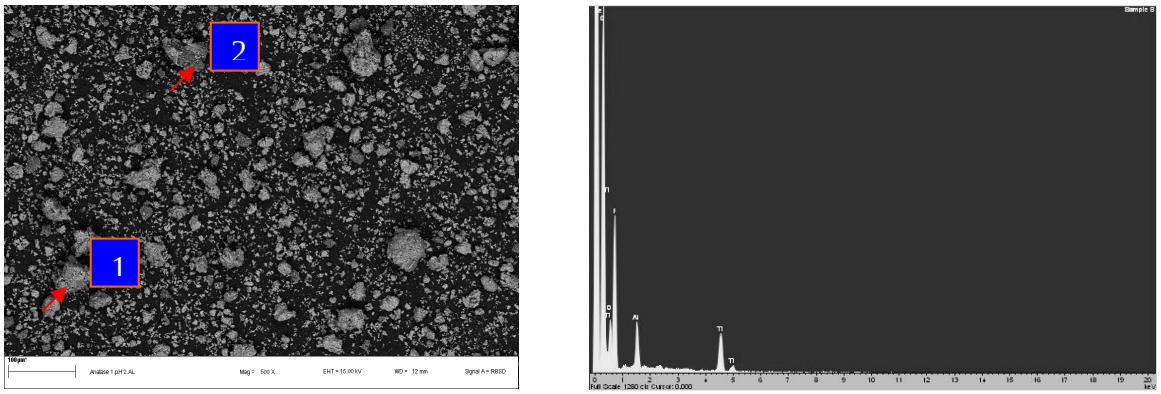
Figure 4. 2: Particle size distribution of the final titanium product

Table 4. 1: ***Comparison of particle size parameters of the precursor and titanium product***

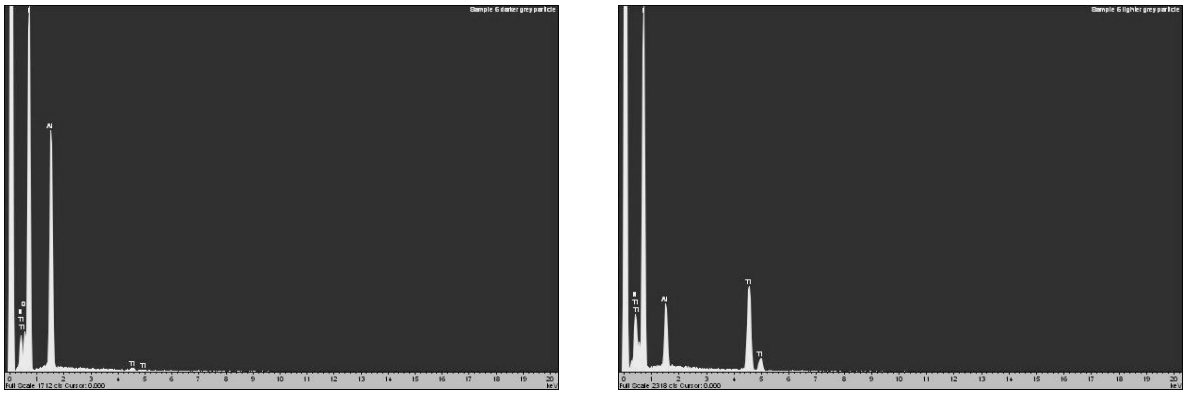
Sample	**d_{10}/ μm**	**d_{50}/ μm**	**d_{90}/ μm**
Precursor	36.0	77.9	156.0
Product	13.0	55.2	158.1

It is evident from figures 4.1 and 4.2 that the final titanium product after heat treating at 1300^{o}C has a finer but wider range of particle size distribution compared to the precursor. The reason for this observation has been attributed to the decomposition of and loss of material from the precursor as it is heated. The coarser particles of the product are likely a result of the partial sintering that occurs when the product is soaked for prolonged time periods at temperature to allow for the complete sublimation of aluminium fluoride. A full description of the possible causes of the observation is given in the next chapter in section 5.1.

4.1.2 SEM Analysis of the precursor



(a) (b)



© (d)

Figure 4. 3: SEM analysis of the precursor (a) SEM micrograph (b) Overall EDS spectrum (c) EDS for spot 1 (d) EDS for spot 2.

The micrograph shows that the powder size is in the micron range and that the particle shape of the raw precursor is roughly spherical. It is also evident that the precursor is made up of two phases which appear as dark and light particles on the micrograph represented by points 1 and 2 respectively. The dark phase, marked 1, is depleted of titanium while the lighter phase, marked 2, is titanium rich. The spot spectra in figures 4.3c and 4.3d show the above statement clearly. It is important to note the relative proportions of the elements in the overall spectrum, figure 4.3 (b), as this gives a direct

guide to the approximate chemical composition and hence chemical formula of the precursor.

Lighter elements like hydrogen had to be analysed separately as these could not be detected by the scanning electron microscope.

Table 4. 2: ***XRF and ICP-MS scan results for the precursor***

Element	**weight %**
Ti	22.20
Al	5.20
F	56.00
Fe	0.05
N*	13.01
H*	3.40
Total	99.86

(* Obtained from ICP-MS)

It is from these analyses and the X-ray diffraction patterns of the precursor that the approximate chemical formula of the precursor was established. The X-ray diffraction pattern of the starting precursor in figure 4.4 shows that the precursor is made up of predominantly two phases which phases are both complex salts of ammonia.

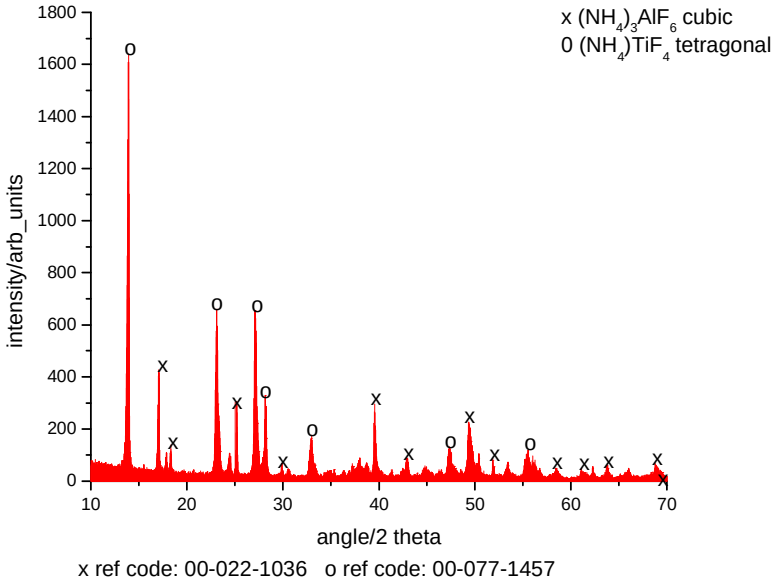


Figure 4. 4: XRD pattern of the raw precursor

Figure 4.4 shows the XRD pattern of the starting precursor and two phases are identified as the main constituents of the precursor. $(NH_4)_3AlF_6$, PCPDF (2002) card number00-022-1036, and NH_4FeF_4, PCPDF (2002) card number 01-077-1457, which are cubic and tetragonal in structure respectively, matched the XRD pattern of the precursor. However, the XRF and ICP analyses, and even the EDS spectrum, show that the precursor contains a negligible amount of iron. It is then logical to conclude that this phase can not be present in the precursor and that the matching was most probably due to NH_4FeF_4 being isostructural with the actual phase in the precursor. The patent by Pretorius [1] discusses this aspect in detail. They noted that they had produced a novel salt, NH_4TiF_4, whose XRD pattern is not in any of the existing PCPDF (2002) databases but is closely matched by that of NH_4FeF_4 [1]. Consequently, the precursor was deduced to be made of two

complex salts namely $(NH_4)_3AlF_6$ and NH_4TiF_4. These appear in the SEM micrograph as the dark and light phases respectively as earlier explained.

4.2 Thermal Analysis

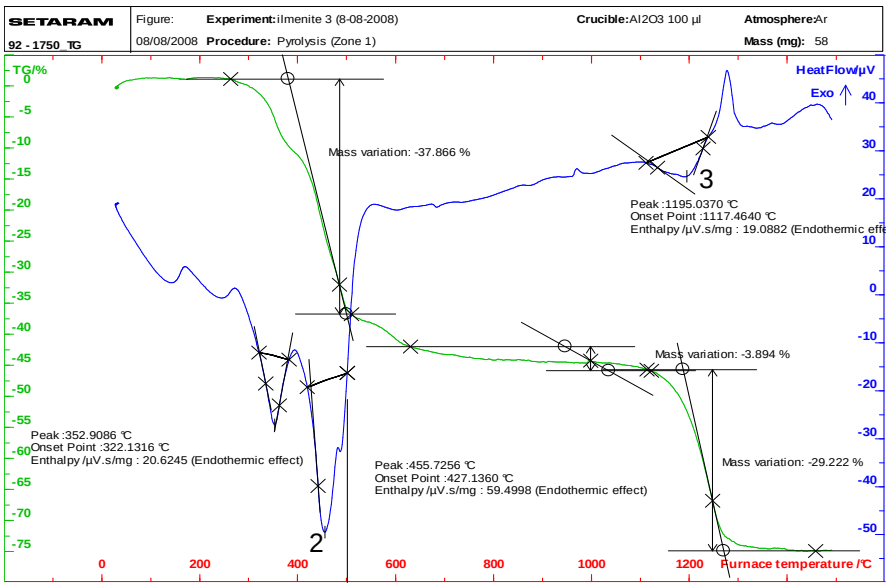


Figure 4. 5: TGA/DTA trace of precursor in UHP argon

The thermal decomposition of the precursor proceeds by a series of reactions as marked by the endothermic peaks on the DTA curve. The TGA curve shows mass losses associated with the reactions and it can thus be concluded that the precursor decomposes releasing volatile products and also that a final residue remains since the mass loss is not 100%.

Table 4. 3: ***Mass losses observed under varying gas linear flow rate at 1300^{o}C***

Linear flow rate/ m/min	**Temperature/ ^{o}C**	**Time/min**	**(mass loss/theoretical) x 100%**
0.5	1300	120	64
1.0	1300	120	75
2.0	1300	120	94
3.0	1300	120	100
3.5	1300	120	100

Table 4.3 shows the mass losses after soaking the precursor at 1300^{o}C for 2 hours under various gas linear flow rates. The mass loss increases as the linear flow rate is increased and reaches a maximum around 3.0m/min. Further increases of the linear flow rate show no effect on the expected mass loss.

4.2.1 SEM analysis of product at various gas linear flow rates

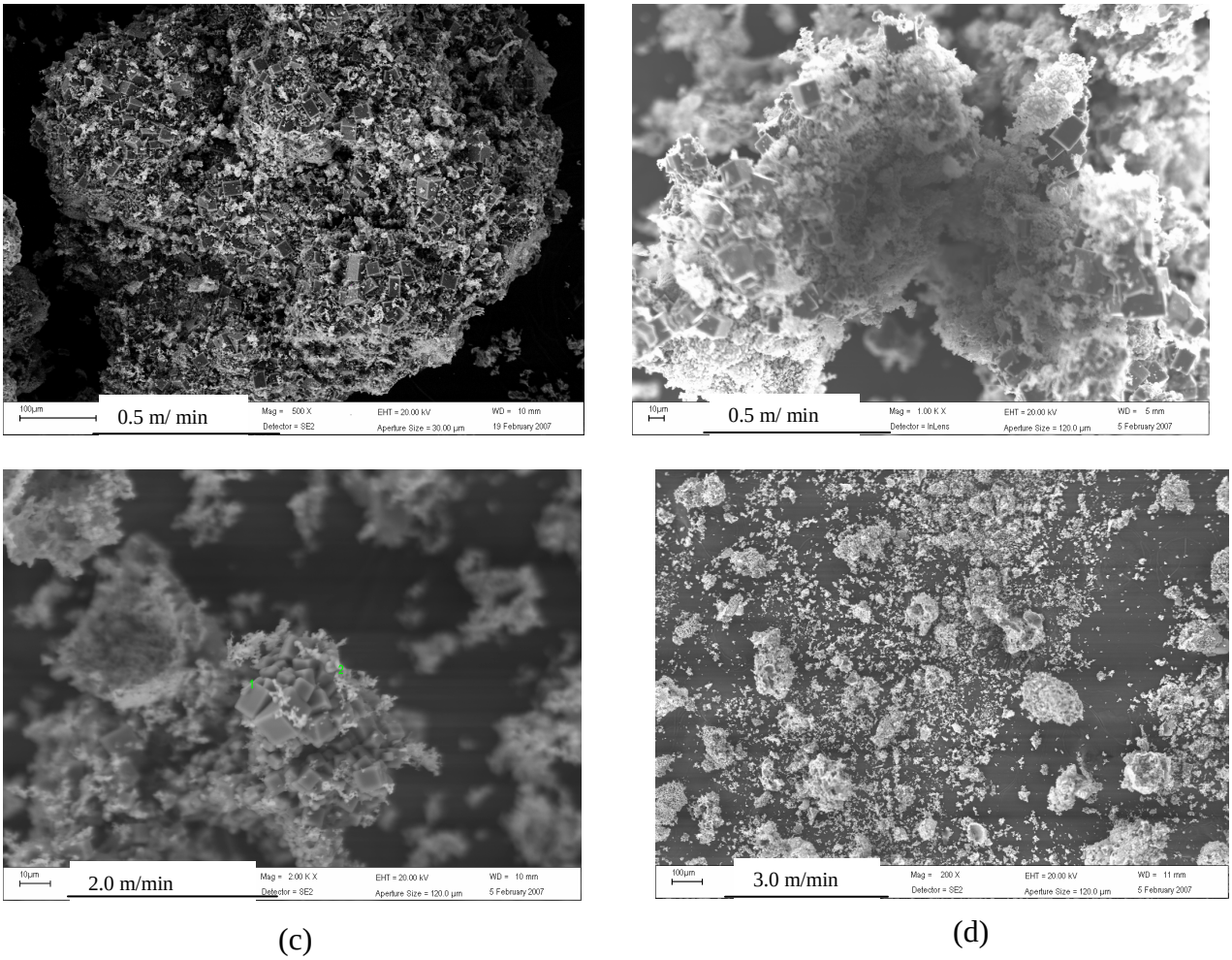


Figure 4. 6: **SEM micrographs of pyrolysis products after heating the precursor for 2 hours at 1300^{o}C and linear gas flow rates of (a) 0.5m/min (b) 1.0m/min (c) 2.0m/min and (d) 3.0m/min**

The cubic crystallites observed in figures 4.6 (a), (b) and (c) are AlF_3. The amount of these crystallites diminishes as the flow rate increases suggesting that the gas flow rate has an effect on the transportation of AlF_3 from the reaction zone.

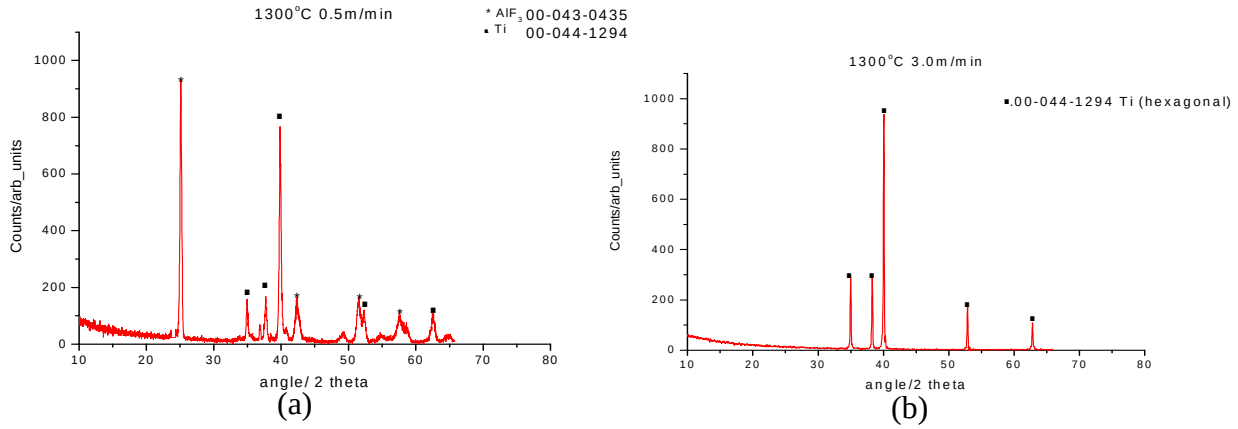


Figure 4. 7: XRD patterns for product after soaking at 1300°C with linear gas flow rate at

(a) 0.5m/min and (b) 3.0m/min

Table 4.4 shows the relative XRD peak intensities of AlF_3 using the most intensive peak at 25° 2 theta (as the standard (I_o)) for the various flow rates considered.)

Table 4. 4*: Linear gas flow rate and the corresponding relative XRD peak intensities (I_i/I_o) of AlF_3 after reduction of the precursor to Ti with Al and soaking for 2 hours at 1300°C*

Gas linear flow rate/ m/min	**I_i/I_o**
0.5	1.00
1.0	0.63
1.5	0.25
2.0	0.05
3.0	0.001
3.5	0.001

It is evident that the amount of AlF_3 that remains in the powder is dependent on the linear gas flow rate. At low linear flow rate not all the AlF_3 sublimes.

4.3 Stepwise thermal decomposition of the precursor

The results of this section are presented fully per decomposition temperature considered. The products from each stage of processing are fully analysed and the new phases obtained are compared with the starting or previous phases identified. In this way logical inferences can be drawn as to the nature of the reactions that occur during the various stages of processing. All the tests and results considered are complementary in nature and augment each other in such a way that concrete conclusions can be made.

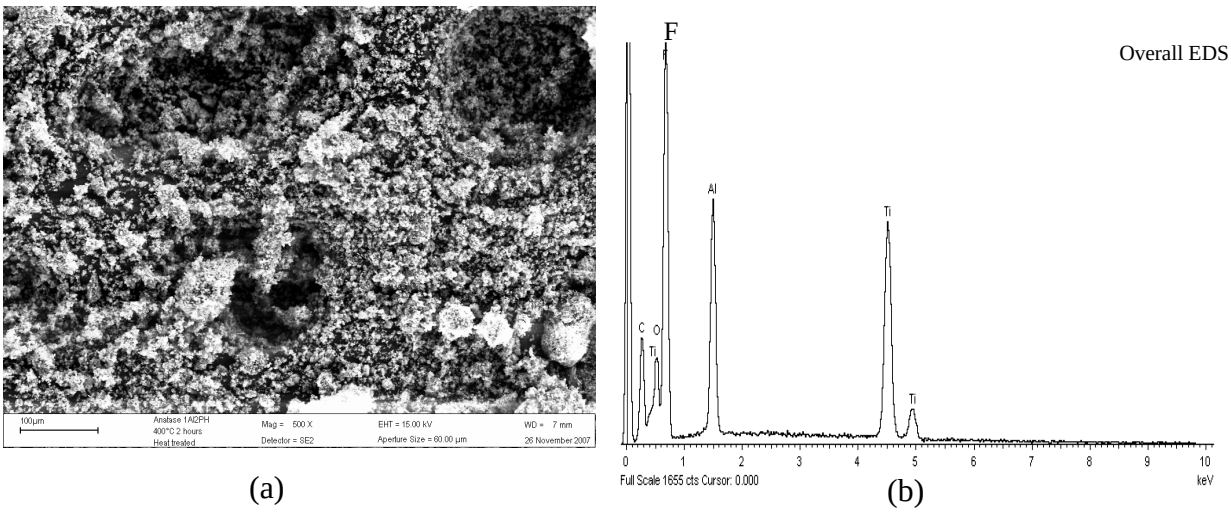


Figure 4. 8: SEM analysis of product after decomposing precursor at 400^{o}C and soaking for 2 hours (a) SEM micrograph (b) Overall EDS

The SEM analysis in figure 4.8 shows that relative peak intensities of titanium and aluminium have increased at the expense of that of fluorine in comparison to those of the starting precursor shown in figure 4.3. At this stage all that is possible to deduce is that the compositional change

that is observed in the EDS spectra is due to loss of material in a manner that little or no titanium or aluminium is lost in the process. Mass loss can only be due to formation of gaseous products which are then carried away by the argon gas. As such these gaseous products contain little or no titanium or aluminium but are made predominantly of fluorine. The mass loss observed after heat treating at 400^{o}C was 13% while the theoretical mass loss that was expected was 12.5% as will be elaborated in chapter 5.

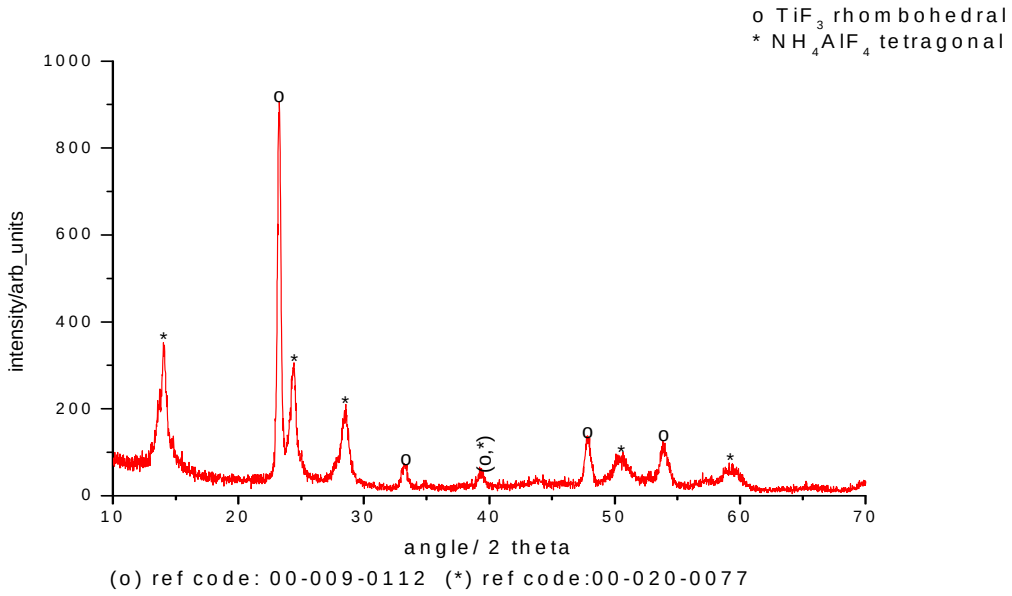
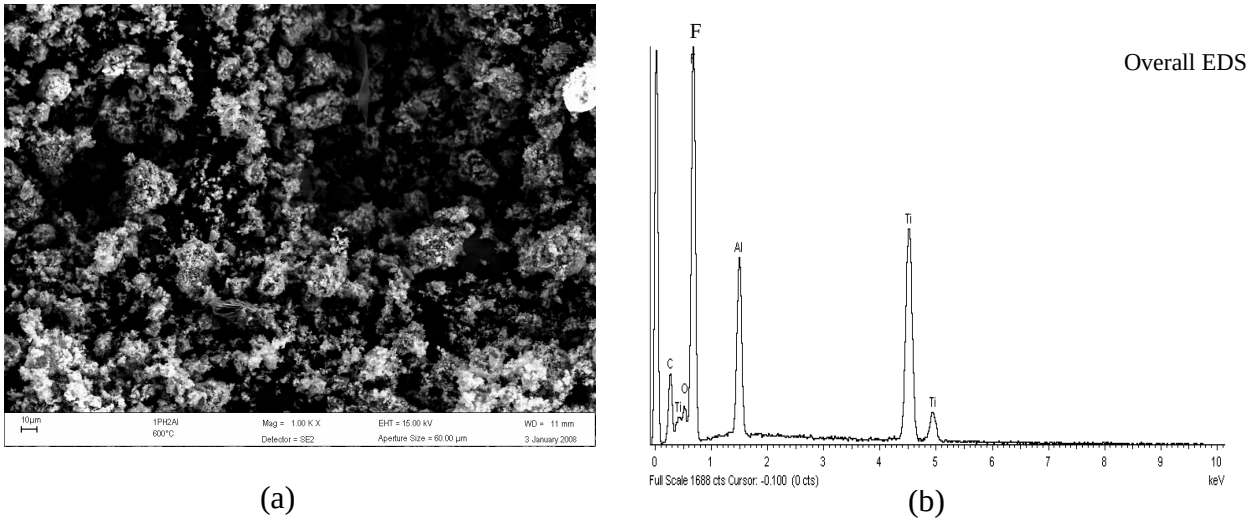


Figure 4. 9: **XRD Analysis of product after decomposing precursor at 400^{o}C in UHP Argon**

From the XRD pattern in figure 4.9 it is noted that at 400^{o}C the precursor decomposes forming completely new products. The products of decomposition are TiF_3, PCDF (2002) card number 00-009-0112, and NH_4AlF_4, PCDF (2002) card number 00-020-0077.

Table 4. 5: ***Nitrogen analysis of product after decomposing precursor at 400^{o}C for 2 hours***

Sample	**Weight % N**
Sample 1	3.12
Sample 2	2.98
Sample 3	2.96
Average	**3.02**
Starting precursor	**13.0**



(a) (b)

Figure 4. 10: SEM analysis of product after decomposing precursor at 600^{o}C (a) SEM (b) overall EDS

Figure 4.10 shows the SEM analysis of the product after heat treating the precursor at 600^{o}C and soaking at that temperature for 2 hours. The mass loss during the heat treatment was around 43%. The theoretical mass loss expected after soaking at this temperature is around 38% which is thus agreeable with the observed experimental result within the margins of experimental error.

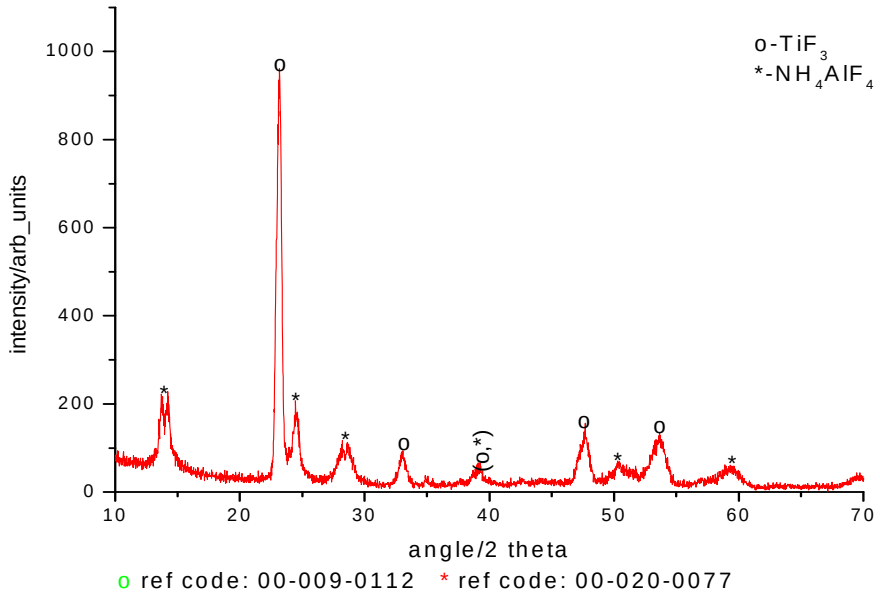
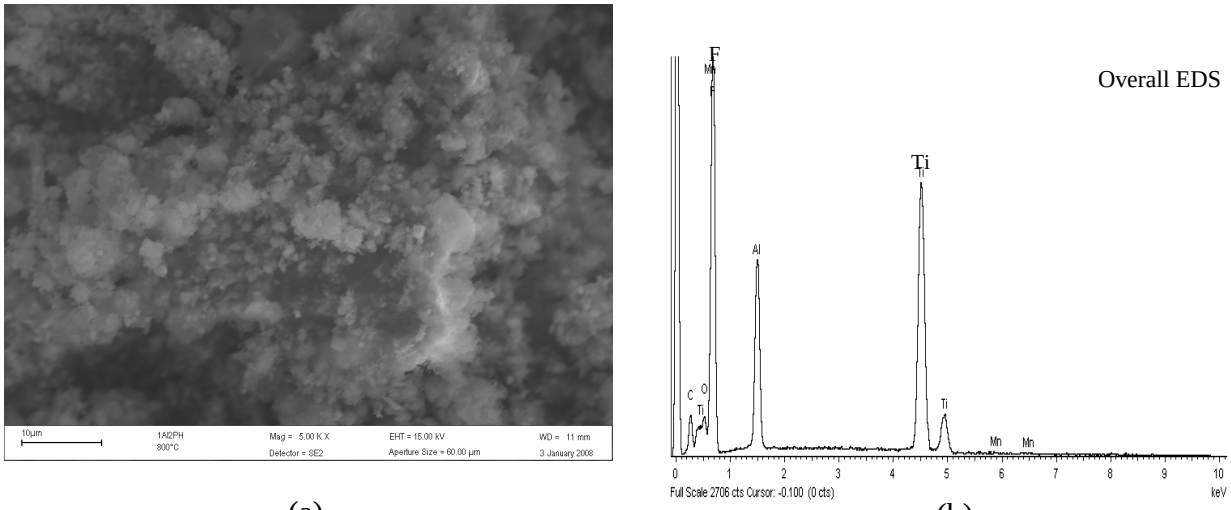


Figure 4. 11: XRD Analysis of product after decomposing precursor at 600^{o}C in UHP Argon

Table 4. 6*: Nitrogen analysis of product after decomposing precursor at 600^{o}C for 2 hours*

Sample	**Weight % N**
Sample 1	2.87
Sample 2	2.99
Sample 3	2.90
Average	**2.92**

Table 4.6 shows the nitrogen analysis from ICP-MS of three samples that were obtained from the product after heat treating the precursor at 600^{o}C for 2 hours. The level of nitrogen in the product confirms the presence of NH_4AlF_4 as shown in the corresponding XRD pattern in figure 4.11. It follows then that the phase NH_4AlF_4 persists in the product at least up to 600^{o}C.



(a) (b)

Figure 4. 12: SEM analysis of product after decomposing precursor at 800^{o}C and soaking for 2 hours (a) SEM (b) Overall EDX spectrum

Figure 4.12 shows the SEM analysis of the product after heat treating the precursor at 800^{o}C and soaking for 2 hours. The peak intensities of titanium and aluminium in the overall EDS spectrum continue to increase relative to that of fluorine. This is supported by the TGA curve in Figure 4.5. The increase in the intensities of these two peaks seems to support the argument that the gases contain negligible or no titanium or aluminium. It is possible then that the volatile products could be fluorides or at least should contain fluorine as a constituent. The mass loss observed in figure 4.5 at 800^{o}C is around 45% which again agrees with what had been expected in theory, 44%.

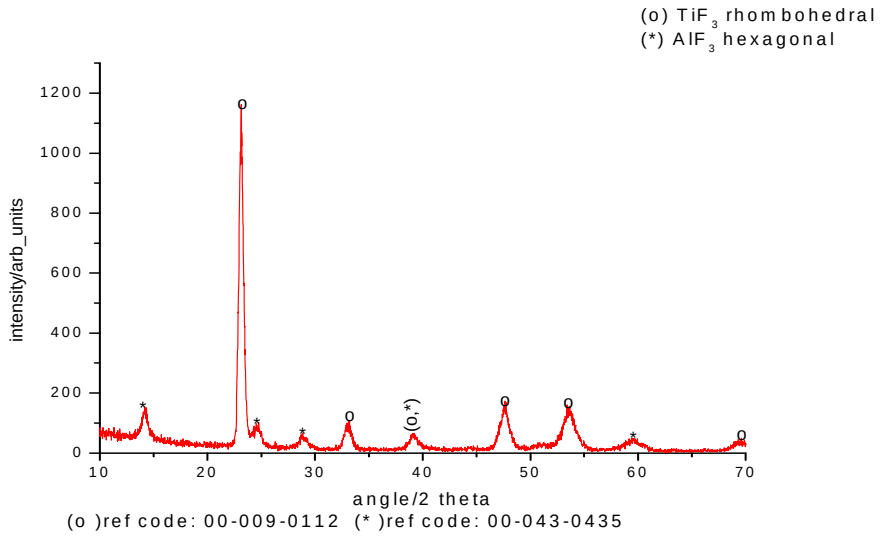


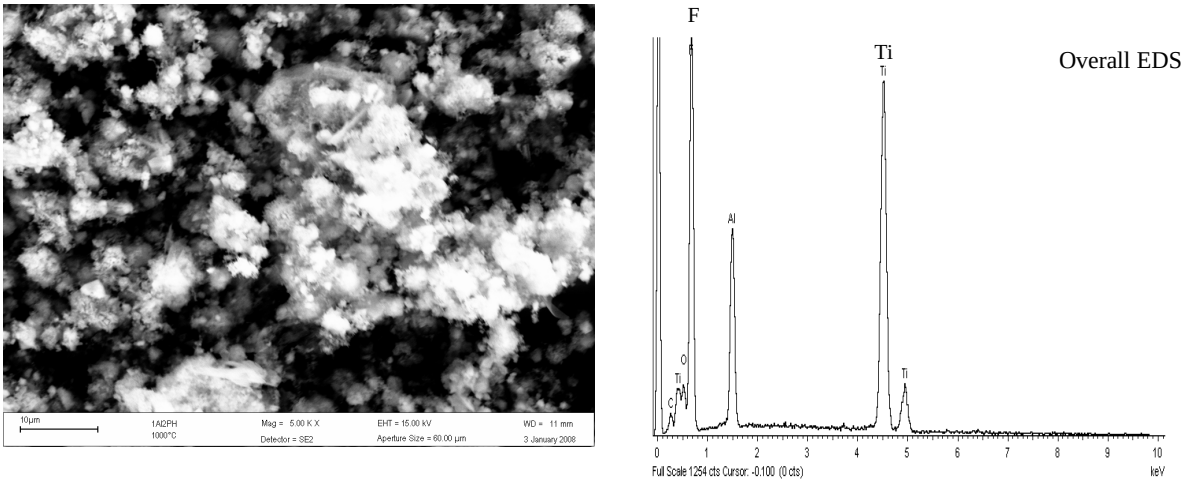
Figure 4. 13: **XRD of product after decomposing precursor at 800^{o}C and soaking for 2 hours**

Apart from the further increase in the intensity of the TiF_3 peak, what is apparent in figure 4.13 is that the phase NH_4AlF_4 is no longer present in the powder. It is also clear that a completely new phase AlF_3, JPSCD card number 00-043-0435 and with a hexagonal crystal structure, is now present. It is logical to make the inference that the NH_4AlF_4 salt is just an intermediate which decomposes to form the AlF_3. Consequently, the AlF_3 is formed at the expense of NH_4AlF_4.

Table 4. 7: ***Nitrogen analysis of product after decomposing precursor at 800^{o}C for 2 hours***

Sample	**Weight % N**
Sample 1	<0.01
Sample 2	<0.01
Sample 3	<0.01
Average	**<0.01**

Table 4.7 shows a negligible amount of nitrogen in the product after heat treating the precursor at 800^{o}C for 2 hours and this rules out the possibility of the salt NH_4AlF_4 being a constituent of the powder. In fact, the result supports the XRD analysis in figure 4.13 which shows AlF_3 instead of NH_4AlF_4. It follows then that NH_4AlF_4 decomposes between 600 and 800^{o}C to form AlF_3 and NH_4F. NH_4AlF_4 is thus an intermediate product and, as will be elaborated in chapter 5, its decomposition produces AlF_3 and gaseous ammonium fluoride as products. This is supported by the TG trace in figure 4.5 which shows a small mass loss in the temperature range 500 to 800^{o}C.



(a) (b)

Figure 4. 14: SEM analysis of product after decomposing precursor at 1000^{o}C for 2 hours (a) SEM (b) Overall EDS spectrum

Figure 4.14 shows the SEM analysis of the product obtained after heat treating the precursor at 1000^{o}C for 2 hours. The titanium and aluminium peaks in the EDS in figure 4.14(b) have significantly increased relative to the fluorine peak in comparison to the SEM analysis of the product after heat treating at 800^{o}C in figure 4.12. This increase in

aluminium and titanium content in the product relative to the products at lower temperatures, coupled with small mass loss in the TGA trace in figure 4.5, suggests that the volatile product contains little or no aluminum or titanium. The volatile product thus contains fluorine predominantly suggesting that it could be a fluoride.

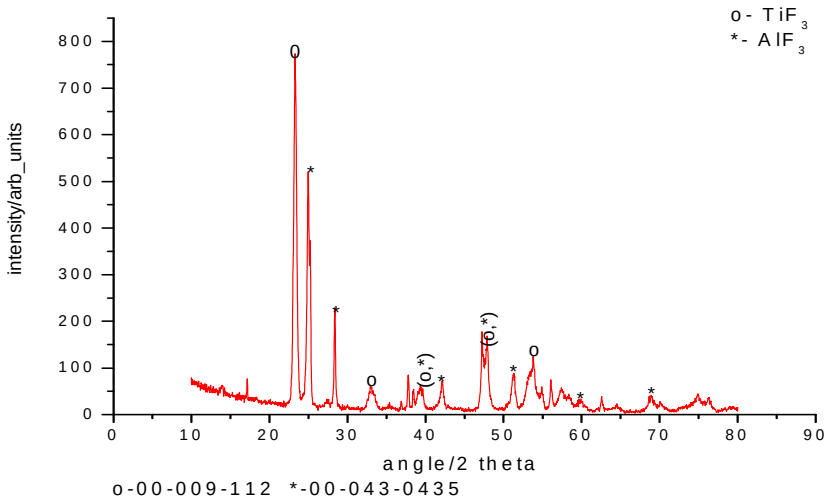
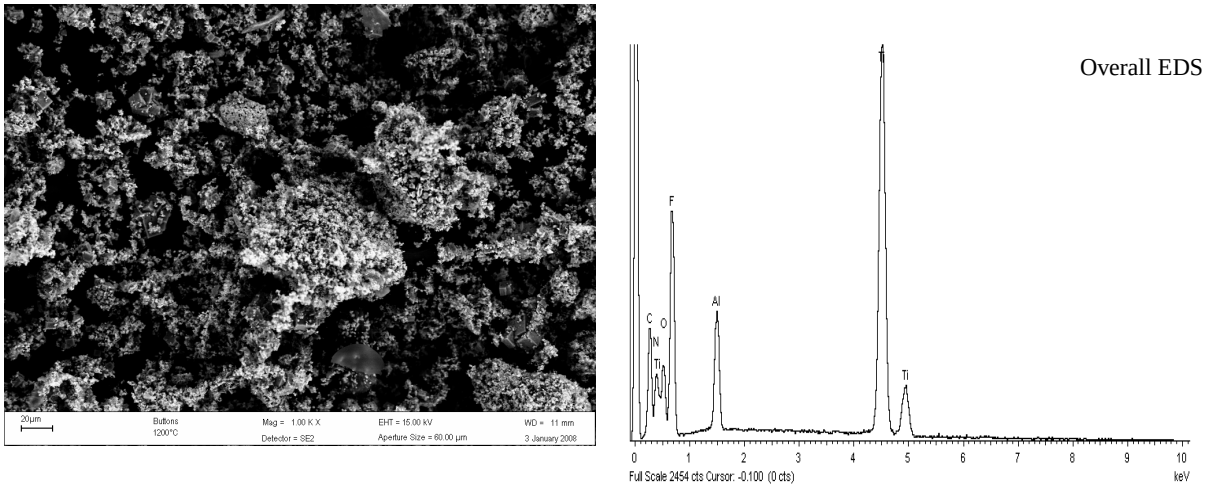


Figure 4. 15: XRD Analysis of product after decomposing precursor at 1000^{o}C for 2 hours

Figure 4.15 shows that the product persists as a mixture of TiF_3 and AlF_3 up to this temperature. However it is noted that the AlF_3 crystal structure has changed from hexagonal to tetragonal suggesting some form of allotropic transformation between 800 and 1000^{o}C.



(a) **(b)**

Figure 4. 16: SEM analysis of product after decomposing precursor at 1200^{o}C for 2 hours
(a) SEM (b) Overall EDX spectrum

Figure 4.16 shows the SEM analysis of the product after heat treating the precursor at 1200^{o}C and soaking for 2 hours. The relative peak intensity of aluminium has decreased relative to the EDS spectrum in Fig 4.12. It is arguable that the mass loss observed at this stage, also shown in figure 4.5, could be due to loss of volatile products containing aluminium. Since AlF_3 is the only phase containing aluminium in the product, it follows then that the observed decrease in the aluminium peak intensity in the EDS spectrum is due to loss of AlF_3 from the powder. AlF_3 sublimes from the precursor and this is also supported by the TGA/DTA trace in Fig 4.5 which shows that there is a mass loss beginning around 1100^{o}C and that this is a separate process as indicated by the presence of the endothermic DTA peak around the same temperature.

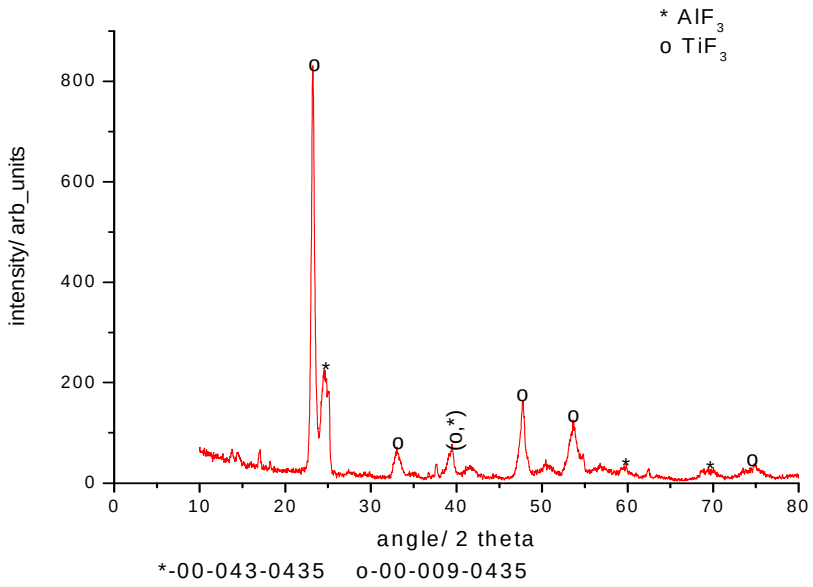
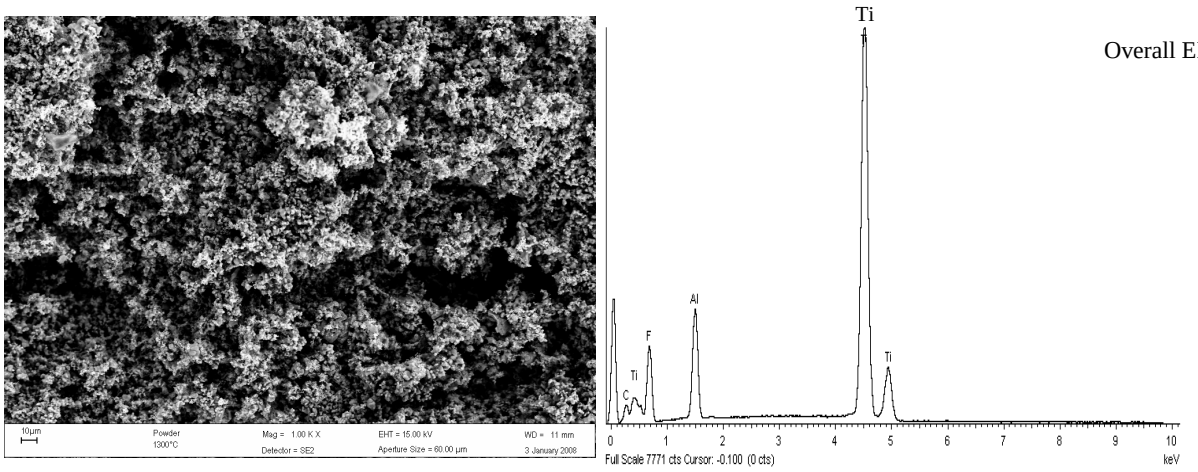


Figure 4. 17: XRD Analysis of product after decomposing precursor at 1200°C in UHP Ar

Figure 4.17 shows the XRD pattern of the product after pyrolising the precursor at 1200°C for 2 hours. Compared to figure 4.15, the phases present in the product are still the same but the peak intensities of AlF_3 have significantly decreased. This suggests some loss of AlF_3 from the product as temperature is increased and this is supported by the mass loss observed around this temperature in figure 4.5. This mass loss might be due to the sublimation of AlF_3 and during the laboratory trials this was observed in the discoloration of water bubblers in figure 3.1 around this temperature.



(a) (b)

Figure 4. 18: SEM analysis of product after decomposing precursor at 1300^{o}C (a) SEM (b) Overall EDX spectrum

Figures 4.18 and 4.19 show the SEM and XRD analyses of the product after heat treating the precursor at 1300^{o}C for 2 hours under argon stream of 2.6m/min. Figure 4.18 shows a significant decrease in the peak intensities of fluorine and aluminium relative to figure 4.16. Similarly the XRD pattern in figure 4.19 shows a decrease in the AlF_3 peak intensities relative to the pattern in figure 4.17. This suggests further loss of AlF_3 from the product through sublimation as temperature is increased from 1200 to 1300^{o}C. It had in theory been expected that the total mass loss after soaking the precursor at 1300^{o}C would be 55 % but figure 4.5 shows a loss of 75%. There is loss of 20% more material than expected. This could probably be due to the fact that the loss might not be solely due to the sublimation of aluminium. Some other phase might as well be vaporizing at this temperature. It will be shown in chapter 5 that the vapour pressure of TiF_3 is much higher than that of AlF_3 at this temperature and it is thus possible that TiF_3 could also be subliming off leading to this excessive mass loss.

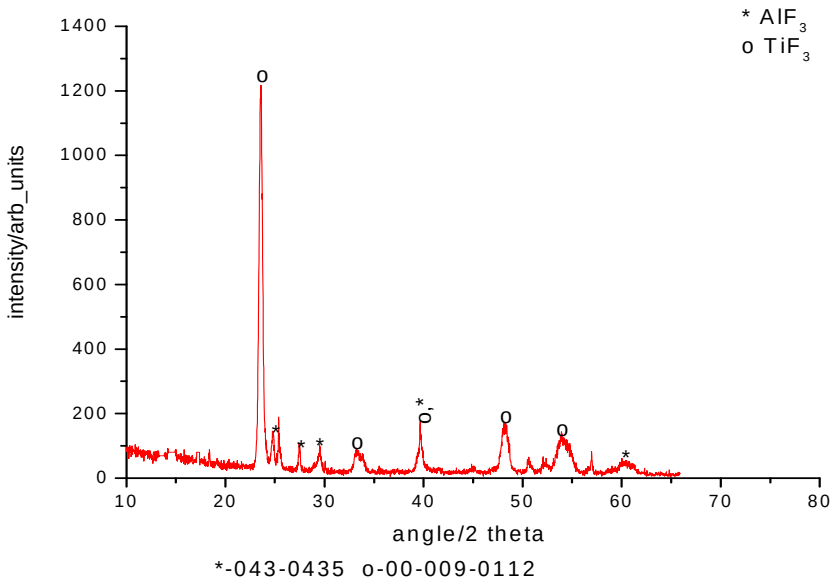
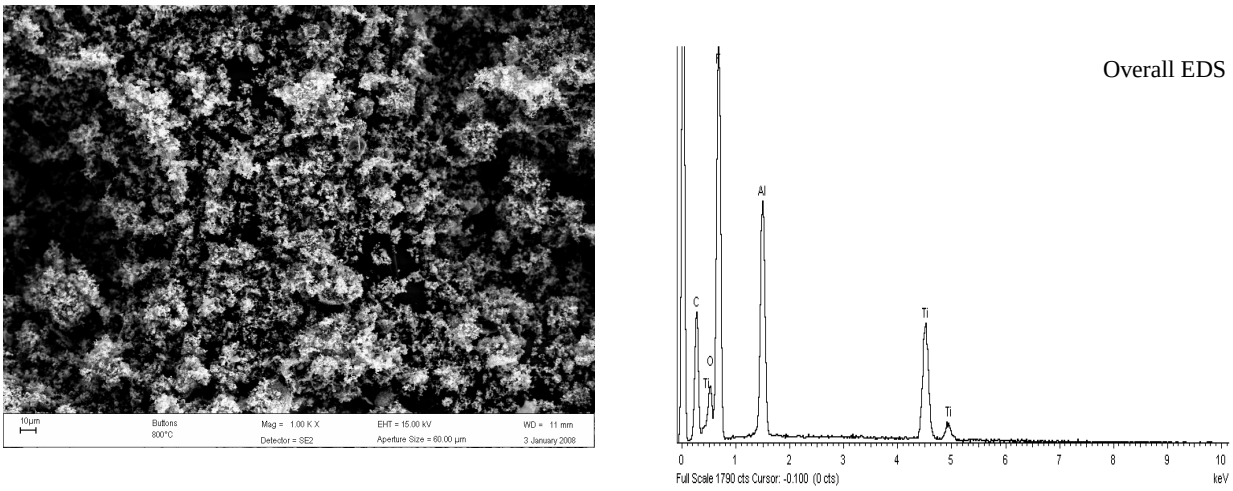


Figure 4. 19: XRD Analysis of product after decomposing precursor at 1300°C in UHP Ar



(a) (b)

Figure 4. 20: SEM analysis of the titanium product after reduction at 800°C for 2 hours (a) SEM micrograph (b) Overall EDS

4.4 REDUCTION OF THE PRECURSOR WITH ALUMINIUM

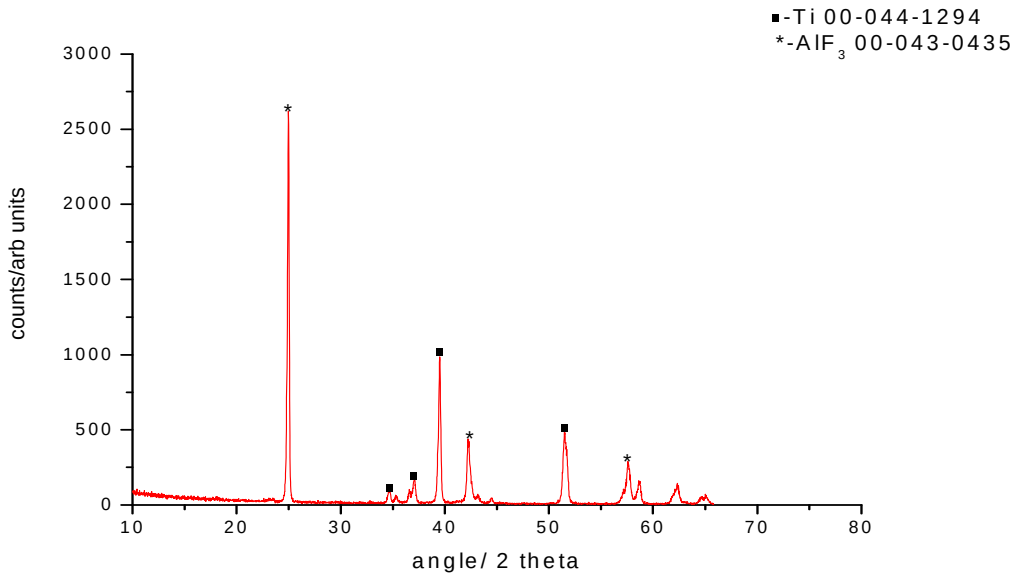


Figure 4. 21: XRD pattern after reduction of precursor with aluminium at 800^{o}C

Figures 4.20 and 4.21 show the SEM and XRD analyses of the product after heat treating the precursor premixed with 12.5 wt% Al at 800^{o}C and soaking at that temperature for 2 hours respectively. The EDS spectrum in figure 4.20 (b) shows that aluminium and fluorine are still present in the product while the XRD pattern in figure 4.21 shows that elemental titanium has been formed and that AlF_3 is the other phase present. The fluorine detected by the EDX spectrometer is therefore due to AlF_3 and not TiF_3. Based on earlier characterisation results of the products obtained from pyrolising the precursor in the absence of aluminium, it can be argued that the presence of AlF_3 is due to the temperature being too low for its sublimation. A higher soaking temperature and allowing

for a judicious soaking period are necessary after reduction to allow for the sublimation of the AlF_3 from the titanium product.

4.4.3 Characterisation of product after sublimation of AlF_3

Both the EDX spectrum and XRD pattern in figures 4.22 and 4.23 respectively showed a relatively clean product with the only observed elements in the EDS spectrum being titanium and traces of aluminium and iron. The XRD pattern further confirmed this and showed that there is predominantly one phase present in the heat treatment products.

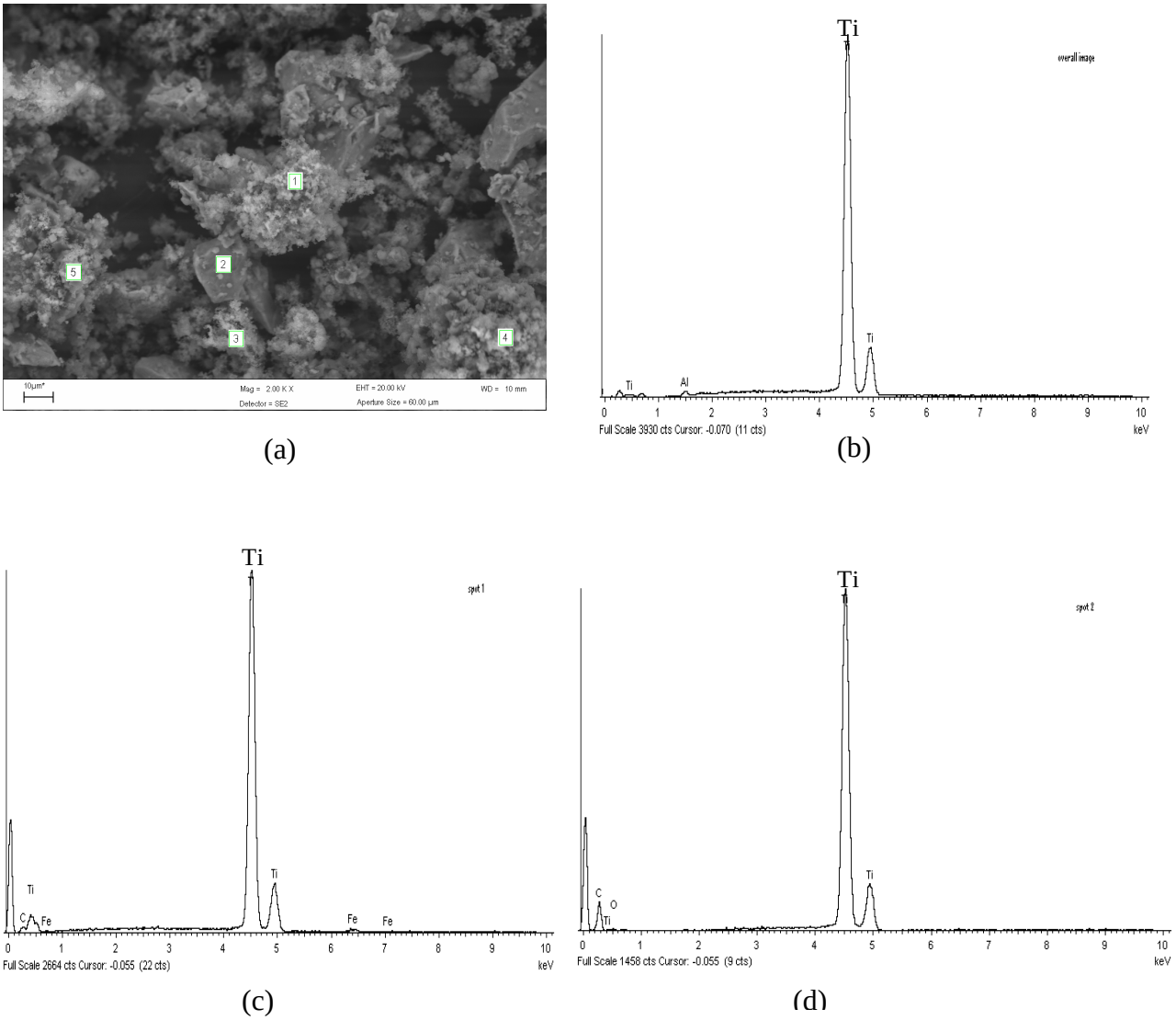


Figure 4. 22: **SEM analysis of product after reduction of precursor with aluminium at 1300°C for 2 hours (a) SEM micrograph (b) Overall EDX spectrum (c) EDS spot 1 and (d) EDS spot 2**

Figure 4.22 shows the SEM micrograph and the corresponding EDX spectra of the final product after heat treating the precursor premixed with a stoichiometric amount of aluminium at 1300^{o}C for 2 hours. The very small Al peak observed in the overall EDX spectrum in figure 4.22 (b) could be due to the fact that some TiF_3 sublimes off leaving elemental Al as excess as earlier explained in this chapter.

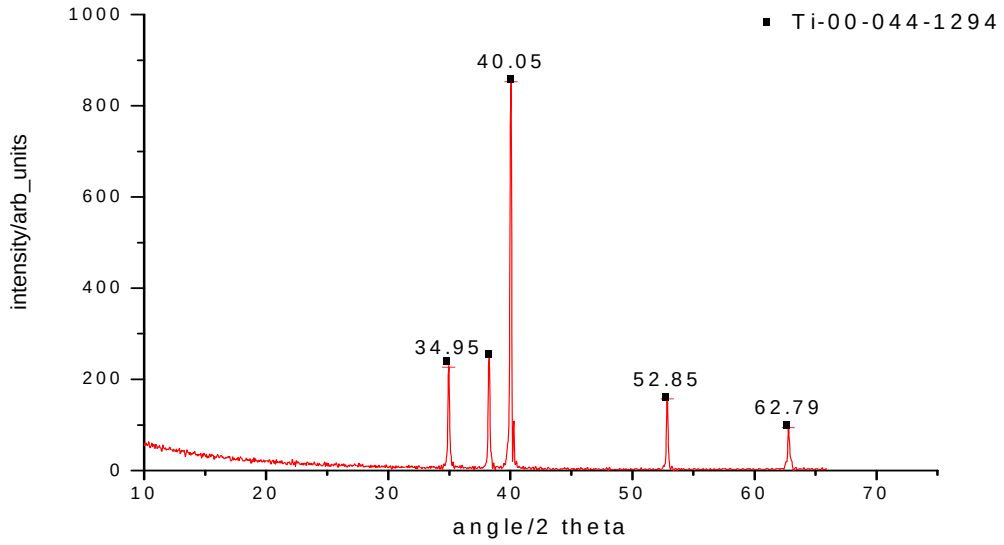


Figure 4. 23: XRD pattern of product after reduction and soaking at 1300^{o}C for 2 hours

The absence of cubic crystallites in the SEM micrograph means that AlF_3 is no longer present. This is also supported by the EDS spectra which now show no or minimal intensities of aluminium and fluorine peaks. So, although the reduction to form titanium takes place at a temperature as low as 800^{o}C, it is necessary to raise temperature to 1300^{o}C in order to rid the product of AlF_3 through its sublimation.

4.5 Chemical Vapour Deposition (CVD) of AlF_3 on Titanium

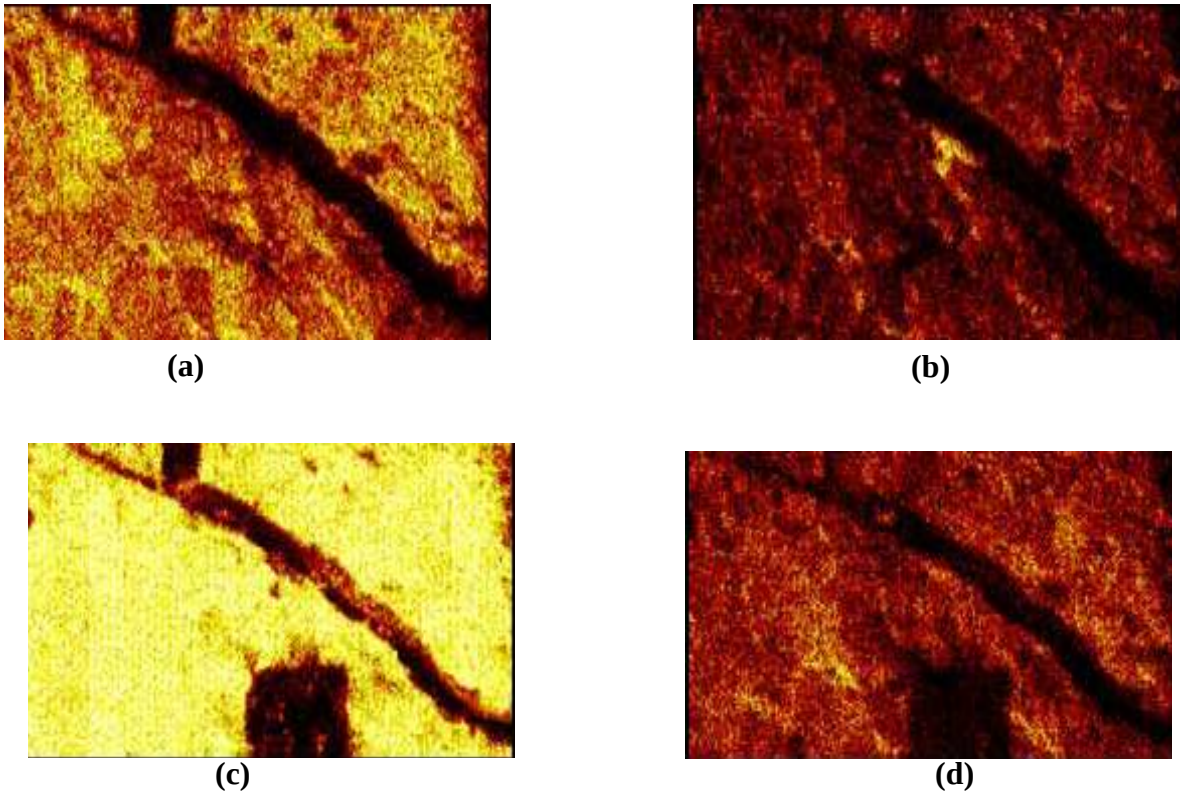


Figure 4. 24: ToF-SIMS images of passivated product (a) Al ion image before sputtering (b) Ti ion Image before sputtering (c) Al ion image after sputtering (d) Ti ion image after sputtering

Figure 4.24 shows ToF-SIMS images of the surfaces of the product that was obtained after reduction of the precursor and soaking the product for 90 minutes in a closed boat to allow for sublimation and resublimation of AlF_3 on to the surface of the powder in order to form a coating. After sputtering the powder surface, figures 4.24(c) and (d) show that the coating in not homogeneous and is partly part of the bulk powder. This heterogeneity is likely to reduce the ability of the AlF_3 coating to raise the spontaneous ignition temperature of the powder significantly.

4.6 Kinetics of the decomposition of the precursor and sublimation of AlF_3

The progress of the pyrolysis of the precursors is here considered in two parts to make the analysis of the kinetics relatively simple. As was noted in the TGA curve in figure 4.5, there are two predominant mass loss temperature regimes in the temperature range from ambient to 1400^{o}C. The first mass loss is observed between 400 and 600^{o}C and the second TG negative slope (mass loss) is observed between 1100 and 1300^{o}C. Two graphs were then constructed by pyrolising the precursor separately between these two temperature ranges and are presented below

4.6.1 Thermal analysis

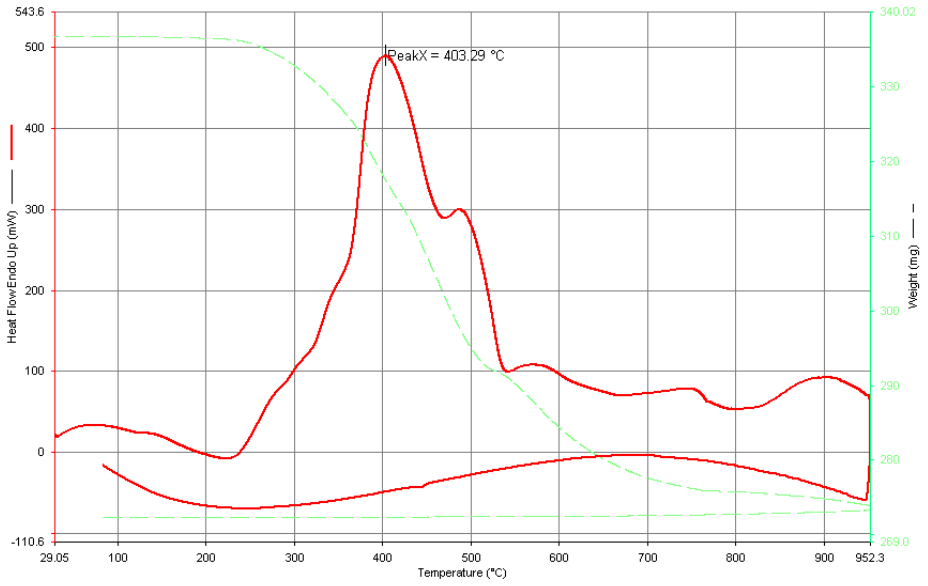


Figure 4. 25: TGA-DSC trace of precursor in UHP Argon

Table 4. 8: ***Mass variation of precursor with temperature and soaking time***

Amount of powder/g	Temp/^{o}C	Soaking time/min	Mass loss $\Delta m / g$	% theoretical mass loss
10.00	300	30	0.00	-
10.00	350	45	0.00	-
10.00	380	30	1.40	82.3
10.00	380	45	1.67	98.2
10.00	380	60	1.85	108.8
10.00	450	30	3.12	84.3
10.00	450	45	3.35	90.5
10.00	450	60	3.80	102.7
10.00	800	30	4.50	104.6
10.00	800	45	4.80	111.6
10.00	800	60	5.10	118.6

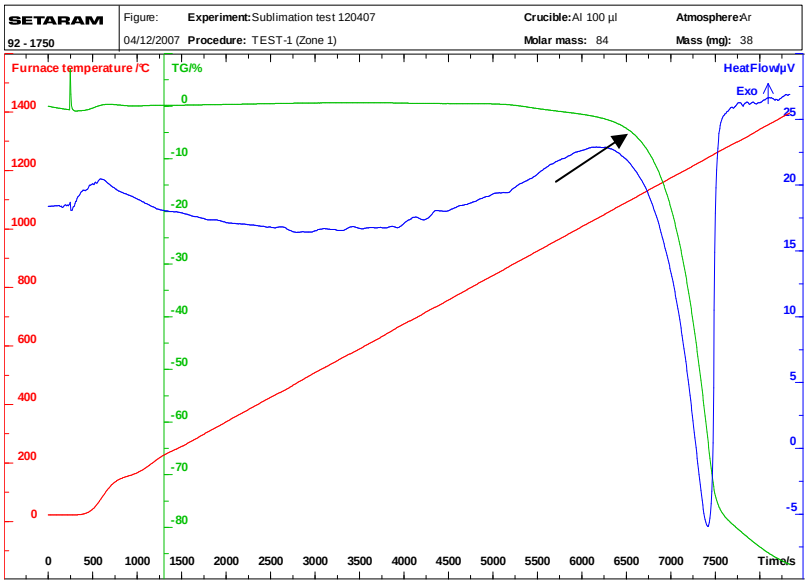


Figure 4. 26: TGA/DTA trace of AlF_3

Figure 4.26 shows the TGA-DTA trace of AlF_3 heated from ambient temperature to 1400^{o}C. The mass loss shown by the green curve in figure 4.26, commencing at the point of inflexion marked by the arrow, marks the sublimation of AlF_3. In essence the

sublimation occurs at one defined temperature and not over a range. The tangent of the TGA slope will be equal to dC/dt and can be, together with mass measurements from the tube furnace samples, used to approximate the rate of sublimation and the rate equation. The results obtained from soaking the AlF_3 in the tube furnace for various time periods and temperatures are shown in table 4.9 below. The relative peak intensities of AlF_3 were also recorded using the most intensive peak of AlF_3 at 25.2^o theta as the standard (I_o).

Table 4. 9: ***Mass variation with soaking temperature, time and linear flow rate***

Mass of powder/g (m_o)	**Temp/^{o}C**	**Ar linear flow rate/^{o}C**	**Soaking time/min**	**Mass loss** $\Delta m / g$	**%** $\Delta m / m_o$	I_i / I_0
5.65	1200	1.13	30	3.81	84.7	2.90
5.65	1200	1.13	45	3.80	84.4	2.90
5.65	1200	1.13	60	3.63	80.7	3.10
5.65	1200	2.26	30	3.98	88.4	1.58
5.65	1200	2.26	45	4.01	89.1	0.95
5.65	1200	2.26	60	4.18	92.9	0.40
5.65	1300	1.13	30	4.03	89.6	2.10
5.65	1300	1.13	45	3.89	86.4	1.90
5.65	1300	1.13	60	3.88	86.2	1.40
5.65	1300	2.26	30	4.12	91.6	0.29
5.65	1300	2.26	60	4.21	93.6	0.16

The rate of sublimation of aluminium fluoride is, like any other reaction, sensitive to temperature and the variation of the rate constant with temperature will follow the Arrhenius equation. The mass losses recorded are therefore expected to increase with temperature as shown in table 4.9. Secondly, the sublimation takes a finite time and hence requires adequate time at any temperature above the threshold for it to proceed. From the table above, the general inference is that the sublimation rate increases with temperature and the extent of the process increases with the time period allowed. Graphic

plots of the data in table 4.9 are given in section 5.5.2 and the rate equation and activation energy are also determined.

Chapter 5: Discussion of Results

5.1 Particle size distribution of the precursor and the titanium product

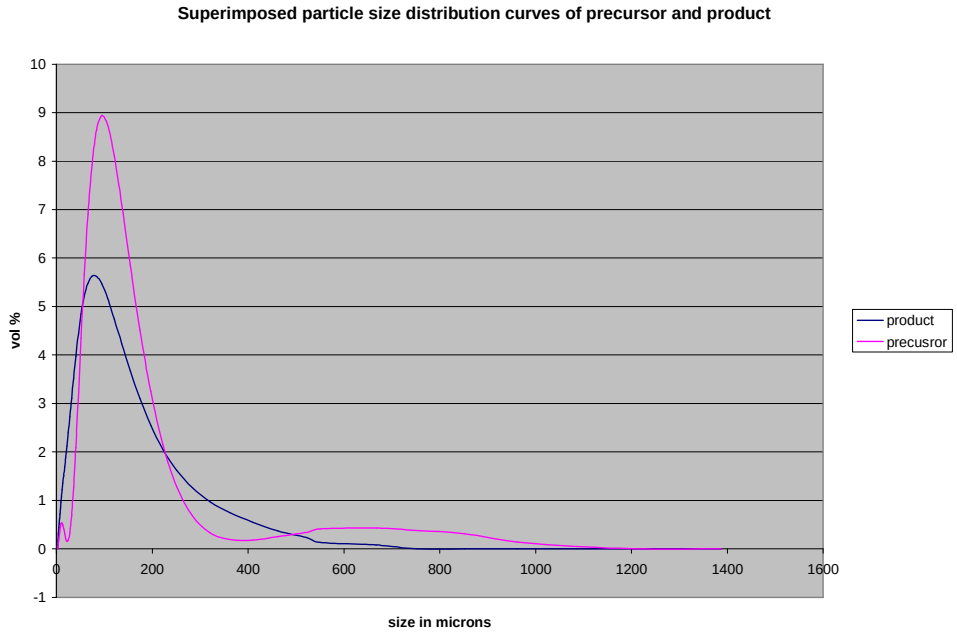


Figure 5. 1: Superimposed particle size distributions of the precursor and Ti product

The precursor is composed of coarser particles compared to the final titanium powder product. If the d_{50} values of the precursor and titanium powder are considered to be d_{p50} and d_{Ti50} respectively, then $(d_{p50} - d_{Ti50})/d_{p50} = 0.29$. This represents an average particle size reduction of approximately 29%. This is understandable because during the pyrolysis of the precursor a lot of material is lost as gas. The shrinking core model has been found to be applicable here in that any material that escapes as gas does so at the expense of the material that was originally in the precursor and hence the size and

morphology of the remaining the particles. More importantly, the gases that escape are not due to the vaporization of phases that were originally in the precursor. The volatile products are formed from the original phases of the precursor. This argument is schematically presented in Figure 5.2 below.

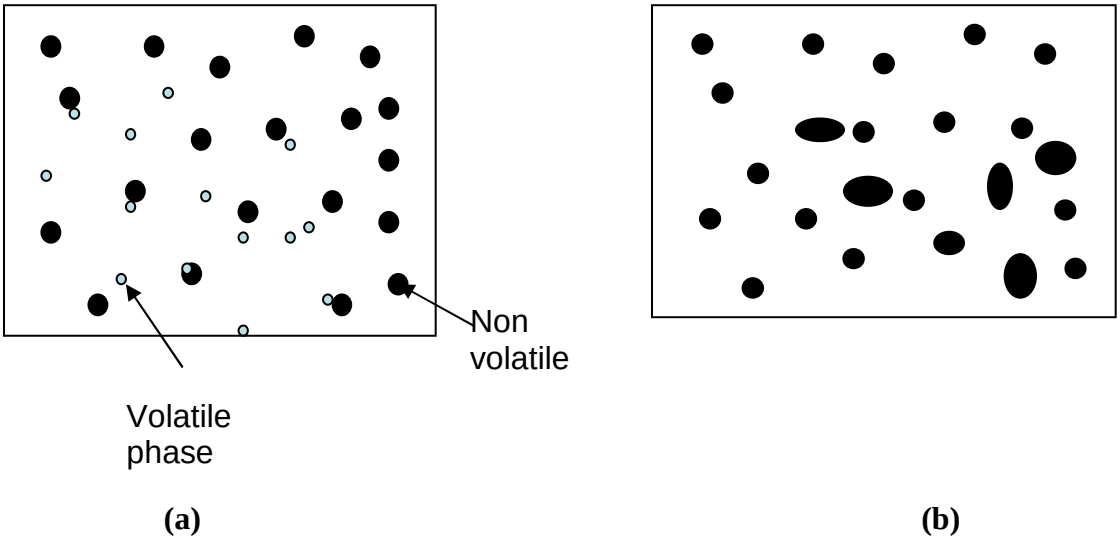


Figure 5. 2: Schematic showing (a) a pre-existent volatile phase and (b) Volatile phase forming due to decomposition of the starting material

The process represented by the schematic in Fig 5.2(a) is one in which the volatile phase is preexistent, and hence is a separate phase, in the precursor. The escape of this phase at the appropriate temperature would not significantly affect the size and even shape of the residual non volatile phase. The situation in Figure 5.2(b) depicts a case where the volatile phase is not existent in the starting precursor but is formed at the appropriate temperature from the decomposition of the phase(s) originally present. It is this hypothesis that seems to support what is observed with the precursor being studied in this work. This can be elaborated with the aid of the shrinking core model represented in the schematic below

The shrinking core model

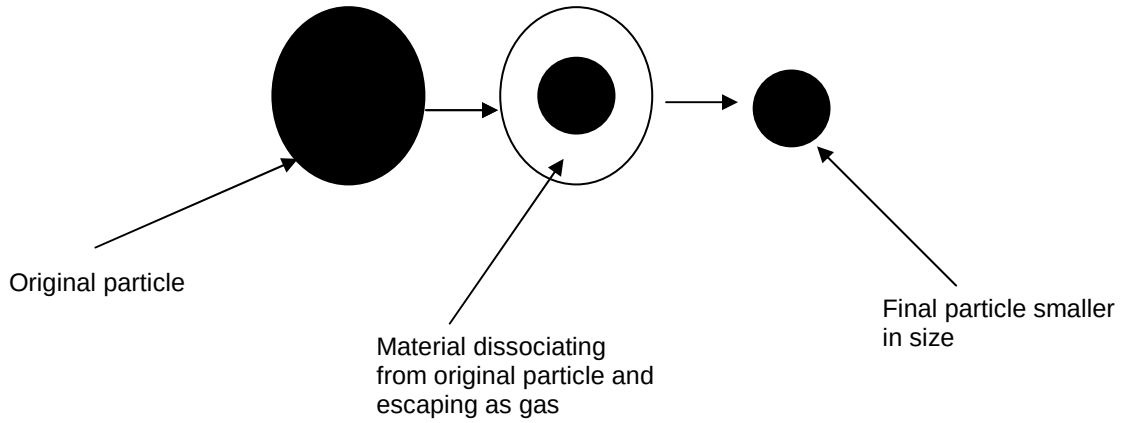


Figure 5. 3: Schematic of the shrinking core model

SEM Analysis of product before and after sublimation of AlF_3

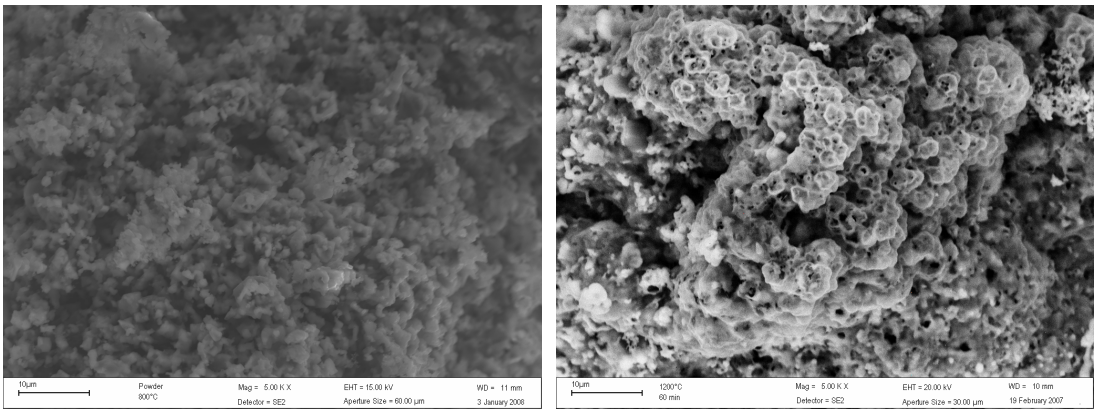


Figure 5. 4: SEM Analysis (a) 800^{o}C (b) 1200^{o}C after sublimation of AlF_3

Figure 5.4 shows the SEM micrographs of the precursor after heat treatment at 800 and 1200^{o}C. The morphology represented by the micrograph in Fig 5.4(b) shows the blow

holes due to escape of AlF_3 as earlier described. The open structure immediately suggests that some form of heat treatment or compaction would be necessary in order to close the porosity caused by the escape of AlF_3.

5.2 Characterisation of the starting precursor

This section looks in detail at the results obtained during the analysis of the raw precursor with an emphasis on how the results support the chemical formula that was finally given to the precursor. It shows that the analyses in total are not a replica of one another but are complimentary and considered together allowed for the inferences and deductions that are made herein.

As mentioned in section 4.1.2, the morphology of the precursor seems to suggest that the precursor is made up of predominantly two phases. The dark phase contains no titanium while the lighter phase is titanium-rich but contains aluminium. When the relative peak intensities are considered coupled with the results obtained from ICP-MS analysis, the bar chart below is constituted

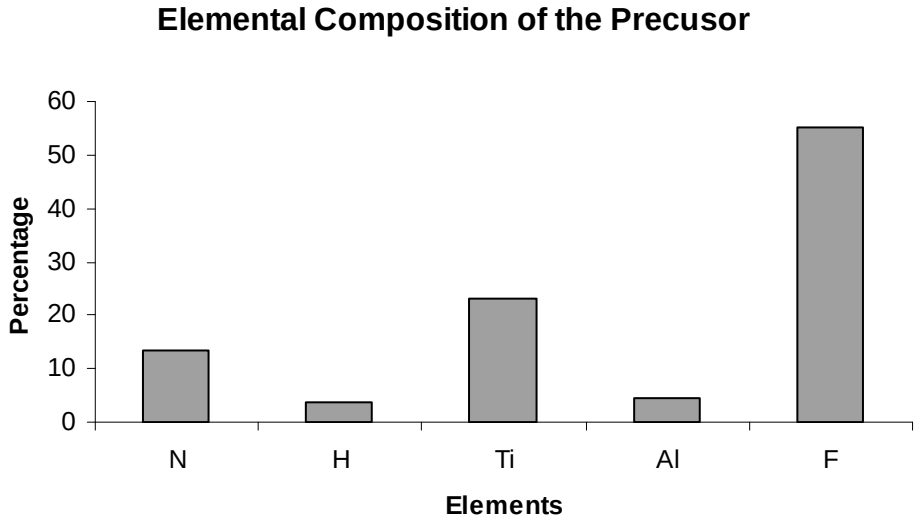


Figure 5. 5: Elemental composition of precursor determined from XRF and ICP-MS in weight %.

The chemical composition of the precursor as shown in Figure 5.5 suggests that the elements N,H,Ti,Al and F are present in the ratio 4:1:6:1:14 respectively. The closest chemical formula approximating this elemental ratio is $(NH_4)_6Ti_3AlF_{18}$. It is reasonable to argue that the precursor can be represented by the chemical formula $(NH_4)_6Ti_3AlF_{18}$ but bearing in mind that there are two phases as observed on the morphology of the SEM micrograph in figure 4.3(a) and also supported by the spot EDS spectra and XRD pattern of the virgin precursor in figure 4.4. The oxidation state of titanium according to the argument above would thus be +3.

The XRD pattern of the raw precursor in Figure 4.4 shows that the precursor is made up of two distinct phases in support of the morphology of the precursor observed in the SEM micrograph in Fig 4.3(a). The precursor comprises two salts namely NH_4TiF_4, which is almost isostructural with NH_4FeF_4, and $(NH_4)_3AlF_6$ as the second phase. It can thus be argued that the light phase in figure 4.3(a) is the NH_4TiF_4 salt (the titanium-rich phase) while the darker phase is the $(NH_4)_3AlF_6$ salt. The $(NH_4)_3AlF_6$ salt has a cubic crystal structure and the most intense peak of its XRD pattern at 18.278^o 2θ is in (111) direction while the crystal structure of the novel salt NH_4TiF_4 is unknown. However, based on the similarity of the XRD pattern of this salt to that of NH_4FeF_4, it can be argued that the crystal structures closely resemble each other. The two phases should thus be almost isostructural and the cautious deduction that NH_4TiF_4 has an orthorhombic crystal structure can be made. Further to this, considering that the titanium atom is smaller than the iron atom, it can be inferred that the lattice parameters of the NH_4TiF_4 unit cell should be smaller than of NH_4FeF_4 resulting in the cell volume

of NH_4TiF_4 also being correspondingly smaller. Table 5.1 shows the cell parameters of the salts and the calculated values for the novel salt.

Table 5. 1: lattice parameters of the three complex salts

Phase	a ($\overset{o}{A}$)	b ($\overset{o}{A}$)	c ($\overset{o}{A}$)	α, β, γ	Cell Volume $\overset{o}{A}^3$	Most Intense Peak I_o	Direction
NH_4AlF_4	3.59	3.59	6.34	90^o	82	13.867	(001)
NH_4TiF_4*	**7.54**	**7.54**	**12.64**	**90^o**	**719**	**13.868**	(002)
NH_4FeF_4	7.6	7.6	12.75	90^o	730	13.891	(002)

(* calculated values)

The lattice parameters of the novel salt NH_4TiF_4 have been approximated using the lattice spacings (d (hkl)) as determined by the X-ray diffractometer and the relationship

$$1/d^2(hkl) = \frac{(h^2 + k^2)}{a^2} + \frac{l^2}{c^2} \quad \text{.....Eqn (5.0)}$$

The *a* and *b* values were calculated in the (020) direction while the *c* value was calculated in the (002) using Eqn (5.0).

5.2.3 Thermogravimetric and thermal analysis of the precursor

The DTA trace in fig 4.4 shows three distinct endothermic peaks during the pyrolysis of the precursor in an inert atmosphere, in this case UHP argon. Heat flow peaks in any thermal analysis indicate the temperatures at which reactions, both chemical and

physical, occur. The thermal decomposition of the precursor in the temperature range from ambient to 1300^{o}C is therefore characterized by three distinct reactions. The first two peaks marked 1 and 2, in figure 4.4 and 5.12 occur at temperatures very close to each other and hence make a double peak. Since it has been shown already that the sublimation of AlF_3 from the precursor takes place at a much higher temperature, it follows that the reactions responsible for the double peak are the ones describing the decomposition of the two complex salts NH_4TiF_4 and $(NH_4)_3AlF_6$. It is also noted that the effect of these two reactions is the loss of material and hence mass from the precursor as supported by corresponding TGA curve in figure 4.4. The salts, or at least one of them, dissociate forming some volatile products. Considering the salts above, the only logical way in which the salts can dissociate is as shown in eqns (5.1) and (5.2) below

$NH_4TiF_4 = TiF_3 + NH_4F\uparrow$ Eqn (5.1)

$(NH_4)_3AlF_6 = NH_4AlF_4 + 2\ NH_4F\uparrow$ Eqn (5.2)

At 400^{o}C NH_4F is a gas, and its loss through vaporization is thus the one responsible for the observed mass loss around this temperature. The melting point of TiF_3 is 1400^{o}C and under atmospheric pressure the sublimation temperature of AlF_3 is around 1200^{o}C so the two compounds are definitely solid in the temperature range from ambient to 1100^{o}C and hence can not be responsible for the observed mass loss in this temperature range. The reaction represented by Eqn (5.1) above supports the presence of TiF_3 in the XRD pattern of product after pyrolising the precursor at this temperature (Figure 4.9). The complex salt NH_4AlF_4 is shown to be present according to the XRD pattern and in agreement with equation 5.2 above. It is concluded that the salt decomposes according

to Eqn (5.2) and that NH_4AlF_4 is formed as an intermediate salt since it does not persist beyond 700^oC. At this temperature, NH_4F is gaseous and hence is lost from the sample. Consequently, the mass loss observed between 400^oC and 600^oC is not due to one reaction but is a combination of the dissociation of the two salts. In both reactions, however, the volatile product is NH_4F. In fact, this was observed during experimentation. Above 400^oC in the tube furnace white fumes were observed and these made the bubbler water milky and persisted up to around 900^oC. The fumes persisted to higher temperatures if the furnace was ramped faster. The water in the bubbler was turned milky around 400^oC and the intensity of the colour increased with time. The mass losses that were observed at the various soaking temperatures are listed in table 5.2 and compared to the theoretical expected. The table also shows the elemental and phase compositions of the residues obtained after soaking at these temperatures.

Table 5. 2: ***Mass losses and residue composition at various soaking temperatures***

Temperature/^{o}C	Theoretical mass loss/%	Observed mass loss/%	Elemental composition of residue (EDS)	Phase composition of residue (XRD)
380	12	13	F,N,Al,Ti	NH_4AlF_4, NH_4TiF_4
500	38	43	F,N,Al,Ti	NH_4AlF_4, TiF_3
600	45	45	F,N,Al,Ti	NH_4AlF_4, TiF_3
700	46	45	F,Al,Ti	AlF_3, TiF_3
800	46	45	F,Al,Ti	AlF_3, TiF_3
900	46	47	F,Al,Ti	AlF_3, TiF_3
1000	46	47	F,Al,Ti	AlF_3, TiF_3
1200	46	55	F,Al,Ti	AlF_3, TiF_3
1300	55	75	Ti, F	TiF_3

The extra 20wt% loss was attributed to the volatilization of TiF_3 although facilities to test the assertion were not present.

5.2.3 XRD Analysis of products of pyrolysis

The XRD pattern of the product obtained after pyrolising the precursor at 400^{o}C supports the argument given above. Fig 4.8 shows that the product is made up of two phases namely TiF_3 and NH_4AlF_4 and since the phases in the original precursor are NH_4TiF_4 and $(NH_4)_3AlF_6$ it follows that TiF_3 is formed from the dissociation of NH_4TiF_4 and that NH_4AlF_4 is as a result of the dissociation of the other salt as represented by eqns (5.1) and (5.3) respectively. The XRD pattern at 700^{o}C shows that

intermediate salt NH_4AlF_4 is no longer present in the product. Instead AlF_3 is matched as the present phase. The salt NH_4AlF_4 thus thermally decomposes between 600 and 700^oC forms AlF_3 as represented by Eqn (5.4) below

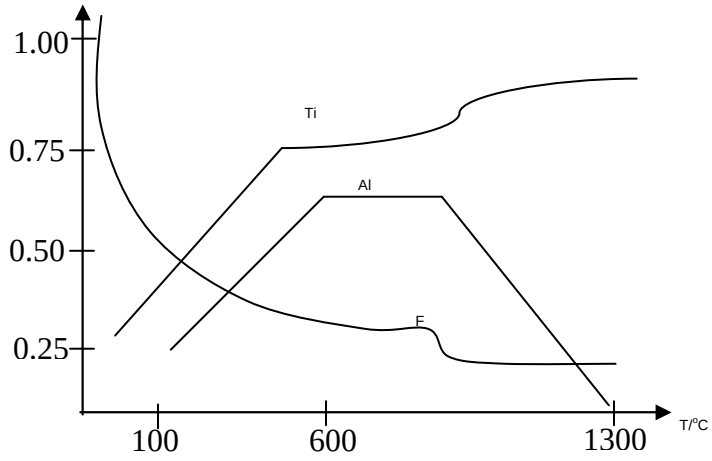
$NH_4AlF_4 = AlF_3 + NH_4F \uparrow$ Eqn (5.4).

This reaction explains the further mass loss observed after the double peak. The product persists as TiF_3 and AlF_3 with no further chemical changes observed except that above 1100^oC the AlF_3 starts to sublime. This is supported by the endothermic peak on the DTA curve and the corresponding mass loss observed around this temperature on the TGA/DTA curve in figure 4.4. This is further supported by the decrease in the peak intensities of AlF_3 in the XRD patterns from 1000 to 1300^oC in figures 4.14(b), 4.16(b) and 4.18(b). It is interesting to observe that the salt $(NH_4)_3AlF_6$ plays no positive role in the process as it does not contain the metal of interest, Ti. In fact its presence is detrimental to the final yield and quality of the final product obtained as will be discussed later in this chapter.

5.2.4 SEM Analysis of products

Although the EDS spectra of the products show the same elements Al, Ti and F, the proportions of these change continually from ambient temperature to 1300^oC. Considering the EDS spectra of the original precursor in Figure 4.3 up to that of the product after decomposing the precursor at 1000^oC, shown in figure 4.14, it is evident that the intensities of the peaks of Ti and Al increase significantly at the expense of that of fluorine. This is understandable since in this temperature range the main volatile product is NH_4F. So, the ammonium fluoride carries away the fluorine leaving the product depleted of fluorine but richer in titanium and aluminium. In a way the

precursor is beneficiated through its decomposition and vaporization of the volatile material since these do not contain titanium. A graphical representation of the variation of the EDS peak intensities of Ti, Al and F from ambient temperature to 1300^{o}C is shown in figure 5.6(a). A similar plot but considering the peak intensities of all the phases observed in the XRD patterns of products of pyrolysis is given in figure 5.6(b).



(a)

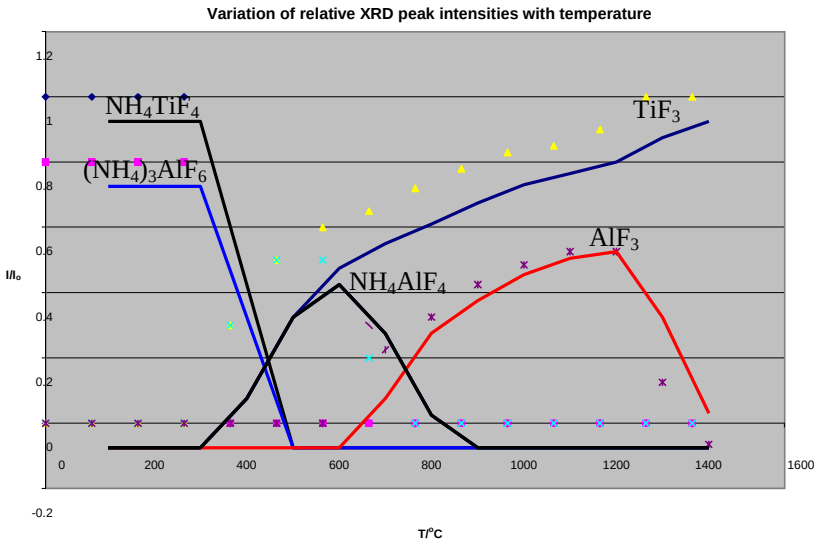


Figure 5. 6 (a) Variation of EDS peak intensities (b) Variation of XRD peak intensities with Temperature

5.3 Optimization of gas linear flow rate

The percentage variation of the total mass loss from the precursor after pyrolysis under varying gas flow rates was also an important indication of the effectiveness of the gas flow in carrying away the volatile products. The data in table 4.3 is plotted in figure 5.7 below to show mass loss variations with the flow rate of UHP argon.

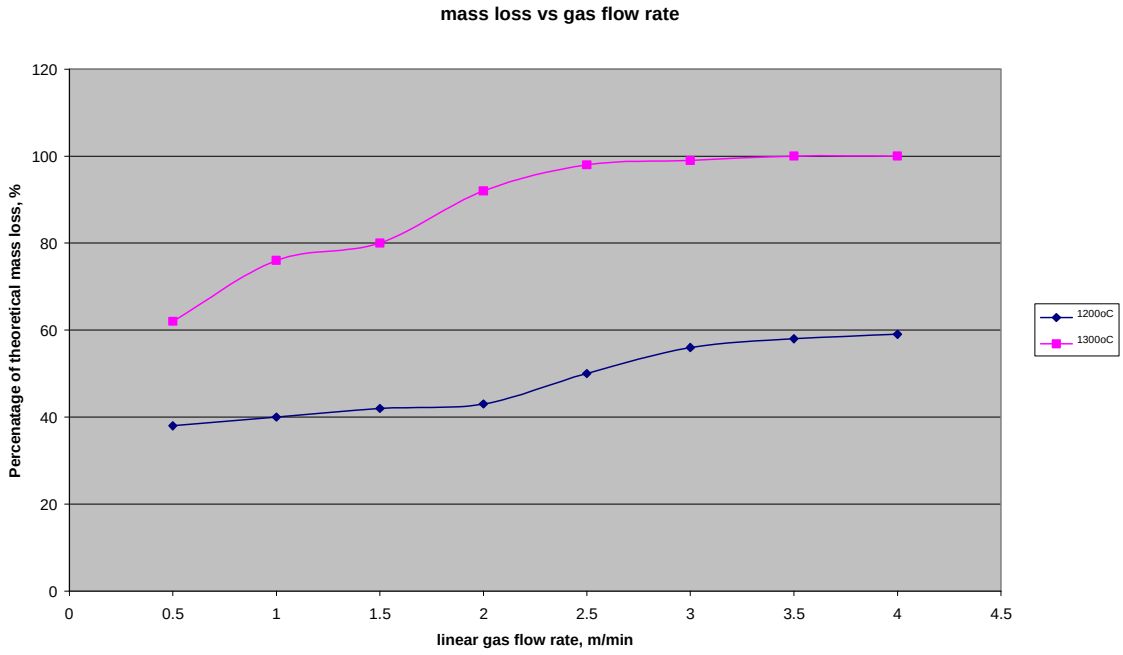


Figure 5. 7: **Variation of mass loss with gas flow rate at 1300^{o}C after soaking for 2 hrs**

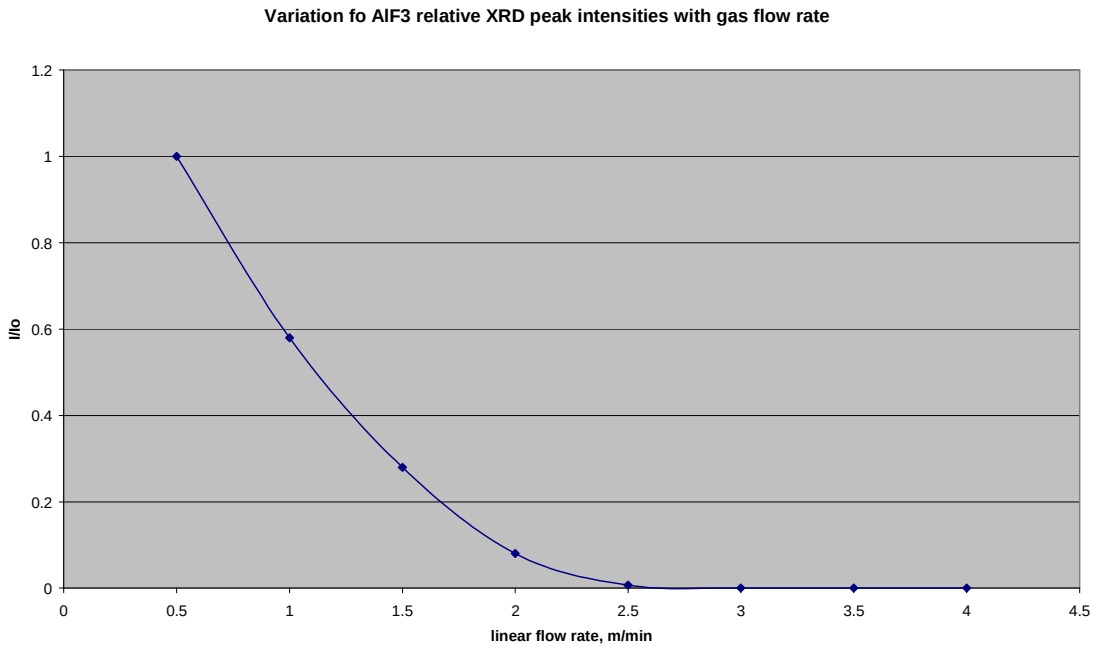
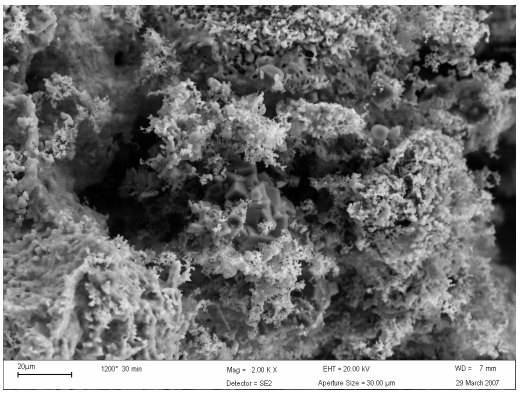
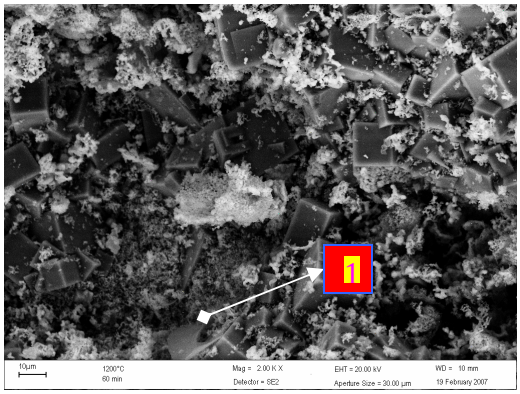


Figure 5. 8: Variation of AlF_3 XRD intensities normalised to its value at 0.5m/min with gas flow rate at 1300^{o}C

Apart from providing an inert atmosphere over the precursor and product, the inert gas also served as a carrier gas removing all volatile products from the reaction zone. In order not to have equilibrium being established, the inert gas has to have enough momentum to carry away the products from the vicinity of the reactants and hence keep the driving force of the reactions in the desired direction. At very low linear flow rates the level of the remaining AlF_3 in the product is highest owing to less transport. This is further supported by observing the SEM micrographs below. Below the threshold gas linear flow rate, instead of the amount of AlF_3 in the product decreasing with time it does not. In fact the grains even coarsen with time and grow in to larger cubic crystallites.

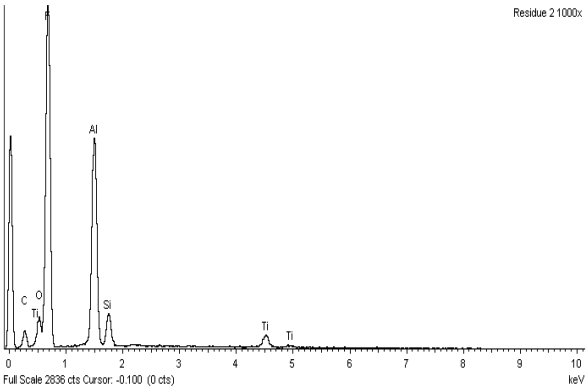


(a)



(b)

Figure 5. 9: **SEM micrographs of product (a) 1.3m/min 10 minutes (b) 1.3 m/min 60 minutes at 1300^{o}C**



(c) EDS for spot 1

Since the momentum of the inert gas is not adequate to sweep away the AlF_3, the partial pressure of AlF_3 above the product rises resulting in a drastic reduction in the rate of sublimation of the AlF_3 remaining in the product. As soaking time increases the AlF_3 particles coalesce through bigger particles cannibalizing smaller ones to form much coarser particles by Ostwald ripening or gas-phase transport through vaporization and condensation as shown in Fig 5.9(b). On the contrary when the linear flow rate is such that its momentum is enough to carry away the volatile products, the partial pressure of

AlF_3 is kept low and hence the driving force remains in the direction of sublimation. Thus with time the amount of AlF_3 in the product decreases and ideally should come to zero as shown in figure 5.10.

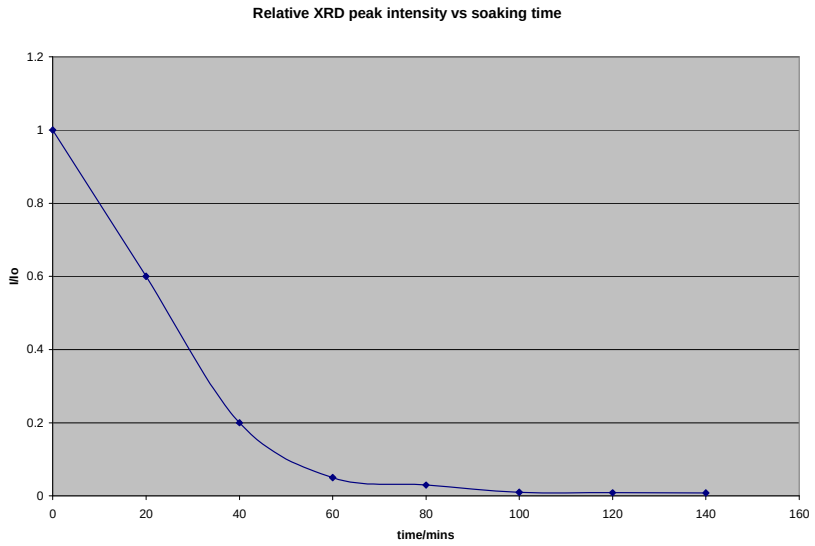


Figure 5. 10 (a): **Variation of AlF_3 relative peak intensities with soaking time at 1300^{o}C and 2.6m/min gas linear flow rate.**

The linear flow rate (flux) of the inert gas should thus be, for the experimental arrangement used in this study, above 2.6 m/min in order for the stream to have enough momentum to carry away the volatile products from the reactor. Volumetric flow rate is the same on any section of the system but the linear flow rate will vary according to cross sectional profiles. However, the flow rate alone is not a sufficient condition for the removal of AlF_3 from the product. The temperature should be high enough for the aluminium fluoride to have sufficient vapour pressure. Figure 5.10 (b) below shows the influence of temperature and linear flow rate on the removal of aluminium fluoride from the product.

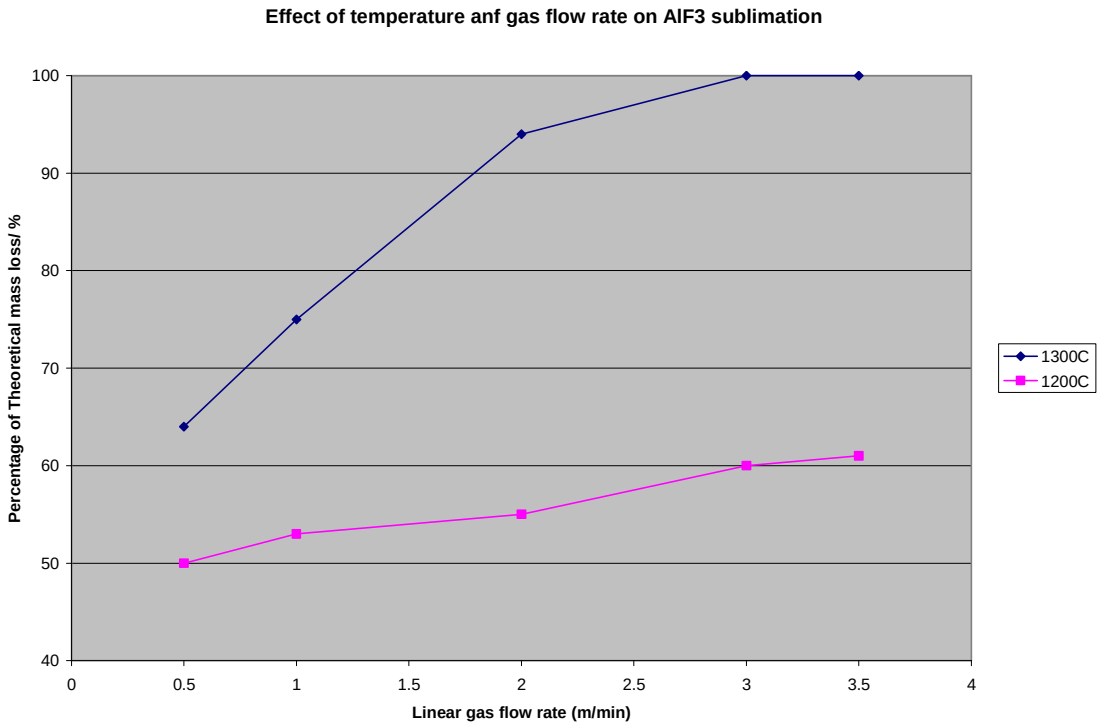


Figure 5.10 (b): Effect of temperature and gas flow rates on the sublimation of AlF_3

5.4 Reduction of the precursor with aluminum

Before reduction of the precursor but after pyrolising at any temperature between 700 and 1300^{o}C it is noted that there are only two phases in the product. Firstly, the SEM micrographs, particularly after 1000^{o}C, show two distinct phases (refer to figures 4.16 and 4.18). The cubic crystals represent AlF_3 while the other phase is TiF_3. Fluorine thus exists in two completely different forms. After subliming off almost all the AlF_3 at 1300^{o}C for 2 hours the morphology no longer shows the cubic crystallites but the EDS spectrum still shows that fluorine is present. The reduction of TiF_3 with aluminum is thermodynamically feasible. Considering the reduction reaction represented by eqn (5.7) below

$TiF_3 + Al = Ti + AlF_3$ eqn (5.7)

The reduction step is also observed on the superimposed TG/DTA traces of a stoichiometric mixture of the precursor and aluminium and of the pure precursor shown in figure 5.11 below

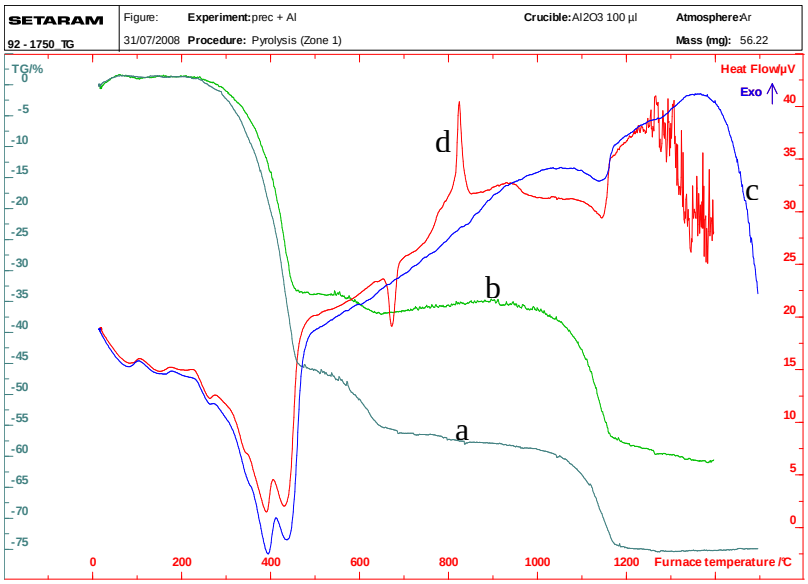


Figure 5. 11: **Superimposed TG/DTA traces of precursor and premixed with Al**

Key: a: TG curve of the raw precursor

b: TG curve of the precursor premixed with 12% Al

c: DTA curve of the virgin precursor

d: DTA curve of the precursor mixed with aluminium

The only striking difference in figure 5.11 is that there are additional endothermic peaks at around 665^{o}C and an exothermic peak around 800^{o}C in the sample with aluminium in comparison to the precursor otherwise the TGA and DTA profiles are very similar. This is understandable considering that the other sample has Al (curve (d)). The extra endothermic peak at 665^{o}C marks the melting point of aluminium

(theoretical mp=660.32^{o}C) [41] while the exothermic peak at around 815^{o}C marks the reduction reaction represented by Eqn (5.7).

5.4.1 Characterisation of the titanium product

The EDS spectrum and XRD pattern of the product after heat treating the precursor mixed with aluminium at 800^{o}C confirm that reduction takes place. Only titanium is detected by EDX spectrometer with very minimal amounts of aluminium and fluorine. The XRD pattern further confirms that the product is elemental titanium, JPSCD card number 00-044-1294. As has been mentioned before, the sublimation of AlF_3 from the powder is diffusion controlled. It was also observed that at 1300^{o}C the produced titanium powder pressurelessly sinters forming a weakly aggregated mass. The effect is thus to lock up the remaining AlF_3 in the structure and close the many diffusion paths that were earlier available in the unsintered powder. The diffusion paths that AlF_3 could traverse to the product surface thus become constricted and limited making the process progressively difficult. Continual agitation of the powder, for example in a rotary kiln, is thus necessary but could not be implemented in our set up. Agitation would break the aggregates formed and would expose the AlF_3 to the powder surface thus lessen the mean diffusion path that the AlF_3 would have to traverse. The effect of agglomeration of the powder on the diffusion rate and hence the reminiscent AlF_3 after soaking is shown in the schematic in figure 5.12.

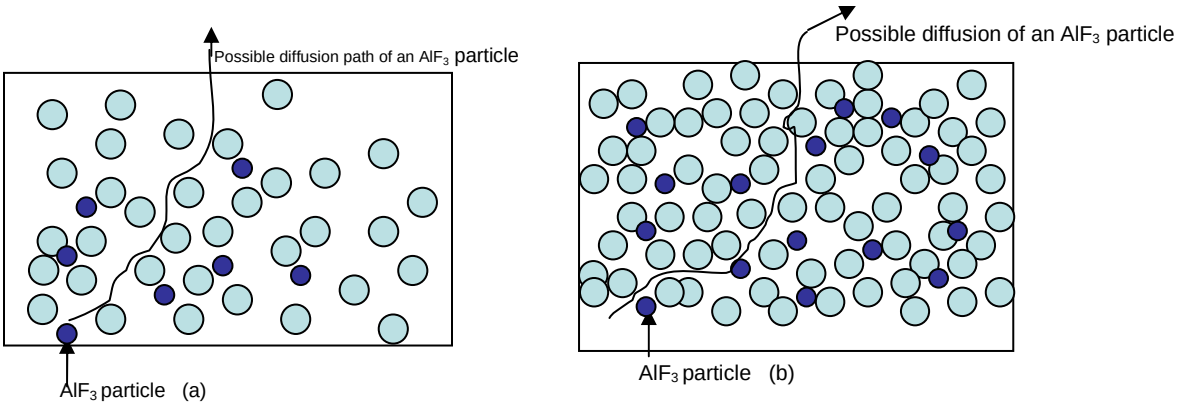


Figure 5. 12: **Schematic of (a) Unsintered product and (b) sintered product**

The progress of the sublimation with temperature is shown graphically in figure 5.12(c). The peak intensities of AlF_3 at 25^o two theta were measured for products that had been obtained from heat treating the precursor at temperatures ranging from 1100^oC to 1400^oC for two hours.

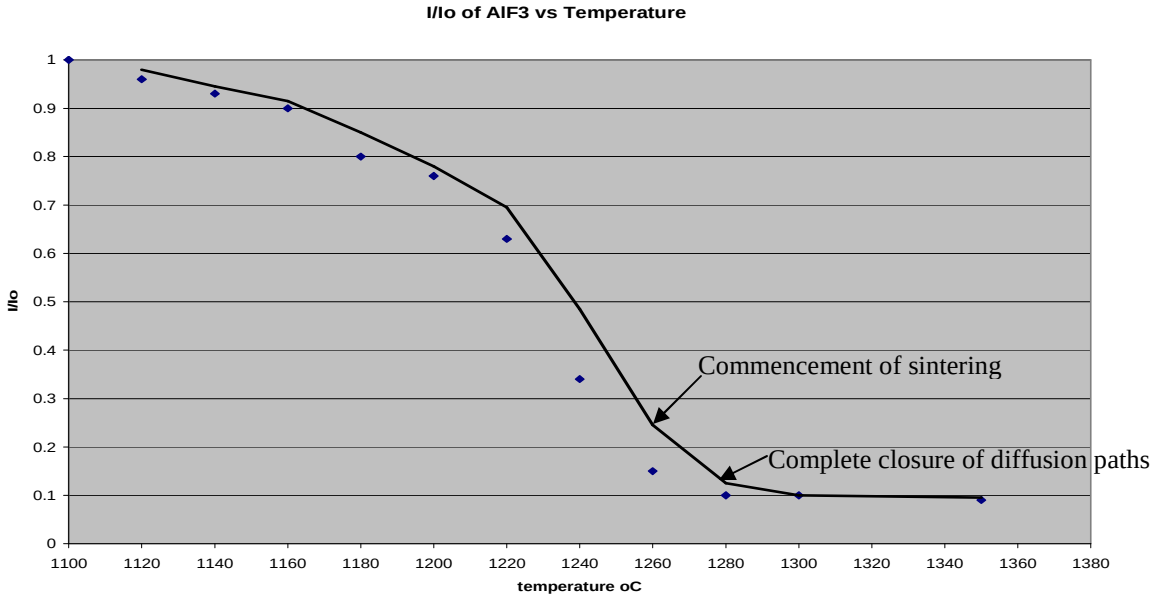


Figure 5.12c: Variation of AlF_3 XRD relative peak intensities with soaking temperature

It was also noted that the final titanium product shows XRD peak shifts suggesting some solvation of smaller atoms in to its unit cells, probably oxygen. The table below compares the XRD peak positions of the product and those expected. The shifts might, however, be due to aberrations of the XRD machine itself.

Table 5. 3*: XRD Peak positions of the product and cp titanium*

Peak Position/2theta	**First peak**	**Second peak**	**Third peak**	**Fourth peak**
Cp Titanium (00-44-1294)	35.094	38.422	40.177	53.005
Product	34.950	38.300	40.050	52.850
(hkl)	(100)	(002)	(101)	(102)
Difference/ 2 theta	0.144	0.122	0.127	0.155

Apart from the 2theta angles of the first peaks, the peak positions show a trend of shifting further to the left as the angle increases. This is common in cases where the unit cells are distorted due to the solvation of a phase into the system. Considering the Bragg equation $n\lambda = 2d\sin\theta$ in the format $\sin\theta = n\lambda/2d$, it is noted that once there is a peak shift the angle of shift will increase as the angle increases. It is arguable therefore that some form of interstitial solution occurs during the processing of the powder. The EDS spectrum of the product in figure 4.22(b) shows a small peak of Al, and it is possible that it is the one responsible for the observed peak shift. The difficulty in accepting the argument is that Aluminium is known to substitutionally alloy with

titanium as its atomic radius is too large for its atoms to fit into the interstices of titanium unit cells. The other problem that might be associated with and responsible for the observed XRD peak shifts and the reminiscent aluminium in the product is that TiF_3 has a high partial pressure at all temperatures and hence tends to vaporize in preference to AlF_3. However, the kinetics is not known hence it might not vaporize at all in the temperature that this work was conducted. Figure 5.13 below is a computer generated thermodynamic graph using the Fact Sage software showing the vapour pressure of gases formed when titanium is in contact with AlF_3 in a molar ratio of 2:1 in argon. Further to the high vapour pressure of TiF_3 relative to AlF_3, the reduction reaction in eqn (5.7) is thermodynamically reversible as shown in eqn (5.11) below

$TiF_3 + Al \Leftrightarrow Ti + AlF_3$ Eqn(5.11)

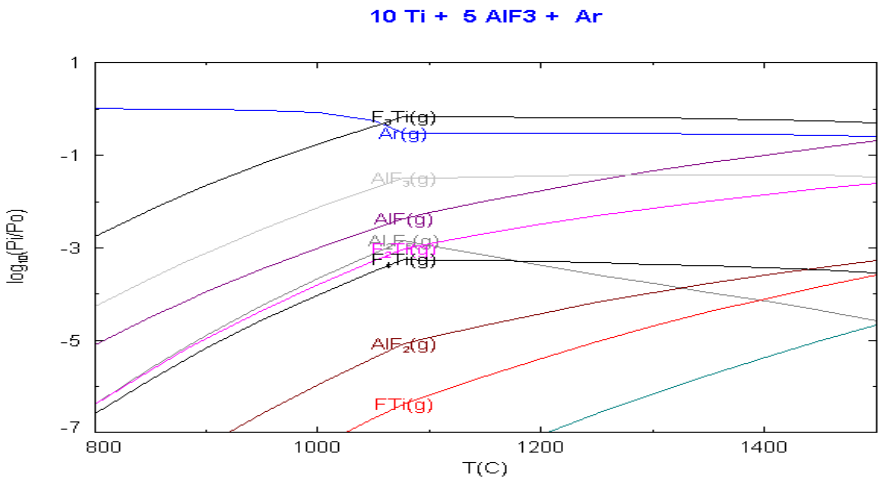


Figure 5. 13: **Variation of vapour pressure of Ti fluorides and Aluminium fluorides with Temperature (computer generated using an SGTE database)**

The implication of eqn (5.11) and figure 5.13 above is that it is possible that once the titanium is formed some of it might react with the AlF_3 present forming TiF_3 and elemental aluminium. The formed TiF_3 might then sublime off leaving the aluminium

dissolved in the titanium as excess. This might be the reason for the small Al peak observed in the EDS spectrum of the product. As the thermodynamics data in figure 5.13 show, TiF_3 has quite a high vapour pressure, higher than that of AlF_3. This would explain the excessive mass loss during the pyrolysis of the precursor of over 80%. Some of the titanium is lost as the TiF_3 evaporates.

5.5 Kinetics Studies

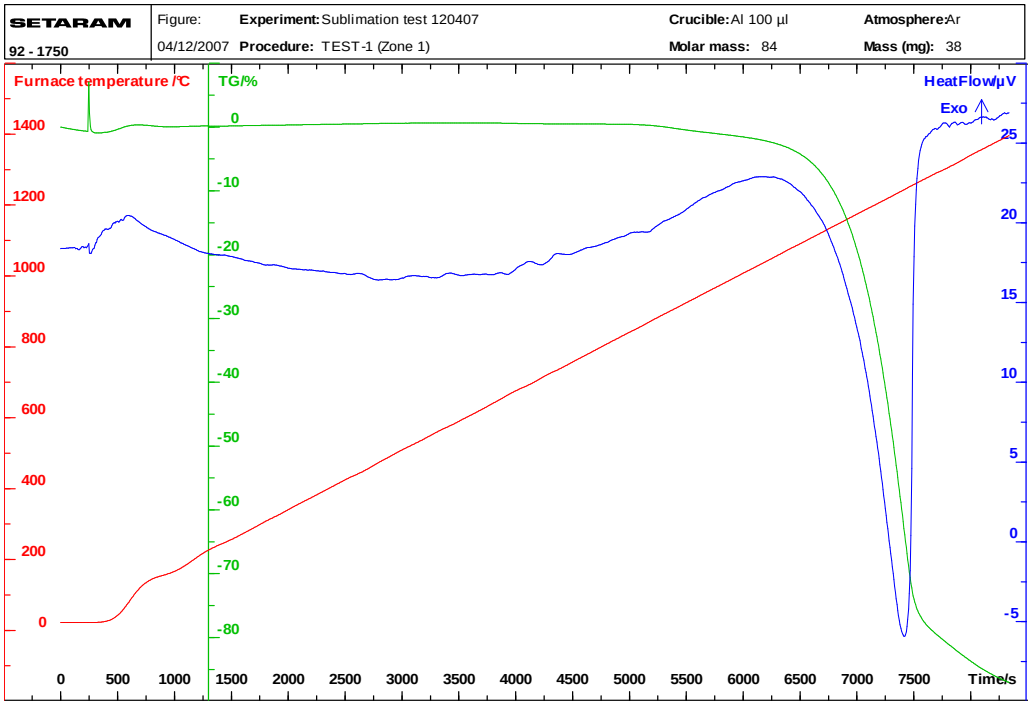


Figure 5. 14: TGA-DTA trace of pure AlF_3

The TG trace in figure 5.14 can be used to approximate rate of sublimation of AlF_3 once the process has commenced. From the TG graphs in all cases where sublimation occurs, and more importantly for the isothermal sections of the graphs, it is apparent that the graphs are linear in which case a relationship of the type $m=m_0-kt$ can be derived where m_0 is the starting mass, in this case 100%, and k is the rate constant

which will depend on temperature. The relationship has been derived for 1100, 1200, 1250 and 1300^{o}C and the rate constants then plotted against the inverse of their absolute temperature according to the Arrhenius equation. The rate constants k for various temperatures is shown in table 5.3 below. These are the constants for the general rate equation

Table 5. 4: ***Rate constants in mg/s for various soaking temperatures***

Temperature/ ^{0}C	**Rate constant mg/s**
1100	0.0225
1200	0.123
1250	0.229
1300	0.27

Most of the TG-DTA runs were conducted with an average mass of 20mg. Shown below is a plot of "half lives" versus mass at a given temperature and for various temperatures.

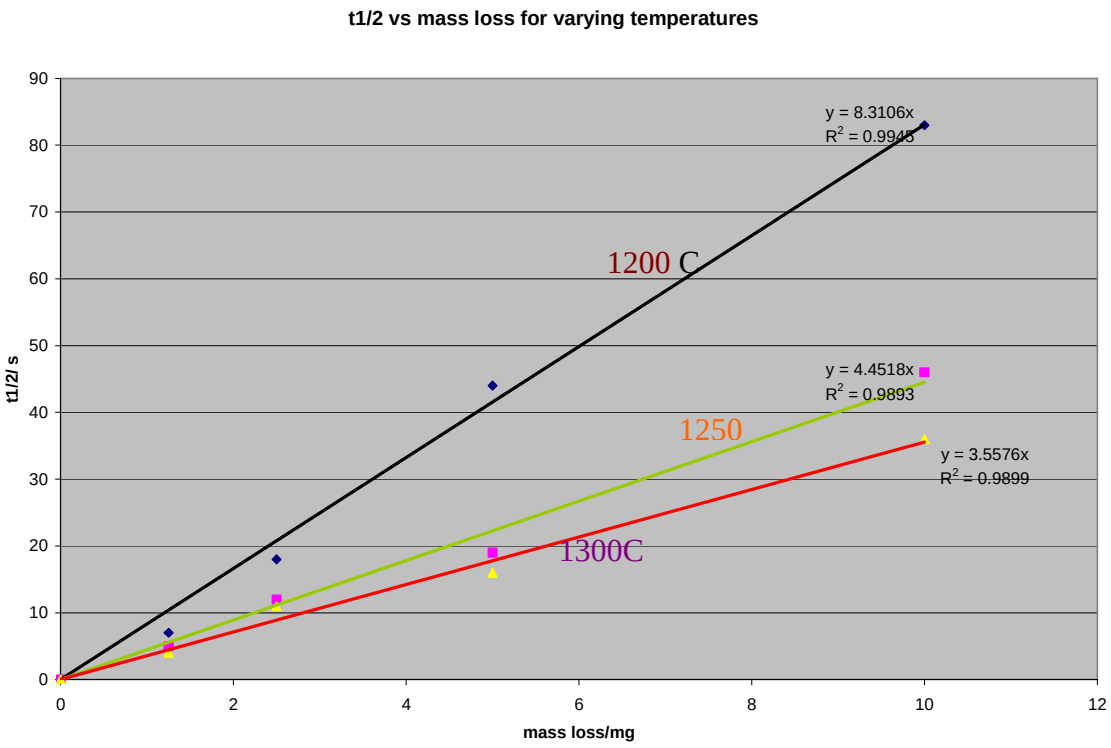


Figure 5. 15: $t_{1/2}$ **vs. mass loss for varying temperatures**

The half life increases with decreasing temperature and increasing initial mass of the AlF_3. It is important to note the rate of mass loss increases ten fold when temperature is raised from 1100C to 1250^{o}C. The natural logarithms of the rate constants in the above cases were plotted against their corresponding inverse absolute temperatures to obtain an Arrhenius plot in figure 5.16.

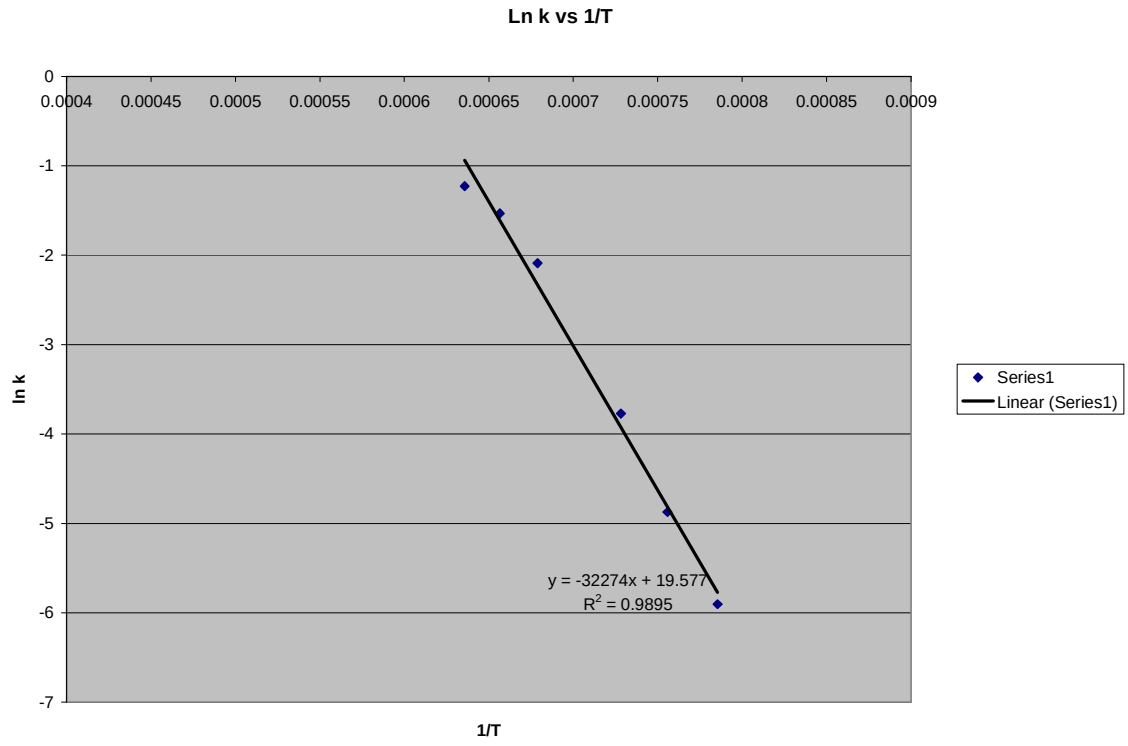


Figure 5. 16*:* A plot of natural log of rate constants versus the inverse absolute T/K

$\frac{d(1/T)}{d(\ln k)} \approx -3.2274\times10^{4}$. The extrapolated intercept, $\ln k_0 = 19.577$. It follows then that

(i) $\frac{E_A}{R} \approx 3.2\times10^{4}\,\mathrm{K}$ and ii) $E_A \approx 268.2 kJ/mol$

$k_i \approx 3.178\times10^{8} e^{-32274/T_i}$ …….eqn (5.12)

Where k_i is the rate constant at temperature T_i and the activation energy $E_A \approx 268 kJ/mol$ **.**

The equation governing the rate of sublimation of AlF_3 at a given temperature T_i is thus governed by equation 5.13

$X_{AlF_3} = 1 - \frac{3.178 \times 10^8 e^{-32274/T_i}}{m_0} t$. ……Eqn (5.13), where X_{AlF_3} is the mass fraction of AlF_3 remaining after t seconds at a temperature T_i. The mass that sublimes in mg at a given temperature T_i after t seconds is thus

$m_s = 3.178 \times 10^8 e^{-32274/T_i} t$ (mg/m^2/s)…….. Eqn (5.14)

The calculated vapour pressure over AlF_3 in Fig. 5.17 fits well with the experimental data. The sublimation temperature is the temperature at which the vapour pressure of the AlF_3 equals the external pressure, $P_i / P_0 = 1$.

Our experiments were conducted under almost atmospheric conditions implying that the sublimation temperature of AlF_3 corresponds to the temperature at which of AlF_3 is 1 atm.

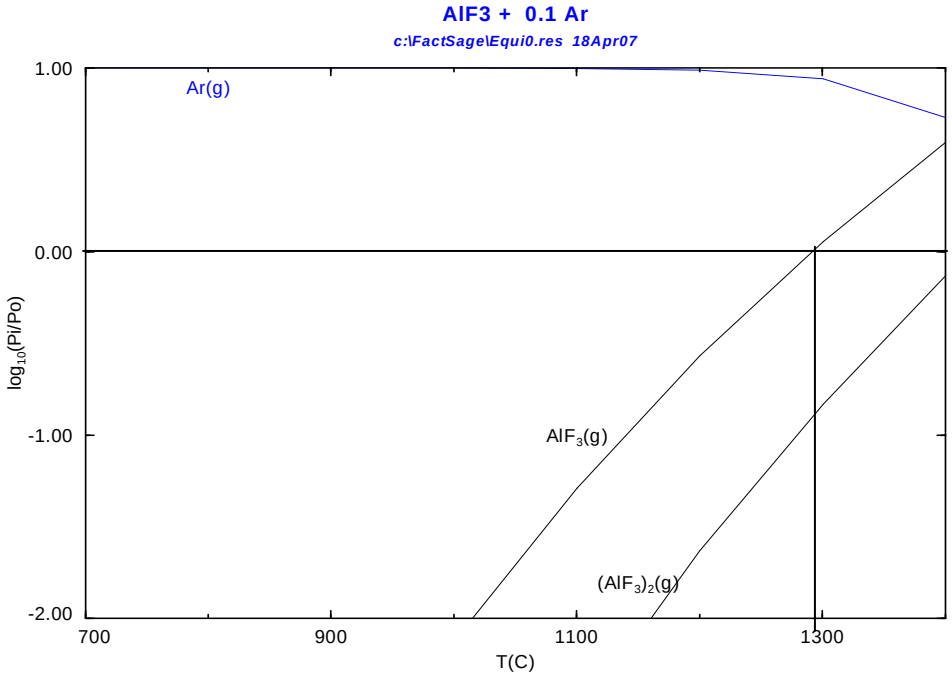


Figure 5. 17: Vapour pressure over AlF_3 as a function of temperature

It is important to notice that both the experimentally determined activation energy and sublimation temperature are in close agreement with theoretical values. The need to raise temperature is necessitated by the need to sublime off the formed aluminium fluoride. The reduction of the precursor has been shown in figure 5.11 to occur at a temperature as low as 800^{o}C and consequently the raising of temperature by a further 500^{o}C is purely for product refinement. This obviously adds on to energy costs associated with the process and becomes one of the disadvantages. It is also this step which exposes the titanium product for extended time periods to high temperature conditions and hence partial oxidation by traces of oxygen in UHP argon. It is also the same unit process associated with the emission of the aluminium fluoride. During the course of the work a number of other differently processed titanium precursors were encountered and it was observed that whenever the phase $(NH_4)_3AlF_6$ was dominant the processing of the precursor became problematic due to excessive aluminium fluoride. So although the positive effects of aluminium fluoride have been well documented and claimed in the patent [1], its excessive presence in the precursor makes the extraction of titanium difficult.

5.6 Recovery of titanium

The titanium content of the precursor is naturally low, at roughly 20% as earlier discussed, and this naturally lowers the yield achievable. The majority of the material that makes up the precursor is lost as gaseous byproducts during heating resulting in a titanium concentrate in the form of TiF_3. Ideally, it would be advantageous and far

better if the precursor could be pyrolysed to TiF_3 and stockpiled as such as this would remove the burden of dealing with bulk materials and low yields. However the recovery of the titanium present in the precursor was very high. Table 5.4 shows the starting precursor and the amount of the titanium formed therefrom. The recovery is calculated using equation (5.15).

Table 5. 5: ***Composition of precursor and of the titanium product from ICP-MS***

Material	**Mass/g**	**%Ti contained**	**Mass of Ti/g**
Precursor	10.00	22.00	2.200
Final Product	2.25	93.8	2.112
AlF_3 byproduct	1.70	5.18	0.088
$NH_4F + TiF_3$*	6.05	0.00	0.000

(* Calculated based on the law of conservation of mass)

If the recovery of titanium is denoted as R_{Ti} then

R_{Ti}= mass of titanium in the product (P_{Ti})/ mass of titanium in the precursor (Pr_{Ti}) or

$R_{Ti}= P_{Ti}/Pr_{Ti}$ …… eqn (5.15)

R_{Ti}= 2.112/2.2 x 100%= 96%.

Recovery is not 100% because, as shown in table 5.4 above, part of the titanium is found in the AlF_3 byproduct collected in the water bubblers. This might not be exactly due to the process but as a result of the experimental set up that was employed. It is possible that due to the high vapour pressure of TiF_3 above 1000^oC, titanium is lost due to the sublimation of TiF_3

A grade of 93.8% for the titanium is understandable noting that no refinement was done on it. The major reason for this relatively low grade is the presence of traces of AlF_3 in the product due to lack of proper facilities to effect complete sublimation of the AlF_3. The reasons for the presence of AlF_3 in the final product are two fold. Firstly, it was deliberate and required that traces of AlF_3 be left in the product so as to raise the spontaneous ignition temperature of the titanium. Secondly, the product partially sinters during the extraction process making the egress of any remaining AlF_3 difficult.

5.8 Summary and proposed process flow sheet

The results and discussion presented can be summarized in the flow sheet in figure 5.18.

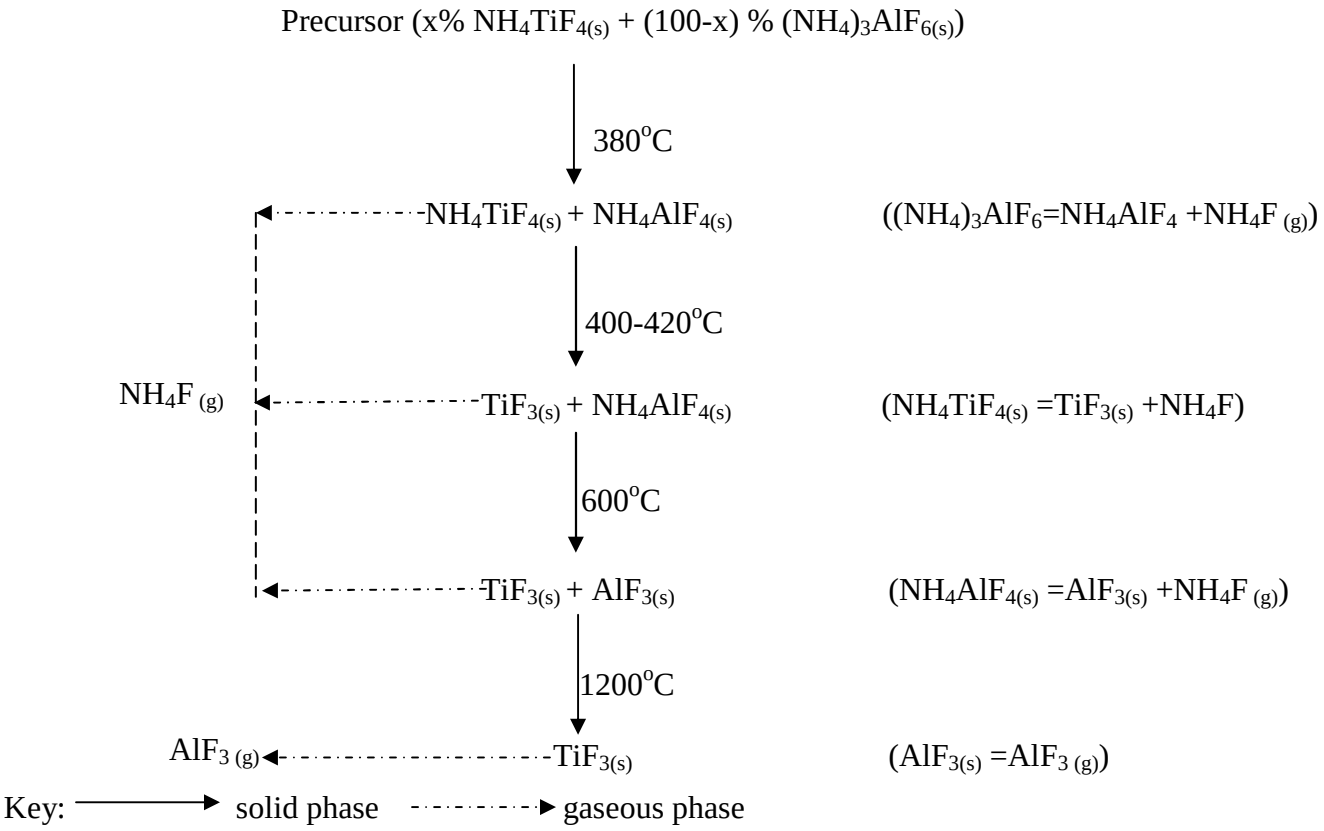


Figure 5. 188: Flow sheet for the pyrolysis of the titanium precursor

The flow sheet in figure 5.18 shows the thermal decomposition of the precursor. The final product, which is also the product of interest, is $TiF_{3(s)}$ while the two byproducts are NH_4F (g) and AlF_3 which is collected in the water bubblers as a white powder. The two byproducts can be further processed as shown in the flow sheet in figure 5.19. The

NH_4F can be treated with aqueous hydrochloric acid to form ammonium chloride and hydrofluoric acid as shown in equation 5.15

$NH_4F_{(g)} + HCl_{(aq)} = NH_4Cl_{(aq)} + HF_{(g)}$ ……. Eqn (5.15)

The $HF_{(g)}$ is thus regenerated and fed back to the system for the digestion of the precursor. It is also clear from the flow sheet that $(NH_4)_3AlF_6$ does not play a role in the production of the Titanium. Its presence lowers the possible yield and results in the generation of excessive AlF_3. It is thus important that during the production of the precursor itself effort be made in ensuring that there is minimal $(NH_4)_3AlF_6$ and that the ratio of the two phases (NH_4TiF_4)/ $((NH_4)_3AlF_6)$ be as high as possible. If that is achieved then the yield will be higher, soaking times to allow sublimation of AlF_3 will be reduced. The chances of then exposing the titanium to incidental oxygen at high temperature will thus be lowered significantly. The production of Ti from the precursor can be done in two ways. Either the precursor can be premixed with a stoichiometric amount of aluminium or the TiF_3 from pyrolysis can be mixed with aluminium and heated to between 800 and 850^oC for reduction. The flow sheet remains exactly the same as the one in figure 5.26 except that between 800 and 850^oC the TiF_3 is reduced to Ti. Figure 5.19 shows the difference

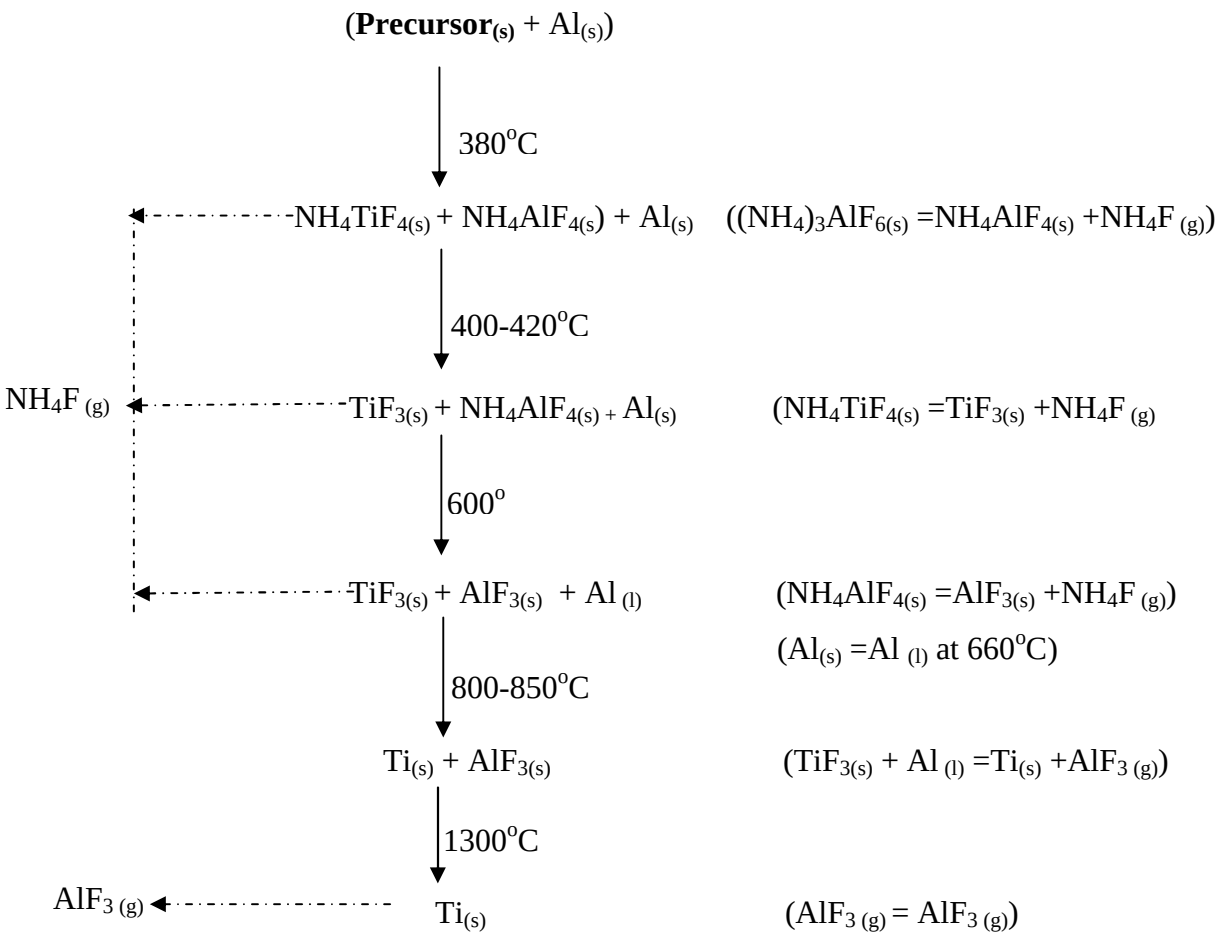


Figure 5. 19: Flow sheet of the process with the precursor premixed with Aluminium

Chapter 6: Conclusions and Recommendations

6.0 Conclusions

The novel titanium precursor salt can be processed to produce titanium. The simple steps of thermal decomposition followed by reduction with premixed aluminium are adequate to produce a reasonable grade of titanium. It has also been shown that apart from being an extractive process, the patented process has the big advantage of being able to self clean the product without need for a separate separation stage as in the case of other metals and their slags. The advantages of powder metallurgy are also apparent in this particular case. The process is also much faster than the Kroll process, which takes several days to run to completion. In general the following conclusions can be drawn from the work that was carried out and the observations that were made

(1) The precursor is a mixture of two complex salts namely $(NH_4)_3AlF_6$ and NH_4TiF_4.

(2) The two salts decompose between 380 and 500^oC to yield AlF_3 and TiF_3 respectively and both lose NH_4F as a gas

(3) In the presence of aluminium, the aluminium melts and wets the mixture around 665^oC and then reduces the TiF_3 to Ti around 830^oC

(4) After the reduction it is necessary to raise the temperature to above 1200^oC in order to sublime off AlF_3 so as to remain with pure titanium

(5) The soaking time required for complete sublimation is dependent on the surface area of the reactor (holding boats), bed thickness and gas linear flow rate. In this case was determined to be between 45 and 60 minutes

(6) At a low scanning rate of 5^{o}K/minute, the process is complete within 10 hours. Higher scanning rates or preheated reactors should be able to achieve shorter residence periods

(7) The product particle size distribution has a wider range than the precursor but on average the product is finer. The few large particles associated with the product have been attributed to sintering.

(8) There seems to be some dissolution of aluminium in the titanium product as supported by the XRD peak shifts and the small peak of aluminium in the EDS of the product as was observed on the SEM images of the product.

(9) Simple chemical vapour deposition (CVD) of AlF_3 on the titanium product is not enough to adequately passivate the titanium from spontaneous ignition due to the heterogeneous nature of the coating

(10) The salt NH_4TiF_4 has an orthorhombic structure and has lattice parameters whose values are very close to those of NH_4FeF_4. Its XRD pattern does not exist in the current databases but is very similar to that of NH_4FeF_4.

(12) The data given in the patent concerning the conditions necessary for the processing of the precursor to titanium are confirmed. However, the claim that leaving a small amount of AlF_3 on the titanium product can passivate titanium has been questioned as the coating in this work has been shown to be discontinuous.

6.1 Recommendations

Based on the observations that were made in the work conducted with the precursor salt the following can be recommended

(1) Since it is TiF_3 that ultimately bears the metal of interest, it is recommended that the precursor be pyrolysed and stockpiled as TiF_3. This way the material will not degrade over time as does the current form of the precursor and, secondly, less bulky materials will be handled during the extraction process proper. The issue of excessive AlF_3 will also be eliminated and shorter soaking times at 1300^oC will become feasible

(2) A method should be devised to allow for some form of agitation of the reactants during the sublimation stage of the extraction process. Apart from improving mixing, it is very important in breaking lumps that form as the product sinters at high temperature. Avoiding sintering of the product will eliminate the problem of remaining AlF_3. One possibility could be to make the sublimation step a separate process on its own and use a fluidized bed or rotary kiln.

(3) High temperature scan rates or preheated reactors should be employed to make the process as short as possible and to avoid holding titanium for extended periods at high temperature

(4) Refinement of the product is necessary in order to obtain grade 1 titanium. Multiple remelting in vacuum could be one possibility.

(5) Ultra high purity argon with no traces of oxygen or nitrogen should be used throughout as even trace quantities of these in the order of ppm are enough to partially nitride and oxidise the titanium product.

References:

1. **G.Pretorious**, *A method of producing titanium, WO2006/079887, 2006, pp 1-45*
2. **C.Leyens and M.Peters,** *Titanium and Titanium alloys: Fundamentals and Applications, Wiley-VCH Verlag GmBH &Co, 2003*
3. **M.Jackson and K.Drung,** *A review of advances in processing and metallurgy of titanium alloys, Materials science and technology, Vol.2, 2006,pp1-13*
4. **E.M.M.Sutter and G.J.Goetz-Grandmont,** *The behaviour of titanium in nitric-hydrofluoric acid solutions, Corrosion Science vol. 30, 1990, pp 461-476*
5. **H.Sibum,** *Titanium and Titanium alloys-From raw materials to semi-finished products, Advanced Engineering materials, Wiley-VCH Verlag GmBH &Co,2003, pp 393-397*
6. **V.Biehl, T.Wack, U.T.Seyfert and J.Brene,** *Evaluation of the haemocompatibility of titanium based biomaterials, Bimolecular Engineering vol19, 2002, pp 97-101*
7. **S.J.Gerdemann,** *Titanium Process Technologies, Journal of Advanced materials and processes, July 2001,pp1-11*
8. **W.J. Kroll,** *A contribution to the history of ductile titanium and zirconium, Journal of the less common metals, 1964, pp 361-367*
9. **G. Z. Chen, D. J. Fray, T. W. Farthing (2000*).* *Direct Electrochemical Reduction of Titanium Dioxide to Titanium in Molten Calcium Chloride,pp2-9*
10. **Wood and Holliday,** *Physical Chemistry: an intermediate course, Butterworths, 1960, pp163-187*

11. **M.Palm, L.Zhang, F.Stein and G.Sauthoff,** *Phases and phase equilibria in the Al-rich part of Al-Ti system above 900^{o}C, Intermetallics, 2002,pp1-7*

12. **Y.Liu,J.Chu,Q.Tong and Y.Zhang,** *Decomposition of Ilmenite by concentrated KOH solution under atmospheric pressure, Int. Journal of mineral processing, vol.81, 2006, pp79-84*

13. **T.H. Okabe, T. Oda and Y. Mitsuda**, *Titanium powder production by perform reduction process (PRP), Journal of Alloys and Compounds, Vol.364, 2004, pp 156-163*

14. **D.Yang and B.Hur**, *The relationship between thermal decomposition properties of titanium hydride and aluminium foaming process, Materials letters 60, 2006, pp 3635-3641*

15. **Y.Liu, L.F.Chen, H.P Tang, C.T Liu, B. Liu and B.Y Yuang**, *Design of powder metallurgy titanium alloys and composites, Journal of Materials science and engineering A418, 2006, pp 25-35*

16. **S.Lavina, E.Negro, R.Gillubizzi, G.Depaloi, G.Pace and V.D.Moto**, *New hybrid inorganic-organic complexes based on poly (3-butylthiophene) and titanium tetrachloride: Synthesis, structure and conductivity, Electrochemica Acta, vol.52, 2007, pp 5062-5070.*

17. **R.J Gross, E.H. Majzoub and S.W. Spangler,** *The effects of titanium precursors on hydriding properties of alanates, Journal of Alloys and Compounds, vol 356/357, 2003, pp 423-428*

18. **H.S. Lee, J.H.Yoon and Y.M. Yi,** *Oxidation behaviour of titanium alloys under diffusion bonding, Thermochimica Acta, vol 455, 2007, pp 105-108*

19. **T.Kapias and R.F. Griffiths,** *Accidental releases of titanium tetrachloride ($TiCl_4$) in the context of major hazards- spill behaviour using REACTPOOL, Journal of hazardous materials, pp 41-52.*

20. **R.Ferreira, C.Avieu, B.Guillaume, J.M.Quinsset,** *Titanium matrix composites by continuous binder-powder coating: An alternative fabrication route, Journal pf composites, part A37, 2006, pp 1831-1836*

21. **K.Gebeur,** *Performance, tolerance and cost of TiAl passenger car valves, Journal of Intermetallics, vol 14, 2006, pp 1831-1836*

22. **Y.G.Zhou, W.D Zheng, H.Q. Yu,** *An investigation of a new near-beta forging process for titanium alloys and its application in aviation components, Journal of Materials Science and Engineering A393, 2005, pp 204-212*

23. **S.Bulatovic and D.M. Wyslouzil**, *Process development for treatment of complex perovskite, ilmenite and rutile ores, journal of Minerals Engineering, vol 12, 1999, pp 1407-1417*

24. **B.T Rubin,** *Kinetics of oxide film repair on titanium, Journal of Electroanalytical chemistry and interfacial chemistry, vol 58, 1975, pp 323-337*

25. **A. Agougjil and T. Brenkacem**, *Synthesis of porous titanium dioxide membranes, Desalination, vol 206, 2007, pp 531-537*

26. **P.L. Threadgrill**, *Prospects for joining titanium aluminides, Journal of Materials science and engineering A192/193, 1995, pp 640-646*

27. **E.Nyberg, M.Miller, K.Simmons and K.S.Weil**, *Microstructure and mechanical properties of titanium components fabricated by a new powder*

injection molding technique, Materials Science and Engineering C25, 2005, pp 336-342

28. **I.Vaquila, L.Vergara, M Passeggi Jr, R. Vidal and J.Ferron,** *Chemical reactions at surfaces: titanium oxidation, Journal of surface and coating technology, vol 122, 1999, pp 67-71*

29. **H.Doug and X.Y. Li,** *Oxygen boost diffusion for the deep case hardening of titanium alloys, Journal of materials science engineering A280, 2000, pp 303-310*

30. **T.E. Norgate, S.Jahanshahi and W.J.Rankin**, *Assessing the environmental impact of metal production processes, Journal of cleaner production, vol 15, 2007, pp 838-848*

31. **P.B Joshi, G.R. Marathe, N.S. Murti, V.K. Kaushik, and P.Ramakrishnan,** *Reactive synthesis of titanium matrix composite powders, Materials letters, 2002, pp 322-328*

32. **E.L. Tavani and N.A. Lacour**, *Making iron(III) tanning salts from a waste of titanium recovery by the sulphate process, Journal of materials chemistry and physics, vol 72, 2001, pp 380-386*

33. **M.J. Thomas, B.P. Waynne and M.W. Rainforth**, *An alternative method to separate and analyse the microtextures and microstructures of α grains and transformed β grains in near α titanium alloy Timetal 834,Journal of materials characterisation, vol 55, 2005, pp 388-394*

34. **K. Okada and S. Ueda**, *A new activation method for titanium sublimation pumps and its application to extremely high vacuums, Vacuum, vol 44, numbers 5-7, 1993,Pergamon Press Ltd, pp 713-715*

35. **P.J David and A. Bendavid**, *Review of the filtered arc process and materials deposition, Journal of thin solid films, vol 394, 2001, pp 1-15*

36. **S.Hashimoto, M.Takeuchi, K.Inoue, S.Honda, H.Awaji.K.Fukuda and S.Zhang,** *Pressureless sintering and mechanical properties of titanium aluminium carbide, Materials Letters 62, 2008, pp 1480-1483*

37. **N.M. Nikitenkov, D.Yu. Kolokolov, I.P.Chenov and Yu.I. Tyarin**, *SIMS investigations of isotope effects of a processed solid surface, Vacuum, vol 81, 2006, pp 202-210*

38. **M.L deBoer, P.I. Cohen and R.L. Park**, *Elastic and inelastic contributions to the auger electron appearance potential spectrum of titanium, Journal of Surface science, vol 70, 1978, North-Holland Publishing Company, pp 643-653*

39. **F.Wagner, N.Bozzolo,D.Van landyuyt and T. Grosdidier**, *Evolution of recrystallisation texture and microstructure in low alloyed Tiatnium sheets, Acta Materialia, vol 50, 2002, pp2345-1259*

40. **David Dye,** *Engineering Alloys (307) Lecture 7: Titanium Alloys, Imperial College,pp1-23*

41. *Ulman's Encyclopedia. of Industrial Chemistry*

42. **H. K. D. H. Bhadeshia**, *Metallurgy of Titanium and its Alloys, University of Cambridge, pp 225-313*

43. **Anne Marie Helmenstin,** *Titanium Facts: Chemical and Physical Properties, University of Cambridge, pp 181-189*

44. **http://wwwchem.uwimona.edu.jm/courses/kroll.skc**

45. **D.R.Lide,** *Handbook of chemistry and physics, 81st edition, 2000-2001, pp452*

46. **W.R. Matizamhuka,** *Masters Dissertation, University of the Witwatersrand, 2006, pp59-60*

APPENDIX A:

Malvern Mastersizer Particle size distribution of product and precursor

Size distribution of starting precursor as Vol%

Size (µm)	Volume In %
0.010	0.00
0.011	0.00
0.013	0.00
0.014	0.00
0.016	0.00
0.018	0.00
0.021	0.00
0.024	0.00
0.027	0.00
0.030	0.00
0.034	0.00
0.038	0.00
0.043	0.00
0.049	0.00
0.055	0.00
0.062	0.00
0.070	0.00
0.080	0.00

Size (µm)	Volume In %
0.080	0.00
0.090	0.00
0.102	0.00
0.115	0.00
0.130	0.00
0.147	0.00
0.166	0.00
0.187	0.00
0.211	0.00
0.239	0.00
0.270	0.00
0.305	0.00
0.345	0.00
0.389	0.00
0.440	0.00
0.497	0.00
0.561	0.00
0.634	0.00

Size (µm)	Volume In %
0.634	0.00
0.717	0.00
0.810	0.00
0.915	0.00
1.034	0.00
1.168	0.00
1.320	0.00
1.491	0.00
1.684	0.00
1.903	0.00
2.150	0.00
2.429	0.00
2.745	0.00
3.101	0.00
3.503	0.00
3.958	0.00
4.472	0.00
5.053	0.00

Size (µm)	Volume In %
5.053	0.00
5.709	0.00
6.450	0.00
7.287	0.00
8.233	0.00
9.302	0.00
10.510	0.00
11.874	0.00
13.416	0.00
15.157	0.00
17.125	0.00
19.348	0.00
21.860	0.00
24.698	0.00
27.904	0.00
31.527	0.00
35.620	0.00
40.244	0.00

Size (µm)	Volume In %
40.244	0.00
45.469	0.00
51.371	0.00
58.041	0.00
65.575	0.00
74.089	0.00
83.707	0.00
94.574	0.00
106.852	0.00
120.724	0.00
136.397	0.00
154.104	0.00
174.110	0.00
196.714	0.00
222.251	0.00
251.105	0.00
283.704	0.00
320.535	0.00

Size (µm)	Volume In %
320.535	0.00
362.148	0.00
409.163	0.64
462.281	5.14
522.296	8.83
590.102	12.61
666.711	15.39
753.265	16.46
851.056	15.53
961.542	12.61
1086.372	8.38
1227.408	3.89
1386.753	0.51
1566.785	0.00
1770.189	0.00
2000.000	

Size distribution of titanium product as Vol%

Size (µm)	Volume In %
0.010	0.00
0.011	0.00
0.013	0.00
0.014	0.00
0.016	0.00
0.018	0.00
0.021	0.00
0.024	0.00
0.027	0.00
0.030	0.00
0.034	0.00
0.038	0.00
0.043	0.00
0.049	0.00
0.055	0.00
0.062	0.00
0.070	0.00
0.080	0.00

Size (µm)	Volume In %
0.080	0.00
0.090	0.00
0.102	0.00
0.115	0.00
0.130	0.00
0.147	0.00
0.166	0.00
0.187	0.00
0.211	0.00
0.239	0.00
0.270	0.00
0.305	0.00
0.345	0.00
0.389	0.00
0.440	0.00
0.497	0.00
0.561	0.00
0.634	0.00

Size (µm)	Volume In %
0.634	0.00
0.717	0.00
0.810	0.00
0.915	0.00
1.034	0.00
1.168	0.00
1.320	0.00
1.491	0.00
1.684	0.00
1.903	0.00
2.150	0.00
2.429	0.00
2.745	0.00
3.101	0.00
3.503	0.00
3.958	0.00
4.472	0.00
5.053	0.00

Size (µm)	Volume In %
5.053	0.00
5.709	0.00
6.450	0.06
7.287	0.18
8.233	0.44
9.302	0.86
10.510	1.50
11.874	2.35
13.416	3.43
15.157	4.68
17.125	6.03
19.348	7.36
21.860	8.54
24.698	9.41
27.904	9.84
31.527	9.75
35.620	9.15
40.244	9.15

Size (µm)	Volume In %
40.244	8.08
45.469	6.66
51.371	5.09
58.041	3.55
65.575	2.20
74.089	0.85
83.707	0.00
94.574	0.00
106.852	0.00
120.724	0.00
136.397	0.00
154.104	0.00
174.110	0.00
196.714	0.00
222.251	0.00
251.105	0.00
283.704	0.00
320.535	0.00

Size (µm)	Volume In %
320.535	0.00
362.148	0.00
409.163	0.00
462.281	0.00
522.296	0.00
590.102	0.00
666.711	0.00
753.265	0.00
851.056	0.00
961.542	0.00
1086.372	0.00
1227.408	0.00
1386.753	0.00
1566.785	0.00
1770.189	0.00
2000.000	

APPENDIX B

Determination of theoretical mass losses during pyrolysis of precursor

The expected mass losses from the thermal decomposition of the precursor were based on the XRF and XRD results of the raw precursor and its thermal decomposition products. Figure 4.4 shows that the precursor is made up two phases only with one phase containing titanium and the other aluminium. It is arguable therefore that all the titanium shown in the XRF is in the phase NH_4TiF_4 and that all the aluminium is in $(NH_4)_3AlF_6$. The theoretical mass losses reported in the table are thus based on the phase composition of the precursor, i.e. 63wt% NH_4TiF_4 and 37wt% $(NH_4)_3AlF_6$, and their decompositions at the various temperatures according to Eqns (5.1) and (5.2).

Temperature/^oC	**Phases present**	**Reaction**	**cumulative weight %**	**Cumulative mass loss as weight %**
20-300	**NH_4TiF_4 $(NH_4)_3AlF_6$**	**Loss of moisture**	**-**	
380-400	**NH_4TiF_4 NH_4AlF_4**	**$(NH_4)_3AlF_{6(s)}=2NH_4F_{(g)} + NH_4AlF_{4(s)}$**	**13**	**13**
400-600	**TiF_3 NH_4AlF_4**	**$NH_4TiF_{4(s)}=TiF_{3(s)} + NH_4F_{(g)}$**	**43**	**30**
600-1250	**TiF_3 AlF_3**	**$NH_4AlF_4=NH_4F + AlF_3$**	**55**	**37**
1300-	**TiF_3**	**$AlF_{3(s)})=AlF_{3(g)}$**	**75**	**53**